A Numerical Model of Thermal Effects in a Microwave Irradiated Catalyst Bed

by

Jason E. Lanz

Thesis submitted to the faculty of the
Virginia Polytechnic Institute and State University
in partial fulfillment of the requirements for the degree of

MASTER OF SCIENCE
in
Mechanical Engineering

Dr. James R. Thomas, Jr., Chairman
Dr. William A. Davis
Dr. Elaine P. Scott

26 March, 1998
Blacksburg, Virginia

Keywords: Catalyst, Microwave, Selective heating, Heat transfer

A Numerical Model of Thermal Effects in a Microwave Irradiated Catalyst Bed

by

Jason E. Lanz

Committee Chairman: Dr. James R. Thomas, Jr.

Mechanical Engineering

(**ABSTRACT**)

Electromagnetic and heat transfer analysis is used to determine possibility of selective heating of nanometer-sized, metallic catalyst particles attached to a ceramic support through microwave irradiation. This analysis is incorporated into a macroscopic heat transfer model of a packed and fluidized catalyst bed heated by a microwave field to predict thermal effects associated with selective heating of the catalyst sites. The model shows a dependence on particle size and microwave frequency on the selective heating of the catalyst sites. The macroscopic thermal effects are shown to be small for a typical experiment. However, changing the support material and catalyst particle size are shown to distinguish the thermal effects associated with selective heating of the metallic catalysts.

ACKNOWLEDGEMENTS

This thesis was only made possible through the help and support of many people. Foremost, I need to thank Dr. James R. Thomas, Jr., for his expertise and patience during this work. I would like to thank my remaining committee members, Dr. Elaine P. Scott and Dr. William A. Davis, for making my studies at Virginia Tech a very worthwhile experience. I would also like to thank Dr. Davis for his time and patience in explaining the electromagnetics involved in this work. I am very grateful to the faculty of the Mechanical Engineering Department at the Virginia Military Institute for their help and encouragement in my pursuit of graduate studies. I must certainly thank my mother for her years of understanding and support, and giving me confidence in all my endeavors. Finally, I would like to thank DuPont and the National Science Foundation, whose funding supported this work.

TABLE OF CONTENTS

LIST OF FIGURES

NOMENCLATURE

$\underline{\underline{A}}$	Coefficient matrix for the Thomas algorithm
A	Surface area of the control volume
A_s	Total surface area
A_c	Contact surface area
a	Waveguide width
a_n	Coefficient for Eq. (3.37a)
$\mathbf{B}$	Magnetic flux density vector
$\underline{B}$	Vector of constants for the Thomas algorithm
b	Waveguide height
C_1	Constant for Eq. (4.31)
C_2	Constant for Eq. (4.31)
C_3	Electric field amplitude reduction constant for Eq. (4.22)
C	Specific heat of alumina
C_p	Constant pressure specific heat
c_n	Coefficient for Eq. (3.37)
$\mathbf{D}$	Electric flux density vector
D	Catalyst bed diameter
D_p	Platinum catalyst particle diameter
d	Catalyst support pellet diameter
$\mathbf{E}$	Electric field vector
$\mathbf{E}_i$	Incident electric field vector
$\mathbf{E}_r$	Reflected electric field vector

$\mathbf{E}_t$	Transmitted electric field vector
E_0	Applied electric field
E_{rms}	Root-mean-squared electric field
$\dot{E}_{gen}$	Energy generated within the control volume
$\dot{E}_{in}$	Energy entering the control volume
$\dot{E}_{out}$	Energy exiting the control volume
$\dot{E}_{st}$	Energy stored within the control volume
f	Frequency
g	Acceleration of gravity
$\mathbf{H}$	Magnetic field vector
H	Height of the catalyst bed
h	Convection coefficient
h_c	Contact conductance
$\mathbf{J}$	Conduction current density vector
k	Thermal conductivity of alumina
k_b	Boltzmann's constant
k_g	Thermal conductivity of the gas
M_b	Molecular weight
$\dot{m}$	Mass flow rate
Nu	Nusselt number
$\mathbf{P}(t)$	Poynting vector (time domain)
P	Perimeter
P_{ave}	Average power
P_∞	Free stream pressure
Pr	Prandtl number
$\dot{q}$	Heat generation per unit volume
q_s''	Heat flux at the surface of the catalyst pellet
Re_d	Reynolds number based on catalyst pellet diameter

$\mathbf{S}(\omega)$	Poynting vector (frequency domain)
S	Arbitrary surface area
R	Radius of alumina catalyst pellet
$\underline{T}$	Temperature vector for the Thomas algorithm
T	Temperature
T_0	Entering gas temperature
T_g	Gas temperature
T_{mean}	Mean gas temperature
T_s	Surface temperature
T_∞	Free stream gas temperature
u_0	Superficial, entering gas velocity
u_1	Interstitial gas velocity
u_{mf}	Arbitrary volume
w	Reactor tube wall thickness
α	Attenuation constant
α_{acc}	Accommodation coefficient
β	Phase constant
Δp	Pressure drop across the catalyst bed
ε	Complex electrical permittivity
ε'	Dielectric constant
ε''	Dielectric loss
ε_r'	Relative dielectric constant
ε_r''	Relative dielectric loss
ε_{eff}	Effective permittivity
ε_0	Permittivity of free space
Γ_{ab}	Reflection coefficient from a to b
μ_w	Gas viscocity at the surface of the pellet
μ_∞	Free stream gas viscocity

μ	Complex magnetic permeability
μ'	Real magnetic permeability
μ''	Magnetic loss
μ_0	Permeability of free space
η	Intrinsic impedance
ω	Angular frequency
Φ	Volume fraction of platinum catalysts
φ	Solid fraction of catalyst support pellets
φ_{mf}	Solid fraction of catalyst support pellets at the minimum fluidization velocity
ρ	Density of alumina
ρ_g	Density of the gas mixture
σ	Electrical conductivity
σ_b	Bulk electrical conductivity
σ_{eff}	Effective conductivity
T_{ab}	Transmission coefficient from *a* to *b*
τ	Relaxation time constant
τ_T	Thermal time constant
χ	Sensitivity coefficient

CHAPTER 1

INTRODUCTION

1.1 Prelude

Microwave processing of materials offers distinct advantages over conventional heating in some applications. The energy of the microwave field can be dissipated directly into the desired media, without the convection and conduction associated with conventional heating. Furthermore, in some applications where the material properties are well understood, microwave heating can offer a greater degree of control over conventional heating techniques.

One such area where microwave processing offers such promise is chemical catalysis. Researchers have reported higher rates of chemical catalysis in the presence of microwave fields. The reaction rates observed have occurred at lower bulk temperatures than in conventional heating. Two possible explanations exist for this phenomenon. The first possibility is that the microwave field is coupling with the desired molecules and altering their rotations in such a way to promote catalysis without increasing the temperature; however, Stuerga and Gaillard [1] have reported that such athermal effects are not probable. A second explanation for the increased reaction rates in heterogeneous catalysis is the possibility of localized heating, without a noticeable contribution to the bulk temperature, in and around the metallic catalyst particles as a result of the microwave field. This second explanation, localized heating, is a primary focus of this study.

At Los Alamos National Laboratory (LANL), an experiment has been designed to study the effects of a microwave field on chemical catalysis. By modeling this

experiment numerically, insight should be gained as to the possibility of localized heating around the catalyst particles.

1.2 Selective Heating Hypothesis

In a typical experiment where microwave heating yielded higher reactions rates and increased reaction selectivity, the catalysts are nanometer-sized metallic particles attached to a porous ceramic support. Since the metallic particles have a higher electrical conductivity than the ceramic support, the particles should couple better than the support to a microwave field, dissipating much of the electromagnetic energy as heat, thus achieving temperatures higher than the support material. However, the temperature rise of the metallic catalysts may not have a significant effect on the measurable bulk temperature of the experiment, owing to the small size of the catalyst particles, and low volume fractions of the particles relative to the support. If the catalyst particles are, in fact, at considerably higher temperatures than the bulk temperatures, this could explain the reports of enhanced catalysis.

1.3 Objectives

The goal of this work is to determine whether the metallic catalyst particles can be selectively heated by a microwave field through an analysis of the electromagnetic interactions with the nanometer-sized catalyst sites, and subsequent heat transfer. A secondary objective is to determine the temperature distribution in a complete catalyst bed to seek measurable thermal effects associated with the possible selective heating of the catalyst sites. The experimental setup proposed by LANL will serve to guide the analysis and numerical modeling of this work.

1.4 Proposed Experiment

The proposed experiment at LANL is designed to study the effect of a microwave field on butane gas flowing through an platinum/alumina, Pt/Al_2O_3, catalyst bed. The desired result of the catalysis is isomerization of the butane molecules which normally

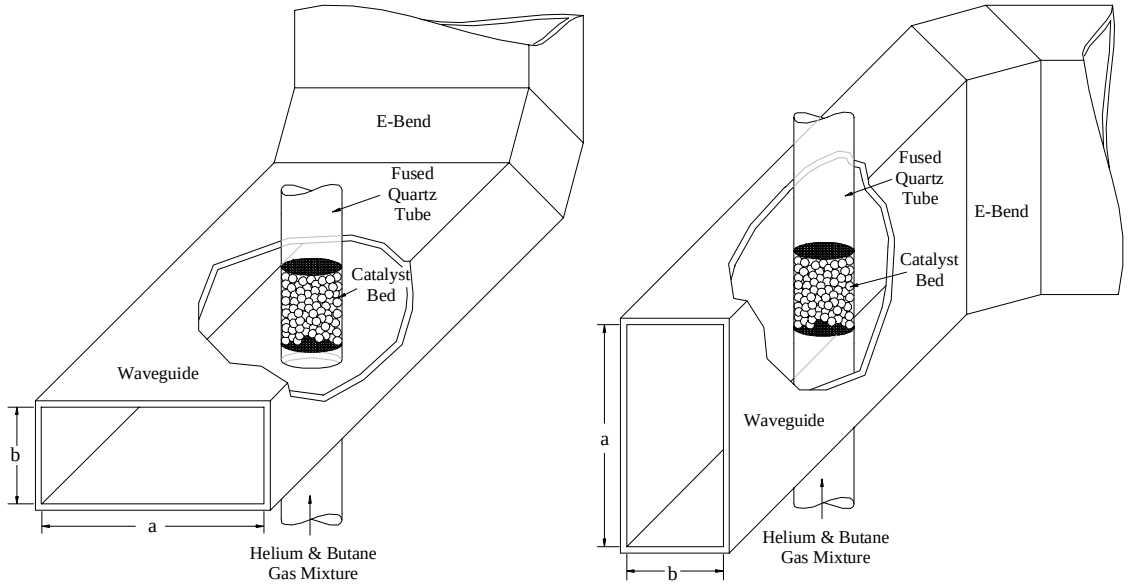

Figure 1.1 Waveguide and reactor tube.

occurs around 300°C. In light of the reports of enhanced catalysis, the isomerization should occur at bulk temperatures below 300°C.

The experimental setup consists of a small catalyst bed inside a reactor tube running through a microwave waveguide. The waveguide is filled with nitrogen to prevent combustion of any hydrogen that may leak from the reactor tube. The microwave applicator is a standard copper WR-284 waveguide with two E-bends. This waveguide can be operated in the TE_{10} mode, where the electric field strength is constant in the direction of propagation along the length of the waveguide; along the width of the guide, a = 7.21 cm, the field varies sinusoidally with one peak amplitude at the half-width. The height of the waveguide, b, is one-half the width, 3.605 cm.

The reactor tube is made of fused quartz with an inside diameter of 2.0 cm and a wall thickness of 2.0 mm. Inside the tube, a bed of catalyst particles is held in place by two screens 2.54 cm apart. The reactor tube can pass through the waveguide in several different orientations, where each orientation produces a different electric field distribution within the bed. First, the tube can pass through perpendicular to the width of the waveguide, as shown in Fig. 1.1(a), so that the axis of the reactor tube is oriented

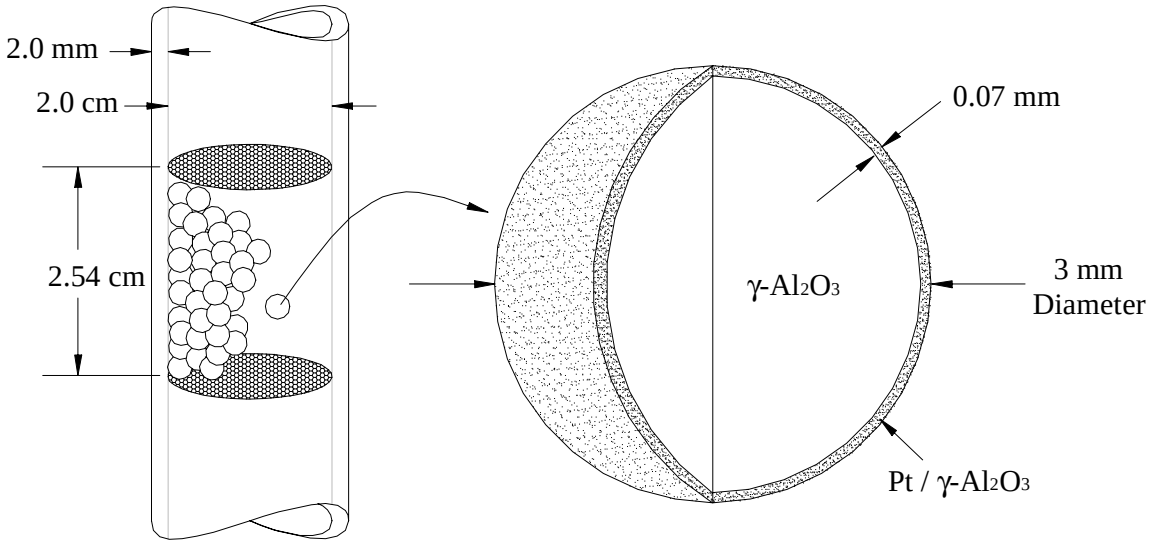

Figure 1.2 Catalyst bed and enlarged cross-section of a catalyst pellet.

parallel to the electric field. Next, the waveguide can be rotated 90 degrees about the length so that the tube now passes perpendicular to the height of the guide, as shown in Fig. 1.1(b); the axis of the bed is oriented perpendicular to the electric field with this orientation. Finally, the reactor tube can run lengthwise through the waveguide, parallel to the propagation of the electric field.

The catalyst bed is 2.0 cm in diameter and 2.54 cm in height and is comprised of catalyst pellets with an average diameter of 3 mm. These pellets can either be arranged in a randomly packed bed, or arranged in such a manner to allow for fluidization given sufficient flow.

The individual catalyst pellets are comprised of a porous gamma alumina, γ-Al_2O_3, and 0.5% platinum, by mass. The gamma alumina differs from crystalline Al_2O_3, due to minor impurities and a 70% reduction in density due to the porosity. The platinum catalysts are attached to the alumina support by immersing the pellet in an aqueous platinum solution. The porosity of the alumina causes the platinum catalysts to be absorbed and attach to the support within the first 70 microns from the surface of the pellet, as shown in Fig. 1.2. The individual platinum catalyst particles range in size from approximately 1 to 20 nm in diameter, as shown in Fig. 1.3.

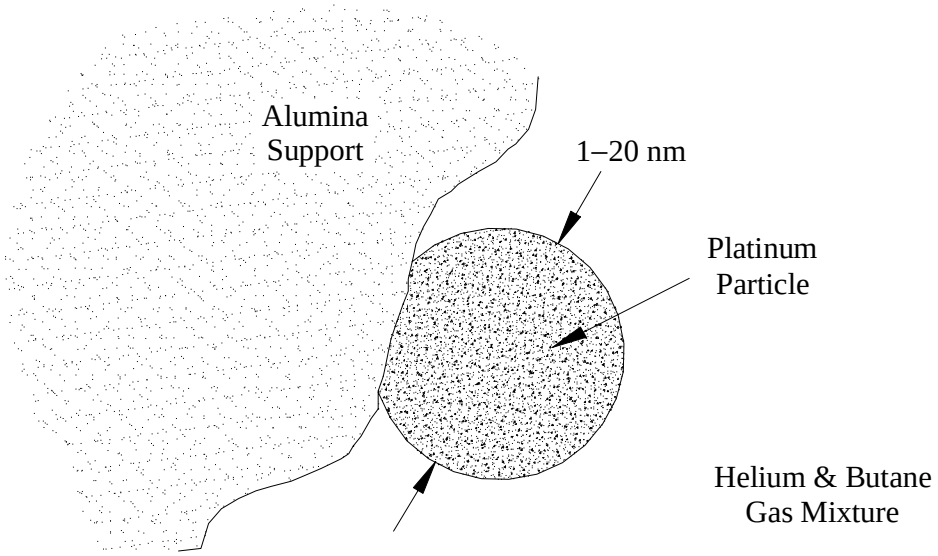

Figure 1.3 Enlarged view of a typical catalyst particle.

The butane gas, C_4H_{10}, flowing through the catalyst bed is diluted with inert helium in an 80% helium, 20% butane mixture, by volume. A low flow rate is required for the isomerization of the butane in the packed bed, arbitrarily chosen as 0.25 l/min of helium and 0.066 l/min of butane, for a combined flow rate of 0.316 l/min. Fluidization of the bed may be required to prevent overheating under high electric field strengths. The minimum flow required to fluidize the bed is approximately 45 times greater than the proposed flow for the packed bed; however, such a high flow rate may not allow for sufficient butane isomerization.

A strong microwave field will be needed if the catalyst particles are to be heated significantly above the bulk temperature. If the gamma alumina support were essentially lossless, the bulk of the microwave energy would be deposited into the platinum catalyst particles. However, the support is not lossless, and a strong microwave field, say $5 \cdot 10^4$ V/m, will elevate the bed temperature well above 300°C, even in the absence of the lossy platinum catalyst. To keep the bulk temperature below the 300°C, where catalysis will occur regardless of the microwave field, it is necessary to pulse the microwave field for short periods of time. This will allow for significant energy dissipation in the catalyst during the microwave pulse, and also allow the bed to cool in the absence of the microwave field.

1.5 Numerical Heat Transfer Model Overview

A numerical model representing the heat transfer in the microwave irradiated catalyst bed, incorporating various mechanisms for heat generation and transfer, will be developed. The results of the model will then be analyzed to determine the applicability of the model and the various hypotheses in the model. Confirmation of the model and hypotheses would be obtained through comparison to the experimental results, but as of yet no such results are available. However, Roussy [2] presents results from similar experiments that will be used for comparison when applicable.

Numerical models will be developed for both packed and fluidized beds subjected to various electric field scenarios. The catalyst bed models will consider the microwave energy dissipated in the catalyst pellets along the axis of the bed, and subsequent heat transfer to the gas flowing along this axis. To model the individual catalyst pellets along the axis, a one-dimensional model of a single pellet exposed entirely to convection will first be obtained; this model will then be translated along the axis to model the complete bed temperature distribution.

Before the heat transfer model can be developed, the electromagnetic interactions with the catalyst bed must first be understood. Coupling mechanisms for the alumina support and platinum catalysts will be presented, including mechanisms which may lead to selective heating of the catalyst sites. Furthermore, electric field distributions within the waveguide and catalyst bed will be approximated for use as boundary conditions for the heat transfer model.

CHAPTER 2

LITERATURE REVIEW

2.1 Enhanced Catalytic Reactions

Since the 1970s researchers have used microwave energy to promote chemical reactions, where increased reaction rates and selectivity have been reported. Gedye et al. [3] reported dramatically increased reaction rates for a variety of organic compounds in 1988. Roussy and Pearce [4] discuss in detail the increased selectivity involved in methane activation, as well as hexane isomerization over a Pt/Al_2O_3 catalyst. Furthermore, Majetich and Hicks [5] compared forty-five organic reactions under both conventional and microwave heating and observed that most reactions showed drastically reduced reaction times in the presence of microwave heating. It should be noted that the aforementioned works represent only a small subset of papers available on the topic of microwave chemistry.

Several explanations have been proposed to account for the reported increased reaction rates and selectivity. Bose et el. [6] suggest that the enhanced reactions are a result of specific activation of the molecules, though Suerga and Gaillard [1] present a theoretical analysis showing that such specific, athermal effects are not possible. In addition, Westaway and Gedye [7] show that the increased reaction rates for four different organic reactions in a microwave field are a result of higher reaction temperatures, and not specific activation by the microwave field. An alternative explanation is that the microwave field is heating the nanometer-sized platinum catalyst particles to temperatures significantly higher than the bulk temperature of the support,

where such microscopic “hot spots” do not have a noticeable effect on the measurable bulk temperature.

2.1.1 Selective Heating

The metallic catalyst sites may couple strongly with the microwave field compared to the support material, thus achieving temperatures significantly higher than the support. Seyfried et al. [8] studied the effects of microwave irradiation on catalysis and postulated that the increased selectivity and reaction rates may be the result of a number of catalyst sites being at substantially higher temperatures than the measurable bulk temperature.

Whether the catalyst particles can actually sustain temperatures significantly higher than the support environment is debatable. Holstein and Boudart [9] use an energy balance to show that a catalyst particle cannot exceed a 0.03% temperature rise above the support temperature as a result of the heat released from an exothermic catalytic reaction. In contrast, Steinbruechel and Schmidt [10] use a different approach more applicable for the small-scale heat transfer associated with nanometer-sized particles. Accounting for the phonon and electron heat carrier velocities and wavelengths, they determine that catalyst sites may achieve temperature differences upwards of 300°C above the support for very short periods of time, on the order of 10^{-12} seconds, as a result of catalytic reactions. Neither of the two works, however, consider the large amounts of energy possibly generated from the metallic catalysts coupling with a strong electromagnetic field.

Directly measuring the temperature rise of the catalyst particles is a difficult task. The small size of the platinum catalysts make traditional thermocouple and infrared techniques impossible. Hence, the goal of this work is to incorporate microscopic electromagnetic interactions with the catalyst sites into a macroscopic heat transfer model to predict measurable thermal effects associated with possible selective heating of the catalyst sites. It should be noted, though, that one possible approach to directly detecting selectively heated catalyst sites is *neutron resonance radiography* as reported by Frost et al. [11].

2.2 Size-Dependent Conductivity

Small metallic particles, such as the catalyst particles considered in this study, have electrical conductivity values considerably less than the typical bulk values. A reasonable explanation is this reduced conductivity, or increased resistivity, results from the conducting electrons experiencing reduced mobility as the host particle size approaches that of the mean-free-path of the conducting electrons. This effect was predicted theoretically in 1965 by Gorkov and Eliashberg [12]. Nimtz et al. [13] measured this size-dependent conductivity using microwave frequencies; they suggest that the conductivity of a small metals decreases from the bulk value approximately as the cube of the particle diameter for sizes below 500 nm.

The platinum catalyst particles considered in this study are typically between 1 and 20 nm in diameter, which is on the same order as the 11 nm mean-free-path of the conducting electrons for platinum at room temperature [10]. The reduced conductivity allows for internal electric fields within the platinum catalysts, giving rise to internal heating, that would not normally be present inside a perfectly conducting sphere when immersed in an microwave field. This heat generated by the platinum catalysts should have a noticeable effect on the temperature rise of a microwave irradiated catalyst pellet or bed of pellets.

2.3 Mixture Formulae

The presence of the platinum inclusions in the outermost part of the catalyst pellet affects the electric field interactions within that region. Roussy and Pearce [4] offer several analytical and empirical formulae for combining the dielectric properties of the platinum catalysts and alumina support so that the two-material region can be treated as a single, homogeneous material. The analytical Rayleigh formula is derived to model isolated spheres in a dielectric support, such as the catalyst pellets considered in this study. Another analytical mixture theory used by Calame et al. [14] to model porous ceramics is the Maxwell-Garnet theory, also derived for isolated spherical inclusions.

CHAPTER 3

MICROWAVE INTERACTIONS WITH MATERIALS

3.1 Introduction

Microwave radiation has the advantage of depositing energy directly into some media, whereas conventional heating techniques require the heat to diffuse into the media from the surrounding environment; thus, microwave heating can be more efficient than conventional heating for some applications. In particular regard to catalysis, microwave fields may have the effect of selectively activating the catalyst sites, an effect not possible by conventional heating. In addition to coupling with the catalyst particles, microwave fields may also couple with the ceramic catalyst support, dissipating the electrical energy in the form of heat. Since microwave radiation is the primary driver of the catalysis and heat transfer within the catalyst bed, an understanding of how microwaves interact with the materials within the bed is required.

An electromagnetic wave propagating through a medium will interact with the charged particles within that medium. In certain materials, these interactions are quite strong and lead to considerable absorption of the wave into the material; this energy is then either dissipated as heat or stored within the medium. The constitutive parameters of a material which describe this interaction are the electrical conductivity, σ, electric permittivity, ε, and the magnetic permeability, μ. These properties of matter relate the strength of the electric field by three constitutive relations to describe the interaction of the wave with the material.

The constitutive relation describing the interaction of the field with the free electrons within the medium is the conduction current density,

$$\mathbf{J} = \sigma\mathbf{E}, \tag{3.1}$$

where σ is the electrical conductivity of the material, in siemens/meter or S/m, and $\mathbf{E}$ is the electric field vector.

Quantifying the interaction of the electric field with the electric permittivity of the material is the electric flux density,

$$\mathbf{D} = \varepsilon\mathbf{E}, \tag{3.2}$$

where ε is the electrical permittivity of the material in farads/meter, or F/m. The permittivity of a material can be represented in complex notation as

$$\varepsilon = \varepsilon' - j\varepsilon'', \tag{3.3}$$

where the real part, the dielectric constant, represents the energy stored in the material, and the imaginary part, the dielectric loss, represents the ability of the material to dissipate the electric field as heat. The electrical permittivity is discussed in more detail in Section 3.2.

Finally, the magnetic flux density,

$$\mathbf{B} = \mu\mathbf{H}, \tag{3.4}$$

relates the magnetic field intensity, $\mathbf{H}$, to the magnetic permeability of the material, μ, in henries/meter or H/m. As with the permittivity, the permeability can also be expressed in complex notation

$$\mu = \mu' - j\mu'', \tag{3.5}$$

where the real part represents the magnetic energy stored in the material, and the imaginary part, the magnetic loss, represents the ability of the material to dissipate the magnetic field as heat. For most problems of interest in microwaves, μ may be represented by $\mu_0 = 4\pi \cdot 10^{-7}$ H/m, the permeability of a vacuum.

The Poynting vector is used to quantify the amount of power lost by an electromagnetic wave propagating through a medium, where

$$\mathbf{P}(t) = \mathbf{E}(t) \times \mathbf{H}(t), \tag{3.6}$$

or as expressed in the frequency domain,

$$\mathbf{S}(\omega) = \frac{1}{2}\left[\mathbf{E}(\omega) \times \mathbf{H}^*(\omega)\right]. \tag{3.7}$$

For an electromagnetic wave propagating through a control volume of arbitrary surface area, *S*, and volume, *V*, the the power absorbed by the medium is the difference between the exiting and entering electromagnetic fields given by

$$-\int_S \frac{1}{2}\left(\mathbf{E} \times \mathbf{H}^*\right) ds = \int_V \frac{1}{2}\left(\mathbf{E} \cdot \mathbf{J}\right) dV + j\omega \int_V \frac{1}{2}\left(\mathbf{B} \cdot \mathbf{H}^* - \mathbf{E} \cdot \mathbf{D}^*\right) dV, \tag{3.8}$$

where the * indicates the complex conjugate, and field values are represented in peak form. Substituting for the constitutive relations and expressing Eq. (3.8) in terms of the properties of the control volume gives

$$-\oint_S \left(\mathbf{E} \times \mathbf{H}^*\right) dS = \int_V \sigma |\mathbf{E}|^2 dV + \frac{1}{2}\omega \int_V \left(\varepsilon'' |\mathbf{E}|^2 + \mu'' |\mathbf{H}|^2\right) dV + j\frac{1}{2}\omega \int_V \left(\mu' |\mathbf{H}|^2 - \varepsilon' |\mathbf{E}|^2\right) dV. \tag{3.9}$$

The first integral on the right hand side of Eq. (3.9) represents the energy dissipated in the medium through electric conduction, while the second integral on the right hand side represents the energy dissipated as heat through both dielectric and magnetic loss. The final integral on the right hand side represents the net reactive electric and magnetic energy stored in the medium, which does not contribute to the heating of the control volume.

Using a vector equation such as Eq. (3.9) is rather impractical for the present application , so in the following sections several scalar equations will be developed from Eq.(3.9) to describe how the microwave field heats the catalyst bed. Since the materials in the catalytic bed do not have any magnetic properties, the magnetic loss terms in the Poynting theorem will be disregarded. The remaining conductivity and permittivity terms in the Poynting theorem represent the two loss mechanisms by which electromagnetic energy is dissipated as heat: electric conduction and dielectric loss. Both metallic conductors, such as the platinum catalysts, and non-conducting dielectrics, such as the alumina support, will couple with an applied electric field, though in different ways. For a conductor, an external electric field will displace and translate the free electrons, whereas in a non-conducting dielectric the same electric field will only

displace the molecular electron cloud some finite distance. An understanding of both loss mechanisms is required to model the catalytic bed.

3.2 Loss in Dielectrics

Dielectric materials have their electrons bound by atomic and molecular forces, and thus behave as insulators, not normally conducting electricity. When subjected to an electric field, the dominant electric charges will align with the field, as in Fig. 3.1. Some of the energy involved in moving the electron cloud is lost to friction forces with other atoms. This continual alignment and realignment with an alternating field gives rise to the electric field loss and consequent dissipation into molecular kinetic energy. As mentioned in Section 3.1, the dielectric interaction with the field consists of both reactive and dissipative terms which can be expressed in complex form to represent the permittivity of a material, $\varepsilon = \varepsilon' - j\varepsilon''$, where ε' is the dielectric constant and ε'' is the dielectric loss of the material. Out of convenience, these terms are often represented in nondimensional terms relative to the permittivity of free space,

$$\varepsilon_r' = \frac{\varepsilon'}{\varepsilon_0}, \tag{3.10}$$

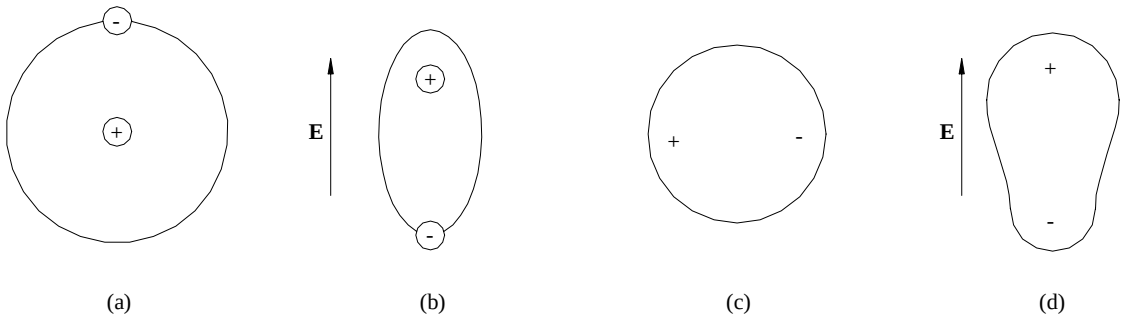

Figure 3.1 Electronic polarization, (a) and (b). Ionic or molecular polarization, (c) and (d).

and

$$\varepsilon_r'' = \frac{\varepsilon''}{\varepsilon_0}, \tag{3.11}$$

where the permittivity of free space, ε_0, is equal to $8.854 \cdot 10^{-12}$ F/m.

Some substances, such as diatomic oxygen and nitrogen, are essentially electrically neutral and couple weakly with the electric field. Other substances such as the polar molecules of water couple extremely well with applied electric fields. The materials which strongly couple with the electric field and dissipate heat are know as *lossy* materials, where the electric energy is lost into the material and dissipated as heat; this dissipation is characterized by the dielectric loss of the material. The second term in Eq. (3.9), can be expressed as a scalar,

$$P_{ave} = \omega \varepsilon_0 \varepsilon_r'' E_{rms}^2 V, \tag{3.12}$$

to account for the average power dissipated in lossy materials by this dielectric heating, where V is the volume of the material, ω is the angular frequency, and the *root mean squared* (rms) value is used for the electric field. Assuming a sinusiodal waveform, the average value of the field is $1/\sqrt{2}$ times the peak value, thus the factor of ½ is missing from Eq.(3.9). Replacing the angular frequency with $2\pi f$, and dividing by the volume gives an expression for the average heat generated per unit volume,

$$\dot{q} = 2\pi f \varepsilon_0 \varepsilon_r'' E_{rms}^2, \tag{3.13}$$

where $\dot{q}$ has units of W/m^3. This expression is used to calculate the heat dissipated by the catalyst support in the microwave field.

3.3 Loss in Conductors

The loss mechanism for conductors differs from that of dielectrics since conductive materials have free electrons which are not tightly bound to any particular atom structure, unlike dielectrics. These free electrons will migrate through the material in the presence of an applied electric field, losing energy by resistive dissipation due to collisions with other electrons and atoms in the lattice structure. The first term on the right hand side of

Eq. (3.9) quantifies this dissipation of electric energy. Expressing the integral in terms of average power yields

$$P_{ave} = \sigma E_{rms}^2 V, \tag{3.14}$$

or on a per unit volume basis:

$$\dot{q} = \sigma E_{rms}^2, \tag{3.15}$$

where $\dot{q}$ has the units of W/m^3. Equation (3.15) quantifies the electromagnetic energy dissipated as heat in the metallic catalyst particles through electric conduction and subsequent resistive dissipation.

3.4 Effective Permittivity

So far, only losses in homogeneous materials have been considered, either pure dielectrics or pure conductors; however, the surface of the catalyst pellets is comprised of a mixture of both dielectric and conductive materials, as depicted in Fig. 1.2. The alumina support and platinum catalysts can be treated as separate entities, calculating the heat generation contribution from each; however, this requires a detailed knowledge of the internal structure and can be quite tedious. More conveniently, several mixture formulae exist for combining the permittivities of two different materials into one effective permittivity[4].

The Rayleigh mixture formula gives an effective permittivity, ε_{eff}, for a material which is comprised of a continuous medium with small, isolated spherical particles dispersed throughout,

$$\varepsilon_{eff} = \frac{\varepsilon_1(2\varepsilon_1 + \varepsilon_2) + 2\Phi\varepsilon_1(\varepsilon_2 - \varepsilon_1)}{2\varepsilon_1 + \varepsilon_2 - \Phi(\varepsilon_2 - \varepsilon_1)}. \tag{3.16}$$

Material 1 represents the support material, material 2 represents the spherical particles, and Φ is the volume fraction of the spherical particles to the support. The ceramic support medium contains both dielectric constant and loss terms, so the permittivity, ε_1, is represented in complex form,

$$\varepsilon_1 = \varepsilon_1' - j\varepsilon_1''. \tag{3.17}$$

Since material 2 is metallic in this case, the loss mechanism is solely through conductivity, so the complex permittivity, ε_2, must be represented in terms of the conductivity. Due to similarity in form, the dielectric loss of metals may be represented by $\varepsilon'' = \sigma/\omega$. Since the free electrons respond rapidly to the applied field there is effectively no stored energy, so the dielectric constant for a metal is simply that of free space. The effective complex permittivity of the metal can now be written as

$$\varepsilon_2 = \varepsilon_0 - j\frac{\sigma_2}{\omega}. \tag{3.18}$$

The relationship in Eq. (3.16) is not valid for conductors when the volume fraction exceeds 30%. At such high volume fractions the metallic inclusions are no longer well isolated and electrons may migrate between the particles along some continuous path; such conduction may give rise to shielding and eddy currents, which create a situation too complex to be modeled by a simple relationship; this phenomenon is known as percolation. For the volume fractions considered in this study, percolation is not a concern.

3.5 Size-Dependent Conductivity

As mentioned in Section 2.2, researchers have reported that the conductivity of metals departs significantly from the bulk value as the size of the material particle decreases. Nimtz [13] has studied the effects of particle size on the conductivity of conductors, and reported that the conductivity decreases significantly from the bulk value as the particle size decreases below the micrometer range. The physical mechanism for such a reduction in conductivity is attributed to quantum constraints. As the size of the particle approaches the same order of magnitude as the wavelength of the electrons, the conducting electrons experience an increase in effective resistance since the electrons are bound to the medium in whole wavelength intervals. This effect has been noticed in semiconductors and other thin conducting films. However, the effect does not decrease the conductivity experienced along the principal axes of conduction in these thin films, since the axes are still long compared to the wavelength of the conducting electrons;

instead, the effect is noticed as anisotropic conductivity, where the conductivity takes on a tensor form and is therefore dependent upon direction. This quantum confinement, though, does have an effect on the conductivity of the spherical, metallic particles considered in this study since all three dimensions are small compared to the wavelength of the conducting electrons.

Nimtz [13] suggests that the conductivity decreases from the bulk value approximately as the cube of the diameter for particles smaller than 500 nm. To incorporate this into a functional relationship for the effective conductivity, the expression

$$\sigma_{eff} = \left(\frac{D_p}{5 \cdot 10^{-6}} \right)^3 \sigma_b, \tag{3.19}$$

is used, where D_p is the metal particle diameter for particles smaller than $5 \cdot 10^{-6}$ meters, and σ_b is the bulk conductivity of the metal. For the nanometer-sized inclusions, this is a reduction of eight orders of magnitude from the bulk value, as depicted in Fig. 3.2.

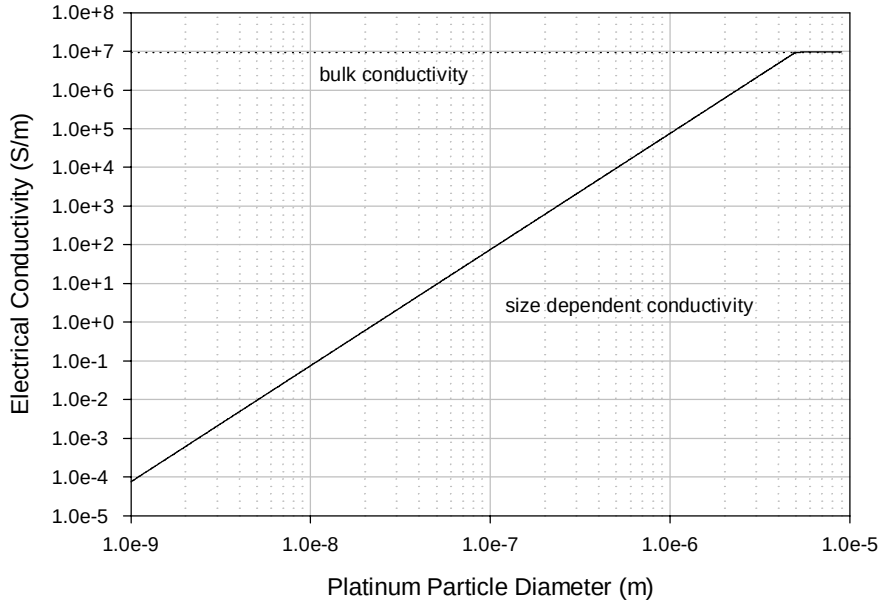

Figure 3.2 Effect of particle size on the electrical conductivity of platinum, as suggested by Nimtz [13].

With such a significant reduction in conductivity, the platinum inclusions no longer behave as good conductors, but may be modeled as either very poor conductors, or even as poor dielectrics.

3.5.1 Maxwell-Wagner Effect

In a normal, conducting sphere the free electrons will respond very rapidly to an applied external field and migrate to the surface; the resulting surface charges shield the inside of the sphere from any electric field. The time required for the charge density, $\mathbf{J} = \sigma \mathbf{E}_2$, inside the sphere to decay to a value of $1/\mathrm{e}$ of its original value is know as the *relaxation time constant*,

$$\tau = \frac{\varepsilon'}{\sigma}. \tag{3.20}$$

For bulk platinum with a dielectric constant, ε', equal to the free space value, $8.854 \cdot 10^{-12}$ F/m, and a conductivity of $2.0 \cdot 10^{7}$ S/m, the relaxation time constant is $4.4 \cdot 10^{-19}$ seconds. Since the period of a 2.45 GHz microwave field is $4.082 \cdot 10^{-10}$ seconds, the relaxation time constant is nearly 9 orders of magnitiude smaller than that of the electric field.

Accounting for the size-dependent conductivity discussed in Section 3.5, a 30 nm platinum particle has an effective conductivity of about $4 \cdot 10^{-2}$ S/m. A first-order approximation of the relaxation time constant accounting for this reduced, effective conductivity is now about $2.2 \cdot 10^{-10}$ seconds, much closer to the half-period of the electric field. As the relaxation time constant approaches the half-period of the microwave field, maximum absorption of electric energy occurs. At this resonant condition Maxwell-Wagner absorption peaks are observed [4].

The Maxwell-Wagner effect is dependent upon the material properties, geometry and frequency. To illustrate this effect on a metallic inclusion, a step electric field is applied to a poorly conducting sphere as illustrated in Fig 3.3. Initially, an internal electric field exists inside the sphere, as the free electrons have had no time to migrate in response to the field. This internal electric field is given by

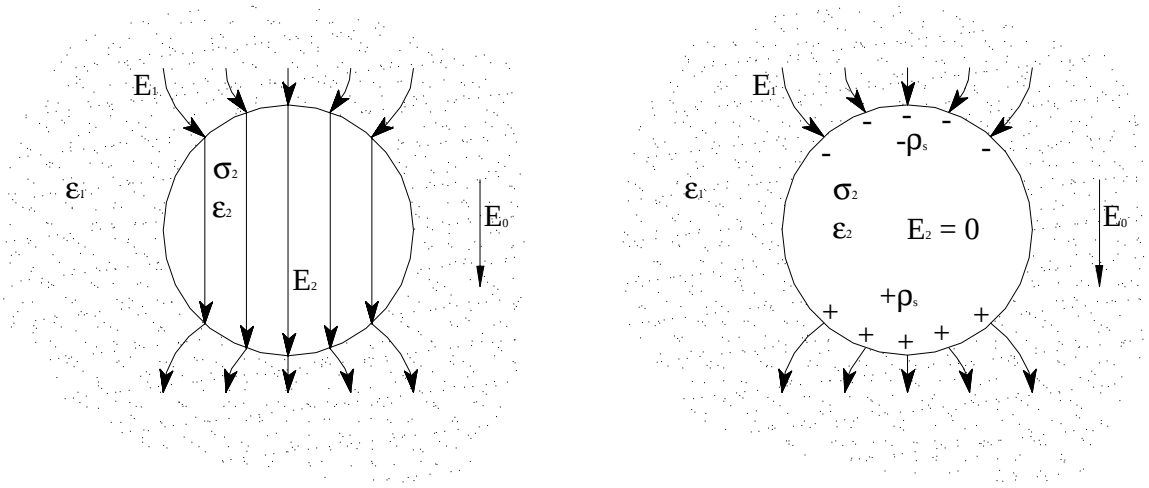

(a) (b)

Figure 3.3 A poorly conducting sphere immersed in an electric field. (a) Initially, no surface charges exist. (b) After a very long time surface charges cancel the external field.

$$\mathbf{E}_2 = \frac{3\varepsilon_1}{2\varepsilon_1 + \varepsilon_2}\mathbf{E}_0, \tag{3.21}$$

where $\mathbf{E}_0$ is the applied, external field. After a sufficiently long time, this internal electric field will decay to a value of zero as surface charges negate the external field, Fig. 3.3(b). If the electron migration is in resonance with the electric field, maximum absorption takes place.

Accounting for this Maxwell-Wagner effect, the power dissipated by this single metallic inclusion can be calculated using the internal electric field and Joule heating, Eq. (3.15). Replacing the step applied field in Eq. (3.21) with a root mean squared a.c. microwave field the heat generation of the particle per unit volume is then

$$\dot{q} = \sigma_{eff} E_{2\,rms}^2, \tag{3.22}$$

where σ_{eff} is the conductivity adjusted for size dependence, Eq.(3.19), and $E_{2\,rms}$ is the average value of the subsequent internal field, Eq.(3.21). By this approach, the heat generated by the metal inclusions is now a function of particle size.

3.6 Electric Field Propagation

As discussed in Sections 3.1, 3.2 and 3.3 an electromagnetic wave will dissipate energy into heat when propagating through lossy media; such dissipation attenuates the amplitude and overall energy of the wave. The overall attenuation and subsequent field distribution are dependent upon the constitutive parameters, σ, ε and μ, as well as the geometries of the wave source and participating media.

An electric field incident upon a medium obeys a conservation of energy such that the incident field is equal to the transmitted field minus the reflected field,

$$\mathbf{E}_i = \mathbf{E}_t - \mathbf{E}_r. \tag{3.23}$$

For an unbounded, uniform plane wave propagating in the x direction with normal incidence on a planar, lossy medium, as shown in Fig. 3.4, the incident wave can be expressed as [15]

$$\mathbf{E}_i = \hat{\mathbf{a}}_z E_0 e^{-\alpha_1 x} e^{-j\beta_1 x}. \tag{3.24}$$

The resulting transmitted and reflected waves are respectively

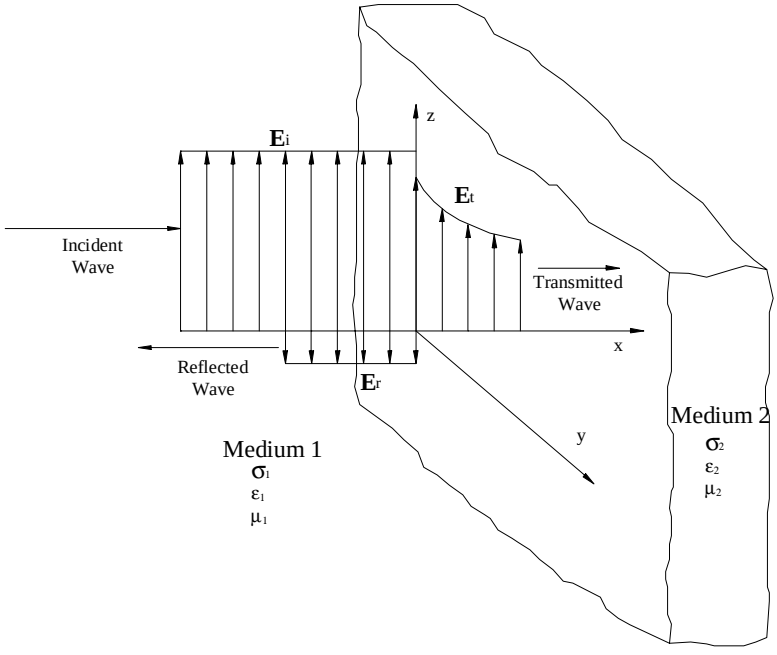

Figure 3.4 A uniform plane wave with normal incidence to a lossy medium.

$$\mathbf{E}_t = \hat{\mathbf{a}}_z T_{12} E_0 e^{-\alpha_2 x} e^{-j\beta_2 x}, \tag{3.25}$$

and

$$\mathbf{E}_r = \hat{\mathbf{a}}_z \Gamma_{12} E_0 e^{+\alpha_1 x} e^{+j\beta_1 x}, \tag{3.26}$$

where T_{12} is the transmission coeffecient, Γ_{12} is the reflection coefficient, α is the attenuation constant, and β is the phase constant; these constants are addressed in the following paragraphs. Eqations (3.23-26) represent unbounded planewaves; however, an electromagnetic wave propagating through a waveguide will take on characteristics related to the geometry of the guide and wavelength of the radiation. These waves will first be discussed in the general forms presented in Eqs. (3.23-26) and later modified to account for the presence of the waveguide and catalyst bed.

The attenuation constant,

$$\alpha = \omega\sqrt{\mu\varepsilon}\left\{\frac{1}{2}\left[\sqrt{1+\left(\frac{\sigma}{\omega\varepsilon}\right)^2}-1\right]\right\}^{1/2}, \tag{3.27}$$

descibes how readily the electromagnetic wave is absorbed into the medium, and the rate at which the field decays.

The phase constant,

$$\beta = \omega\sqrt{\mu\varepsilon}\left\{\frac{1}{2}\left[\sqrt{1+\left(\frac{\sigma}{\omega\varepsilon}\right)^2}+1\right]\right\}^{1/2}, \tag{3.28}$$

accounts for the differences in the speed of light in various materials and subsequent time lag.

The transmission coefficient, T_{12}, is the ratio of the transmitted wave strength to the incident wave strength, and describes the ability of the electric field to propagate between two different media. The transmission coefficient for a wave traveling from medium 1 into medium 2 can be expressed in terms of the intrinsic impedances of the two media,

$$T_{12} = \frac{2\eta_2}{\eta_1+\eta_2} = \frac{\mathbf{E}_t}{\mathbf{E}_i}, \tag{3.29}$$

where the intrinsic impedance of the material, η, is

$$\eta = \sqrt{\frac{j\omega\mu}{\sigma + j\omega\varepsilon}}. \tag{3.30}$$

For free space, the intrinsic impedance is simply the square root of the ratio of μ_0 to ε_0, or 377 Ohms.

Finally, the reflection coefficient, Γ_{12}, quantifies the electric field reflection caused by differences in intrinsic impedance of the materials. The reflection coefficient can either be expressed in terms of the transmission coefficient,

$$\Gamma_{12} = T_{12} - 1, \tag{3.31}$$

or in terms of the intrinsic impedances,

$$\Gamma_{12} = \frac{\eta_2 - \eta_1}{\eta_2 + \eta_1} = \frac{\mathbf{E}_r}{\mathbf{E}_i}, \tag{3.32}$$

where the incident wave is traveling from medium 1 and into medium 2.

3.6.1 Field Transmission

Before the electric field can heat the catalytic bed, the field must first pass through a fused quartz tube in the LANL experiment. Because the constitutive properties of fused quartz and alumina differ, the electric field will behave differently within each medium, leading to reflections which affect the field values.

To quantitatively study the electric field interactions with the catalytic bed it is advantageous to model the ceramic pellets and the free space between the pellets with a single, effective permittivity. The Rayleigh mixture formula could be used to obtain an effective permittivity, but since the formula is derived for isolated spheres, the relationship may no longer be valid for the closely packed pellets within the bed. An alternative approach to calculating an effective permittivity of the bed is to interpolate between free space and a solid bed of alumina based on the volume fraction of alumina, φ, within the bed,

$$\varepsilon_2 = (\varepsilon_{\text{alumina}} - \varepsilon_0)\varphi + \varepsilon_0. \tag{3.33}$$

Using a permittivity for gamma alumina of $\varepsilon_{\text{alumina}} = (4.5 - j0.4)\varepsilon_0$ F/m, and a solid fraction of 0.65, the effective permittivity of the bed is then $\varepsilon_2 = (3.45 - j0.28)\varepsilon_0$ F/m. This mixture of free space and alumina will be designated as medium 2 throughout Sections 3.6.1 and 3.6.2.

The wall of the fused quartz tube surrounding the alumina catalyst bed is only 2 mm thick, and since the intrinsic impedances of the quartz, 265 Ohms, and newly obtained alumina/free space mixture, 202 Ohms, are similar in value, the overall effect of the quartz tube on the electric field may be considered negligible. However, a more formal method of proving this assumption is to look at the reflection coefficients at the various interfaces between the different materials, as follows.

To simplify the geometry of the cylindrical catalyst bed, consider a plane layer of a mixture of alumina and free space, 2 cm in thickness, with layers of fused quartz, 2 mm in thickness on each side, as shown in Fig. 3.5. This planar geometry is not a correct representation of the cylindrical catalyst bed, but is used only for comparative purposes. The reflection coefficient, Γ_{in}, for the geometry shown in Fig. 3.5(a) is approximated by

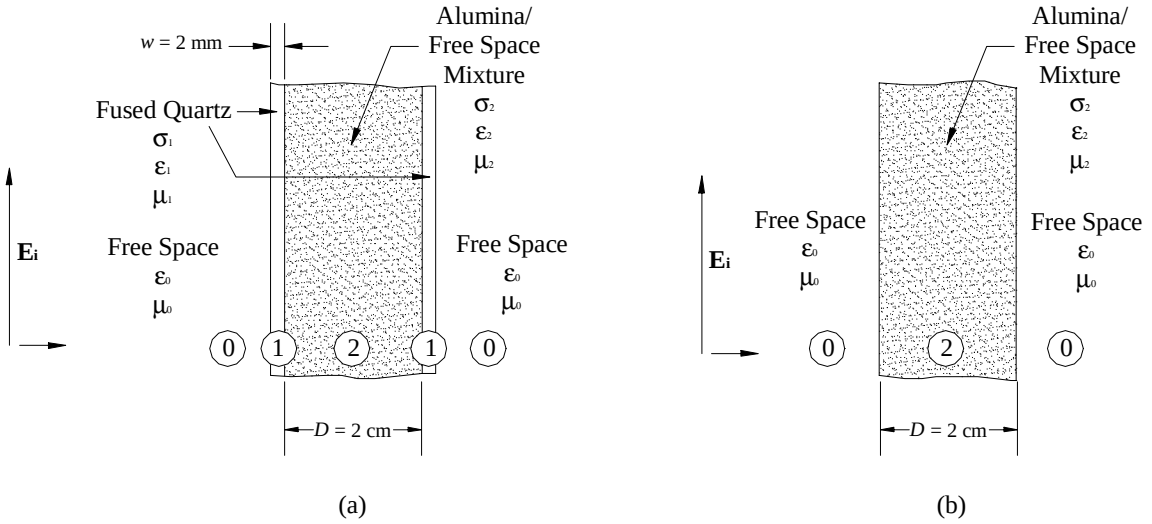

Figure 3.5 (a) A plane comprised of an alumina/free space mixture bound on both sides by a layer of fused quartz , (b) and without the fused quartz cladding.

$$\Gamma_{\text{in}} = \Gamma_{01} + \Gamma_{12} e^{-j2\beta_1 w} + \Gamma_{21} e^{-j2(\beta_1 w + \beta_2 D)} + \Gamma_{10} e^{-j2(\beta_1 w + \beta_2 D + \beta_1 w)}, \tag{3.34}$$

where Γ_{01} is the reflection coefficient from free space into the quartz layer, Γ_{12} is the reflection coefficient from the quartz layer into the alumina/free space mixture, and so on. Using a value of $(3.8 - \text{j}0.0028)\varepsilon_0$ F/m for the permittivity of fused quartz, the magnitude of the right hand side of Eq.(3.34) is 0.482. This reflection coefficient can now be compared to the reflection coefficient obtained by ommiting the two fused quartz layers and considering only an alumina/free space mixture bounded by free space on both sides. The reflection coefficient for this geometry is approximated by

$$\Gamma_{\text{in}} = \Gamma_{02} + \Gamma_{20} e^{-j2\beta_1 D}, \tag{3.35}$$

where Γ_{20} is the reflection coefficient for the alumina/free space mixture back into free space. By neglecting the fused quartz cladding, the magnitude of the right hand side of Eq. (3.35) is 0.535. The reflection coefficients arrived at by Eqs.(3.34) and (3.39) are close enough to justify omitting the fused quartz tube and modelling the catalytic bed solely as a dielectric rod comprised of an alumina/free space mixture.

A first order approximation of the electric field distribution can now be obtained by modeling the bed as a solid dielectric slab, as shown in Fig. 3.5(b). The rate at which the wave decays within the slab goes as the inverse of the attenuation constant, α, of the alumina/free space mixture; this inverse is known as the penetration depth, δ, where $\delta = 1/\alpha$. For a semi-infinite alumina/free space slab, the penetration depth is about 26 cm, by which point the electric field decays exponentially to $1/\text{e}$ of the original field value. This implies that over the 2 cm thickness of the catalyst bed the field will attenuate very little. However, since the catalyst bed is in fact cylindrical, this is only a first order approximation. The geometry of the problem gives rise to electric field reflections internal to the cylinder, as well as field concentrations, which will be looked at in closer detail in the next section.

3.6.2 Field Distributions

The microwave field is directed across the catalytic bed through a copper waveguide, where the electric field is no longer a uniform plane wave, so the plane wave analysis in Section 3.6.1 is not entirely valid. Instead, the wave propagating through the waveguide in the *x* direction is the sum of two plane waves and will have a sinusoidal form across the width, or *y* direction, of the guide. In the proposed experiments, the WR-284 waveguide is operating in the TE_{10}, *transverse electric*, mode with one electric field maximum in the plane parallel to propagation. The electric field strength of a wave propagating in the *x* direction in the TE_{10} mode is represented by

$$\mathbf{E}_i = \hat{\mathbf{a}}_z E_0 \sin\left(\frac{\pi y}{a}\right) e^{-j\beta_0 x}, \tag{3.36}$$

where β_0 is the phase constant for the air inside the cavity, considered free space, and *a* is the width of the waveguide. There is no attenuation constant associated with this equation since there is no dielectric loss associated with the gas in the waveguide. Accounting for geometry, this applied electric field will interact differently with the catalyst bed depending on the orientation, or *polarization*, of the bed with respect to the

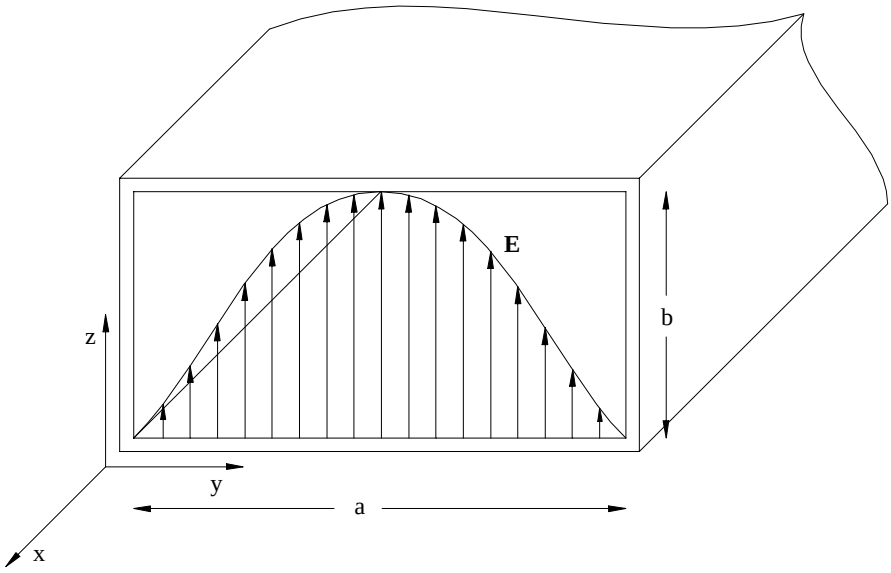

Figure 3.6 A waveguide operating in the TE_{10} mode with an electric field propagating in the *x* direction.

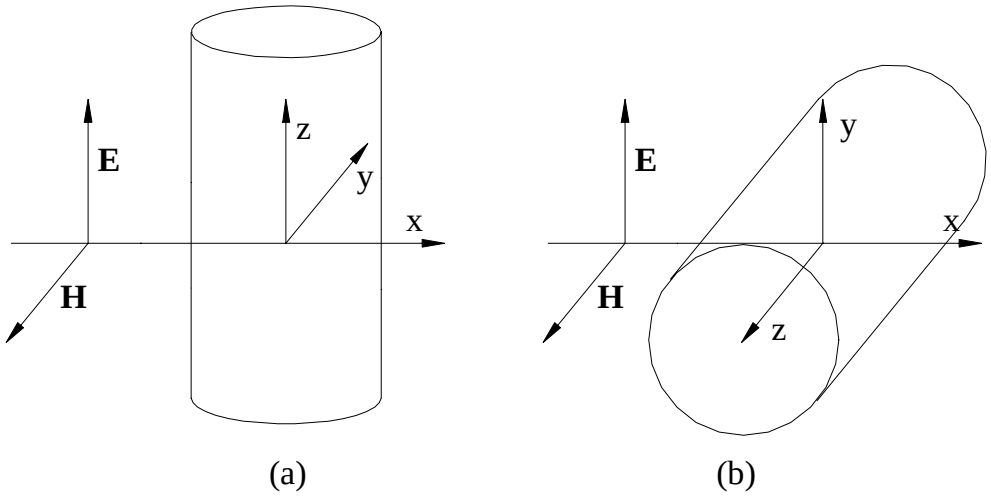

Figure 3.7 A dielectric rod oriented (a) parallel to the electric field and perpendicular to the direction of propagation, and (b) perpendicular to both the electric field and direction of propagation.

field. The two different bed polarizations considered in this study are: first, parallel to the electric field vector and perpendicular to the direction of propagation; second, perpendicular to both the electric field vector and direction of propagation, shown in Fig. 3.7.

The first configuration modeled is that of the catalyst bed as a solid dielectric cylinder comprised of free space and alumina with the axis of the cylinder oriented parallel to the electric field and perpendicular to the direction of propagation, as shown in Fig. 3.7(a) and Fig. 3.8. A cylinder with a ratio of radius to microwave wavelength between 0.1 and 2 falls into the Mie scattering range, where internal reflections within the cylinder produce interference patterns in the electric field; this radius to wavelength region is also known as the *resonance region*. However, the radius to wavelength ratio for the catalytic bed is 0.08, placing it within the Rayleigh scattering range, where the internal interference is minimal. Nevertheless, a solution to a dielectric rod in the Mie scattering range is still applicable for geometries falling in the Rayleigh range, since the resonance terms will be negligible. For the incident wave in Eq. (3.36), Roussy [4] determines the field internal to a dielectric cylinder in the Mie scattering range to be

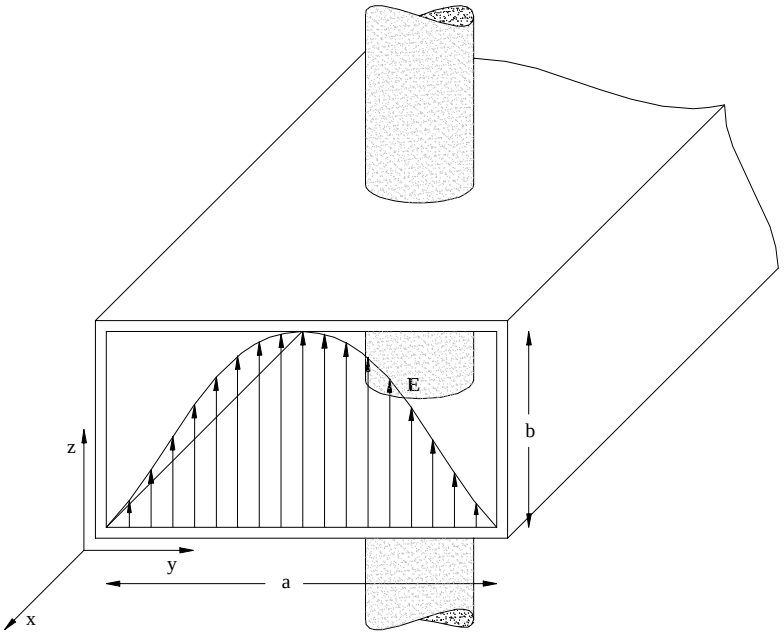

Figure 3.8 Catalyst bed oriented parallel to the electric field and perpendicular to the direction of propagation.

$$\mathbf{E}_t = E_0 \sum_{n=-\infty}^{\infty} j^{-n} c_n J_n(\beta_2 r) e^{jn\varphi} \sin\left(\frac{\pi x}{a}\right) \hat{\mathbf{a}}_z, \tag{3.37}$$

where

$$c_n = \frac{J_n(\beta_0 D/2) + a_n H_n^{(2)}(\beta_0 D/2)}{J_n(\beta_2 D/2)}, \tag{3.37a}$$

and

$$a_n = \frac{-J_n(\beta_0 D/2)}{H_n^{(2)}(\beta_0 D/2)} \left\{ \frac{\dfrac{\varepsilon_2 J_n'(\beta_2 D/2)}{\varepsilon_0 \beta_2 a J_n(\beta_2 D/2)} - \dfrac{J_n'(\beta_0 D/2)}{\beta_0 a J_n(\beta_0 D/2)}}{\dfrac{\varepsilon_2 J_n'(\beta_2 D/2)}{\varepsilon_0 \beta_2 a J_n(\beta_2 D/2)} - \dfrac{H_n'^{(2)}(\beta_0 D/2)}{\beta_0 a H_n^{(2)}(\beta_0 D/2)}} \right\}. \tag{3.37b}$$

The resulting field distribution across the diameter of the cylinder is slightly concave with a maximum at the axis, as shown in Fig. 3.9. The maximum value of the field strength within the bed is 93% of the external, applied field strength. Using this orientation, the presence of the dielectric rod results in only a slight perturbation in the applied field.

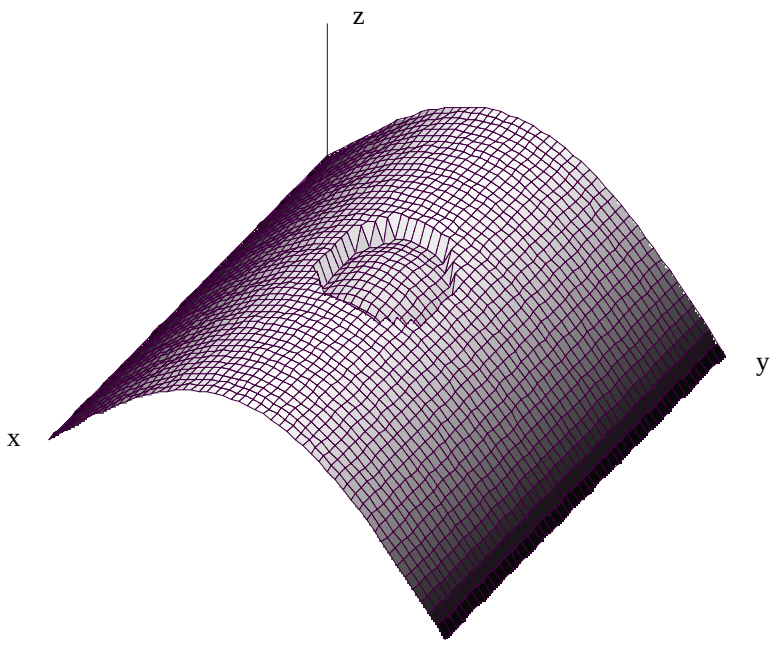

Figure 3.9 Electric field distribution for parallel polarization to the TE_{10} mode. This plot shows the incident and transmitted fields, omitting the reflected field.

Orienting the catalyst bed perpendicular to both the direction of propagation and the electric field, Fig. 3.7(b) and Fig. 3.10, produces a greater change in the electric field pattern, as shown in Fig. 3.11. For an incident plane wave of the form

$$\mathbf{E}_i = \hat{\mathbf{a}}_y E_0 \sin\left(\frac{\pi z}{a}\right) e^{-j\beta_0 x}, \tag{3.38}$$

the resulting internal field is constant and parallel to the applied field, and is quantified by the relationship [4]

$$\mathbf{E}_t = -E_0 \frac{2\varepsilon_0}{\varepsilon_0 + \varepsilon_2} \sin\left(\frac{\pi z}{a}\right) \hat{\mathbf{a}}_y. \tag{3.39}$$

This geometry produces a field strength inside the cylinder only 44% the value of the applied electric field strength, as well as varying sinusoidally across the length of the bed. This transmitted field is only an approximation of the actual field, though the actual field should exhibit the same characteristics.

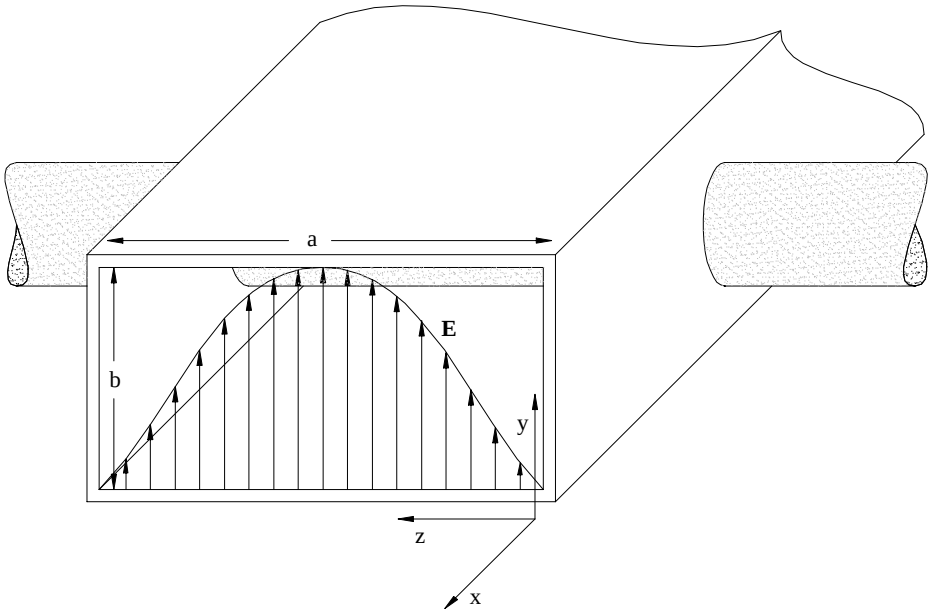

Figure 3.10 Catalyst bed oriented perpendicular to both the electric field and direction of propagation.

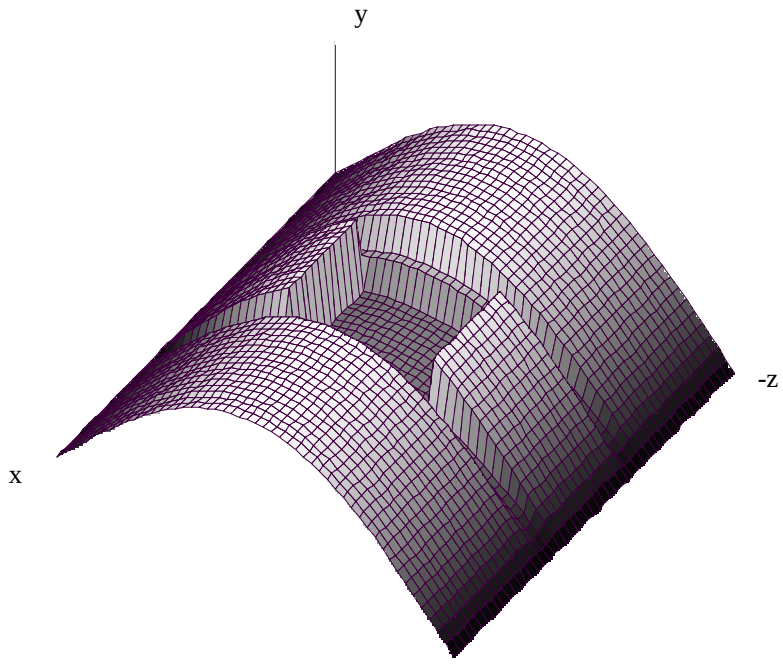

Figure 3.11 Electric field distribution for perpendicular polarization to the TE_{10} mode. This plot shows the incident and transmitted fields, omitting the reflected field.

CHAPTER 4

HEAT TRANSFER MODEL

4.1 Model Overview

A numerical heat transfer model will now be developed for the proposed packed catalyst bed. In addition to the packed bed, the model will also be extended to approximate a fluidized bed as well.

To model the packed and fluidized beds, a model of a single catalyst pellet will first be developed. This single pellet model will then be used to represent a sequence of points along the axis of the beds. The thermal effects within the packed and fluidized catalyst beds can then be studied by varying such parameters as the electric field, catalyst pellet composition, and gas flow rate.

A one dimensional finite-difference formulation will be used in modeling the single catalyst pellet, where heat conduction to neighboring pellets will be ignored. Furthermore, the shape of the catalyst pellet will be approximated as spherical. Using these two assumptions reduces the pellet model to that of an isolated sphere in cross-flow, where the total surface area of the sphere is exposed to convection. The convection boundary condition and catalyst pellet arrangement will then be adjusted to account for either the packed or fluidized bed case.

The electric field constitutes one of the most sensitive parameters in the heat transfer model since the heat generation is a function of the electric field squared; for this reason, variations in the electric field distribution are accounted for when applicable. The electric field within the individual catalyst pellets is assumed constant since the pellet diameter is small compared to the microwave wavelength. However, the electric field

distributions along the axis of the catalyst bed will account for a varying electric field due to polarization of the bed following the approximations made in Sections 3.6.1 and 3.6.2.

Furthermore, the thermal and electromagnetic properties of the materials within the bed will account for temperature dependence.

4.2 Finite-difference Formulation of a Single Catalyst Pellet

Since conduction to other pellets has been neglected, the geometry allows the pellet to be reduced to one dimension, along the radius of the pellet. To model this numerically, a finite-difference approach is employed. For this approach, the pellet can be characterized by three different nodal equations: a general, interior node, the center node, and the surface node exposed to convection, as shown in Fig. 4.1.

For the general, interior node within the pellet, the conduction equation for $T(r,t)$,

$$\rho C \frac{\partial T}{\partial t} = \frac{1}{r^2}\frac{\partial}{\partial r}\left(kr^2 \frac{\partial T}{\partial r} \right) + \dot{q}(r,t), \tag{4.1}$$

will be represented in finite-difference form. The specific heat, C, thermal conductivity, k, and heat generation, $\dot{q}$, are temperature dependent and will vary with the temperature along the radial direction. Because the thermal and electromagnetic properties are functions of temperature, and consequently functions of the pellet radius, the finite-

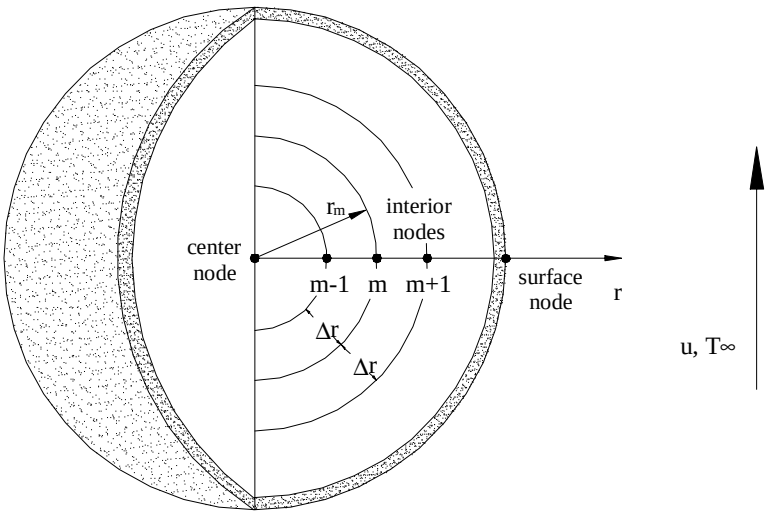

Figure 4.1. Cross-section of the alumina catalyst pellet.

difference equations are derived by the volume integration over a finite-difference node. Multiplying by r^2 and integrating both sides of the equation from $r_{m-\Delta r/2}$ to $r_{m+\Delta r/2}$ gives

$$\rho C \frac{\partial T}{\partial t} \int_{r_{m-\Delta r/2}}^{r_{m+\Delta r/2}} r^2 dr = \int_{r_{m-\Delta r/2}}^{r_{m+\Delta r/2}} \frac{\partial}{\partial r}\left(k r^2 \frac{\partial T}{\partial r} \right) dr + \int_{r_{m-\Delta r/2}}^{r_{m+\Delta r/2}} r^2 \dot{q}(r,t) dr. \tag{4.2}$$

Since the specific heat is not as strong a function of temperature as the thermal conductivity, it is assumed constant with respect to *r*, and brought outside of the integral. Evaluating the integrals in Eq. (4.2), and representing the derivative in finite-difference form using the fully-implicit method gives

$$\rho C\left(\frac{T_m^{p+1} - T_m^{p}}{\Delta t} \right)\left(\frac{r_{m^+}^{\ 3} - r_{m^-}^{\ 3}}{3} \right) = k_{m^+} r_{m^+}^{\ 2}\left(\frac{T_{m+1}^{p+1} - T_m^{p+1}}{\Delta r} \right) - k_{m^-} r_{m^-}^{\ 2}\left(\frac{T_m^{p+1} - T_{m-1}^{p+1}}{\Delta r} \right) + \dot{q}_m \left(\frac{r_{m^+}^{\ 3} - r_{m^-}^{\ 3}}{3} \right), \tag{4.3}$$

where T_m^p and T_m^{p+1} indicate temperatures for an arbitrary node, *m*, at times t^p and t^{p+1}, respectively, and

$$C_m = C\big|_{T_m^{p+1}}, \tag{4.4}$$

$$k_{m^+} = \frac{k\big|_{T_{m+1}^{p+1}} + k\big|_{T_m^{p+1}}}{2}, \tag{4.5}$$

$$k_{m^-} = \frac{k\big|_{T_{m-1}^{p+1}} + k\big|_{T_m^{p+1}}}{2}, \tag{4.6}$$

$$r_{m^+} = r_m + \frac{\Delta r}{2}, \tag{4.7}$$

and,

$$r_{m^-} = r_m - \frac{\Delta r}{2}. \tag{4.8}$$

Equation (4.3) can be rearranged and solved for T_m^p plus a known quantity, yielding

$$T_m^p + \frac{\Delta t}{\rho C_m}\dot{q}_m =$$

$$-\left(\frac{3\Delta t}{\rho C_m \Delta r}\frac{k_{m^-} r_{m^-}^{\ 2}}{r_{m^+}^{\ 3} - r_{m^-}^{\ 3}}\right) T_{m-1}^{p+1} + \left(1 + \frac{3\Delta t}{\rho C_m \Delta r}\frac{k_{m^-} r_{m^-}^{\ 2} + k_{m^+} r_{m^+}^{\ 2}}{r_{m^+}^{\ 3} - r_{m^-}^{\ 3}}\right) T_m^{p+1} \tag{4.9}$$

$$-\left(\frac{3\Delta t}{\rho C_m \Delta r}\frac{k_{m^+} r_{m^+}^{\ 2}}{r_{m^+}^{\ 3} - r_{m^-}^{\ 3}}\right) T_{m+1}^{P+1}.$$

This resulting equation is valid for any general , interior node within the pellet, $0 < r_m < R$.

At the center node, where $r_m = 0$, the temperature profile is axisymmetric, and

$$\left.\frac{\partial T}{\partial r}\right|_{r=0} = 0.$$

thus, the temperatures on either side of the node are equal. Since the temperatures on either side of the node are equal to each other,

$$T_{m-1}^{p+1} = T_{m+1}^{p+1},$$

and likewise,

$$k_{m^-} = k_{m^+},$$

Eq. (4.9) simplifies to

$$T_m^p + \frac{\Delta t}{\rho C_m}\dot{q}_m = T_m^{p+1} - 6\left(\frac{\Delta t}{\rho C_m \Delta r^2} k_{m^+}\right) T_{m+1}^{p+1}, \tag{4.10}$$

at $r_m = 0$. This simplified form of Eq. (4.9) will be used to represent the center node.

The conduction through the surface of the pellet is equal to the convection at the surface,

$$-k\left.\frac{\partial T}{\partial r}\right|_{r=R} = -h\left(T\big|_{r=R} - T_\infty\right). \tag{4.11}$$

However, this boundary condition cannot be directly represented in finite-difference form, since such formulation requires a volume element and Eq. (4.11) applies at a point. Instead, a First Law energy balance will be used to obtain the nodal equation for the surface of the pellet. This energy balance gives

$$\dot{E}_{in} - \dot{E}_{out} + \dot{E}_{gen} = \dot{E}_{st}, \tag{4.12}$$

where

$$\dot{E}_{in} = -kA\frac{\partial T}{\partial r}, \tag{4.13}$$

$$\dot{E}_{out} = hA(T - T_g), \tag{4.14}$$

$$\dot{E}_{gen} = \dot{q}V, \tag{4.15}$$

and

$$\dot{E}_{st} = \rho CV\frac{\partial T}{\partial t}. \tag{4.16}$$

Representing Eq. (4.12) in a finite-difference form consistent with Eqs. (4.9) and (4.10) yields

$$\begin{aligned} &-4\pi r_{m^-}{}^2 k_{m^-}\frac{T_m^{p+1} - T_{m-1}^{P+1}}{\Delta r} - 4\pi r_m{}^2 h\left(T_m^{p+1} - T_\infty\right) + \frac{4}{3}\pi\left(r_m{}^3 - r_{m^-}{}^3\right)\dot{q}_m \\ &\qquad = \frac{4}{3}\pi\rho C_m\left(r_m{}^3 - r_{m^-}{}^3\right)\frac{T_m^{p+1} - T_m^p}{\Delta t}, \end{aligned} \tag{4.17}$$

where h is the convection coefficient, to be discussed in section 4.4. Solving for T_m^p plus known quantities involving $\dot{q}$ and h, in a similar manner to Eqs. (4.9) and (4.10), gives

$$\begin{aligned} &T_m^p + \frac{\Delta t}{\rho C_m}\dot{q}_m + 3h\frac{\Delta t}{\rho C_m}\frac{r_m{}^2}{r_m{}^3 - r_{m^-}{}^3} = \\ &-\left(3\frac{\Delta t}{\rho C_m \Delta r}\frac{k_{m^-} r_{m^-}{}^2}{r_m{}^3 - r_{m^-}{}^3}\right)T_{m-1}^{p+1} + \left(1 + 3\frac{\Delta t}{\rho C_m \Delta r}\frac{k_{m^-} r_{m^-}{}^2}{r_m{}^3 - r_{m^-}{}^3} + 3h\frac{\Delta t}{\rho C_m}\frac{r_m{}^2}{r_m{}^3 - r_{m^-}{}^3}\right)T_m^{p+1}. \end{aligned} \tag{4.18}$$

Equations (4.9), (4.10) and (4.18) constitute a system of algebraic equations which can be written in matrix notation as

$$\underline{\underline{A}} \cdot \underline{T} = \underline{B} \tag{4.19}$$

or

$$\begin{bmatrix} A_{11} & A_{12} & 0 & \dots & 0 \\ A_{21} & A_{22} & A_{23} & 0 & \vdots \\ 0 & \ddots & \ddots & \ddots & 0 \\ \vdots & 0 & A_{m-1,m-2} & A_{m-1,m-1} & A_{m-1,m} \\ 0 & \dots & 0 & A_{m,m-1} & A_{m,m} \end{bmatrix} \cdot \begin{bmatrix} T_1 \\ T_2 \\ \vdots \\ T_{m-1} \\ T_m \end{bmatrix} = \begin{bmatrix} B_1 \\ B_2 \\ \vdots \\ B_{m-1} \\ B_m \end{bmatrix}. \tag{4.20}$$

The diagonal and off-diagonal terms in $\underline{\underline{A}}$ are the coefficients of the T_{m-1}^{p+1},T_m^{P+1} and T_{m+1}^{p+1} terms in Eqs. (4.9), (4.10) and (4.18), and the $\underline{T}$ vector contains those unknown temperatures at time p+1. The $\underline{B}$ vector contains the known constants in Eqs. (4.9), (4.10) and (4.18), temperatures at the current time step, convection and heat generation terms.

The unknown temperatures at time t^{p+1}, $\underline{T}$, can be solved for by matrix inversion,

$$\underline{T} = \underline{\underline{A}}^{-1} \cdot \underline{B}. \tag{4.21}$$

Since the coefficient matrix, $\underline{\underline{A}}$, is tridiagonal, the Thomas Algorithm [16], listed in the appendix on page 97, will be used to solve for the unknown temperature vector. However, with the use of temperature-dependent thermal conductivity and specific heat capacity, these nodal equations are nonlinear with respect to temperature, since $\underline{\underline{A}}$ is a function of $\underline{T}$. To obtain an accurate temperature distribution, the coefficients in $\underline{\underline{A}}$ must be reevaluated at the newly obtained nodal temperatures, then Eq. (4.21) must then be recalculated to solve for a new temperature distribution; this iterative process must be repeated until there is little or no change in subsequent calculations of $\underline{T}$.

With the appropriate convection coefficients, this finite-difference solution may be used to model the temperature distribution within a single pellet in cross flow, or extrapolated to model the temperature distributions of the pellets and gas along the axis of the catalyst bed, as shown in Section 4.5.

4.3 Heat Generation

The heat generated from the microwave field interactions with the alumina and platinum will be the only heat source considered in this study, neglecting any heat gain from exothermic chemical reactions. Since the catalytic bed has constitutive properties

differing from those of free space, the very presence of the bed will affect the distribution of the microwave field, as discussed in Section 3.6, giving rise to regions of higher or lower field strength within the bed. In addition, the constitutive properties of the materials also vary with temperature, so any temperature gradient within the bed will further alter the field distribution.

For this study, the electric field distribution in the waveguide and across the catalyst bed will be assumed independent of temperature. Using this assumption, the electric field distributions developed in Section 3.6 are used in calculating the local heat generation.

Orienting the catalyst bed parallel to the electric field, as shown in Figures 3.8 and 3.9, only a slight perturbation is observed, where the internal field is slightly peaked at the axis of the bed with an electric field strength nearly that of the external field. Since this particular field distribution does not vary along the axis of the bed, and the electric field perturbation is so slight, the internal electric field heating the bed is considered constant with the same strength as the external field, $E_{rms} = E_{0rms}$.

With the catalyst bed oriented perpendicular to the electric field, as shown in Figures 3.10 and 3.11, a greater disturbance of the electric field is observed. The internal field distribution produced by this polarization is constant along the diameter of the bed, but varies along the axis of the bed sinusoidally with the applied external field. The expression

$$E_{rms} = C_3 \cdot E_{0\,rms} \sin\left[\frac{\pi}{a}\left(\frac{a-H}{2} + z\right)\right] \tag{4.22}$$

accounts for the field distribution along the axis of the bed (in the z direction) resulting from the perpendicular polarization, where a is the width of the waveguide, H is the height of the catalyst bed, and C_3 a the constant arrived at in Section 3.6.2, Eq.(3.39), correcting the decrease in wave amplitude inside the catalyst bed, where $C_3 = 0.44$.

As noted in Eq.(4.1), the heat generation is a function of both radius and time. The radial dependence arises from the nonhomogeneity of the catalyst pellet material, as well as the effective permittivity changing with temperature. The time dependence of the heat

generation arises from both the temperature dependence of the dielectric loss and the time variant electric field that may be needed to keep the bed from overheating. At the large electric field strengths needed to promote the desired chemical reactions, the gas flow through the bed may not be sufficient to keep the bed from overheating. To avoid this possibility of overheating, the microwave field will be turned on and off periodically in time; this pulsing will allow the inlet gas flow to cool the bed and keep the bed temperatures within the desired range.

4.3.1 Heat Generation in the Catalyst Support

Ideally, the catalyst support would be comprised of a lossless material; however, the catalyst pellets in the LANL experiments were composed of a porous gamma alumina, approximately one-fifth the density of pure alumina, with various impurities which result in a higher dielectric loss than that of pure alumina. Because of the higher dielectric loss of the gamma alumina, the catalyst support will have the undesirable effect of coupling with the microwave field. Nonetheless, the support is a homogeneous material and the heat generation contribution is given by

$$\dot{q}_m = 2\pi f \varepsilon_0 \varepsilon''_{r\,m} E^2_{rms}, \tag{4.23}$$

where

$$\varepsilon''_{r\,m} = \varepsilon''_r\big|_{T_m^{p+1}}.$$

This expression for the heat generation is valid from the center node out to the radial point where the platinum and alumina mixture begins.

4.3.2 Heat Generation in the Mixture Region

To manufacture the gamma alumina catalyst pellets, the pellets are immersed in a platinum solution to bond the platinum to the support. Since the support is porous, the platinum is absorbed not only on the surface of the pellet, but some depth into the pellet as well; this depth is approximately 70 micrometers. The presence of the platinum can be handled in one of two ways: by using a mixture formula to calculate an effective

permittivity, or accounting for the heat generation as the sum total of the contribution from each individual platinum particle.

4.3.2.1 Mixture Formulae

When using a mixture formula, such as the Rayleigh formula, Eq. (3.16), the heat generation is calculated using Eq. (4.23), where ε_m is the effective permittivity calculated using the mixture formula, discussed in Section 3.4.

4.3.2.2 Heat Generation within a Single Platinum Particle

An alternative approach to calculating the heat generation contributed by the microwave interaction with the metal sites is to consider the sum total of contributions from each individual particle. This is a two-step process: first calculating the heat generation within the platinum particle, and second, determining how the heat is dissipated between the ceramic support and gas.

As shown in Section 3.5.1, the heat generated by an individual metal particle from the electric field is a function of the particle size, and constitutive properties of both the metal and support.

Determining how this heat generation is distributed between the particle, support, and gas depends on several factors: contact conductance with the support, convection coefficient to the gas, and the thermal capacitance of the particle.

Of these three parameters, the most difficult to characterize is the contact conductance between the particle and its support. The work of Steinbruechel and Schmidt [10] implies a value of $5 \cdot 10^6$ W/m^2. Noting that the units of the contact conductance, h_c, differ from the normal units of k, W/m, used in Fourier conduction, the contact conductance coefficient is used in the same manner as the convection coefficient.

Since the diameter of the platinum catalyst is smaller than the mean free path of the helium and butane carrier gas molecules, the normal Nusselt number relationship for a sphere cannot be used to determine the convection coefficient; instead, a convection coefficient is derived from gas kinetic theory. Williams et al. [17] give a coefficient of

$$h = \alpha_{\text{acc}} \frac{P_\infty}{2} \left(\frac{8k_b}{\pi} \frac{T_\infty}{M_b} \right)^{1/2} \frac{1}{T_\infty}, \tag{4.24}$$

where k_b, in this relationship, is Boltzmann's constant, $1.3807 \cdot 10^{-23}$ J/molecule·K. Other parameters involved are the pressure and temperature of the carrier gas, P and T respectively, the molecular weight of the gas, M_b, and the accommodation coefficient, α_{acc}.

The accommodation coefficient is in the range $0 \le \alpha_{acc} \le 1$, and represents the likelihood of a gas molecule coming in contact with the surface to achieve thermal equilibrium with the surface temperature. Most typical engineering surfaces are porous on the microscopic level, thus molecules can easily deflect into surface cavities, and, after several subsequent contacts with the material inside the cavity, achieve thermal equilibrium. For this reason, the accommodation coefficient of most typical engineering materials may usually be approximated as 0.8; however, since the particle in question is a very small isolated sphere, the likelihood of a colliding gas molecule achieving equilibrium with the sphere will be much less than for a large flat surface with many microscopic pores. For this study, the accommodation coefficient will be approximated as 0.1, as inferred from the work of McFall on the accommodation of helium on an amorphous SiO_2 surface [19].

For the 80% helium, 20% butane flow, by volume, discussed in Section 1.4, the average molecular weight is 24.4 AMU, or $4.052 \cdot 10^{-26}$ kg. Using this value of $4.052 \cdot 10^{-26}$ kg for M_b in Eq. (4.24), at a pressure of 101 kPa, and a temperature of 300 K, Eq. (4.24) gives a convection coefficient of approximately 8,500 W/m^2 °C. This convection coefficient is roughly one-half of one percent of the estimated contact conductance, so it is assumed by this analysis that nearly all of the heat generated in the platinum is transferred to the alumina support.

Assuming that all of the heat generated by the platinum is transferred to the support allows this heat generation at the node containing the alumina and platinum mixture to be approximated as

$$\dot{q}_m = (1-\Phi)2\pi f \varepsilon_0 \varepsilon''_{r\,m} E^2 + \Phi \frac{\sigma_{eff\,m} E_2^{\,2}}{2}, \tag{4.25}$$

where Φ is the volume fraction of platinum, and E_2 is the internal electric field within the platinum particle, Eq. (3.21). The resulting Eq. (4.25) individually accounts for the heat generation of both the platinum and the support; in the ideal case of a completely lossless support, the heat generation would be solely from the platinum.

4.4 Convection Coefficients

The model of the catalyst pellet only considers convection at the surface, neglecting any conduction to neighboring pellets. For this study, several differing convection coefficients are considered for comparison. The first coefficient, obtained for an isolated sphere, may be used for a sphere in cross flow, or spheres suspended in a fluidized flow. An additional coefficient is offered for the packed bed model.

4.4.1 Sphere in Cross-Flow

To model the heat transfer of a sphere in cross-flow, Whitaker [20] suggests

$$Nu = 2 + \left(0.4\,Re_d^{\,1/2} + 0.06\,Re_d^{\,2/3}\right) Pr^{0.4} \left(\frac{\mu_\infty}{\mu_w}\right)^{1/4}, \tag{4.26}$$

where

$$Nu = \frac{hd}{k_g}, \tag{4.27}$$

which is valid for $3.5 \le Re_d \le 8 \cdot 10^4$. The gas properties in Eqs. (4.26) and (4.27) are evaluated at the free-stream temperature, except μ_w, which is evaluated at the surface temperature of the pellet.

This correlation may also be used to approximate the convection heat transfer of a bed of suspended fluidized catalyst pellets, assuming the pellets are sufficiently spaced throughout the bed.

4.4.2 Packed Bed Correlation

For the packed bed model, to be developed in Section 4.5, a different convection coefficient from Eq. (4.26) is needed to account for the more complicated flow through a packed bed. Galloway and Sage [21] developed a correlation for flow through a packed bed, which, for a randomly packed bed of spheres reduces to

$$Nu = 2.0 + C_1 \, Re_d^{1/2} \, Pr^{1/3} + C_2 \, Re_d \, Pr^{1/2}, \tag{4.28}$$

where the Reynolds Number is based on the pellet diameter and superficial fluid velocity, and C_1 and C_2 are 1.354 and 0.0326, respectively.

Beasley and Clark [22] found that increasing the coefficients C_1 and C_2 by 50% to values of 2.031 and 0.049, respectively, gives better agreement between numerical modeling and experiment. For the packed bed model presented in this study, these increased values will be used for C_1 and C_2.

4.4.3 Fluidized Bed Correlation

At the minimum fluidization conditions, the pellets in the fluidized bed have only a slightly greater spacing than the packed bed. With the tight packing, catalyst pellets lie in the wakes of other pellets, so the convection coefficient developed for the sphere in cross-flow is inadequate. Zabrodsky [23] suggests that the minimum Nusselt number at the onset of fluidization is a function of the solid fraction of the bed, such that

$$Nu = \frac{2}{1 - \varphi_{mf}^{1/3}}, \tag{4.29}$$

where φ_{mf} is the solid fraction of the bed at the onset of fluidization, to be discussed in Section 4.6.

4.5 Packed Bed Model

The finite-difference model of the single catalyst pellet can now be replicated along the axis of the bed to develop a one-dimensional model of the packed bed. This model

does, however, neglect axial and radial conduction due to contact with neighboring pellets and the cylinder wall.

If the catalyst bed is subdivided into sufficiently small discs, with a height on the order of a pellet diameter, or smaller, as in Fig. 4.2, the temperature across the surface of any catalyst pellets within this thin disc can be assumed constant. With this assumption of constant surface temperature, the mean exiting temperature of the gas may be found through

$$\frac{dT_{mean}}{dz} = \frac{-q_s'' P}{\dot{m} C_p}, \tag{4.30}$$

where the heat flux at the surface of the pellet is represented by

$$q_s'' = h(T_{mean} - T_s), \tag{4.31}$$

and P is the total perimeter of the pellets in the thin disc. Clearly, the perimeter of the pellets will vary throughout the thin disc; however, this discrepancy is resolved when solving for T_{mean}. Solving Eq. (4.30), the mean temperature of the fluid exiting the thin disc is given by

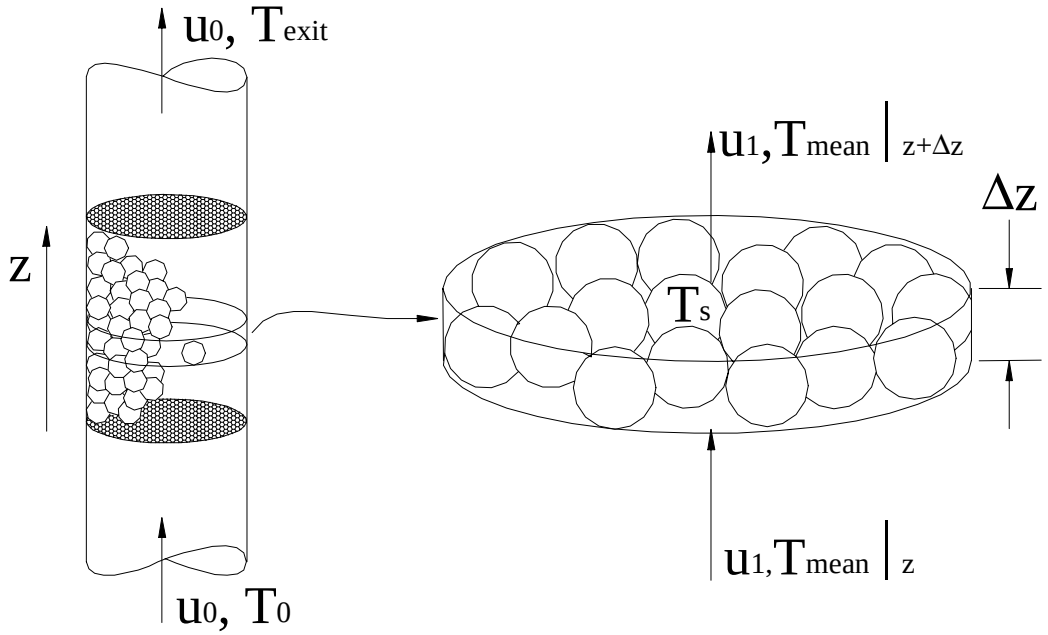

Figure 4.2. Arbitrary horizontal cross-section of the catalyst bed.

$$T_{mean}\big|_{z+\Delta z} = T_s + \left(T_{mean}\big|_z - T_s\right)\cdot e^{-\frac{hP}{\dot{m}C_p}\Delta z}, \tag{4.32}$$

where $T_{mean}\big|_z$ is the mean temperature of the gas entering the disc. The problem of using a characteristic perimeter is avoided by recognizing the quantity $P\Delta z$ as the surface area of the pellets contained within the disc. This solution, though, is only valid for a constant pellet surface temperature, T_s. Since the gas temperature is a boundary condition for the pellet model, the surface temperature of the pellet will change as the mean gas temperature changes. This effect may be accounted for by periodically reevaluating the surface temperature of the pellet at the new gas temperatures as the gas flows through the bed.

The gas will flow around the catalyst pellets with an interstitial velocity of

$$u_1 = \frac{u_0}{1-\varphi}, \tag{4.33}$$

where u_0 is the superficial velocity of the gas entering the bed and φ is the solid fraction of catalyst pellets within the bed. At this rate, the gas will move through the thin disc in a time of

$$\Delta t = \frac{\Delta z}{u_1}. \tag{4.34}$$

If the height of the disc and flow rate are chosen so that the resulting Δt matches the time step of the pellet finite-difference, then for some arbitrary Δz, shown in Fig. 4.3, Eq. (4.32) can be expressed as

$${T_g}_n^{\,p} = {T_s}_{n^-}^{\,p-1} - \left({T_s}_{n^-}^{\,p-1} - {T_g}_{n-1}^{\,p-1}\right)\cdot e^{\frac{-hA_s}{\dot{m}C_p}}, \tag{4.35}$$

where A_s is the exposed surface area of the catalyst pellets within the disc,

$$A_s = \frac{3\pi\varphi(D/2)^2\Delta z}{R}, \tag{4.36}$$

and ${T_s}_{n^-}^{\,p-1}$ is the surface temperature obtained from the pellet finite-difference using the incoming gas temperature, ${T_g}_{n-1}^{\,p-1}$, as the convection boundary condition.

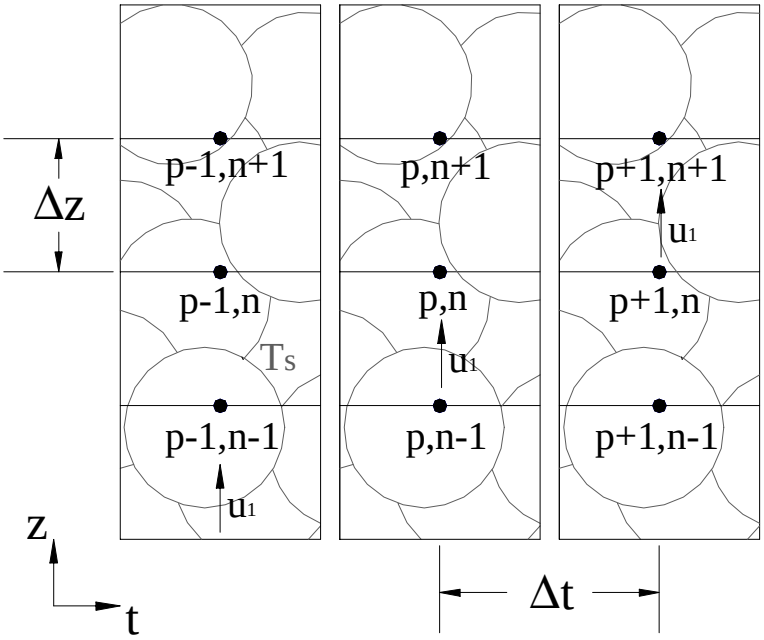

Figure 4.3 Schematic showing axial nodes within the packed bed at various time steps for Eq. (4.38).

Using this solution method, the bed can be divided into N axial sections, obtaining gas temperatures at N+1 nodes, with the first node being the inlet gas temperature, T_0, and a pellet surface temperature between each node. Figure 4.4 outlines the solution technique used by the appended FORTRAN code.

4.6 Fluidized Bed Model

The model developed for the packed bed can be extended to represent a fluidized bed by adjusting such factors as the packing, flow rate and convection coefficient. Equation (4.35),

$$T_{g_n}^{\ p} = T_{s_{n^-}}^{\ p-1} - \left(T_{s_{n^-}}^{\ p-1} - T_{g_{n-1}}^{\ p-1}\right) \cdot e^{\frac{-hA_s}{\dot{m}C_p}},$$

can still be used to represent the heat transfer to the gas in a fluidized bed if the convection coefficient, h, pellet surface area, A_s, and mass flow, $\dot{m}$, are adjusted to account for flow through a fluidized bed.

The solid fraction of catalyst pellets in a fluidized bed at the minimum fluidization velocity is just slightly less than the solid fraction for a normally packed bed [22] and can

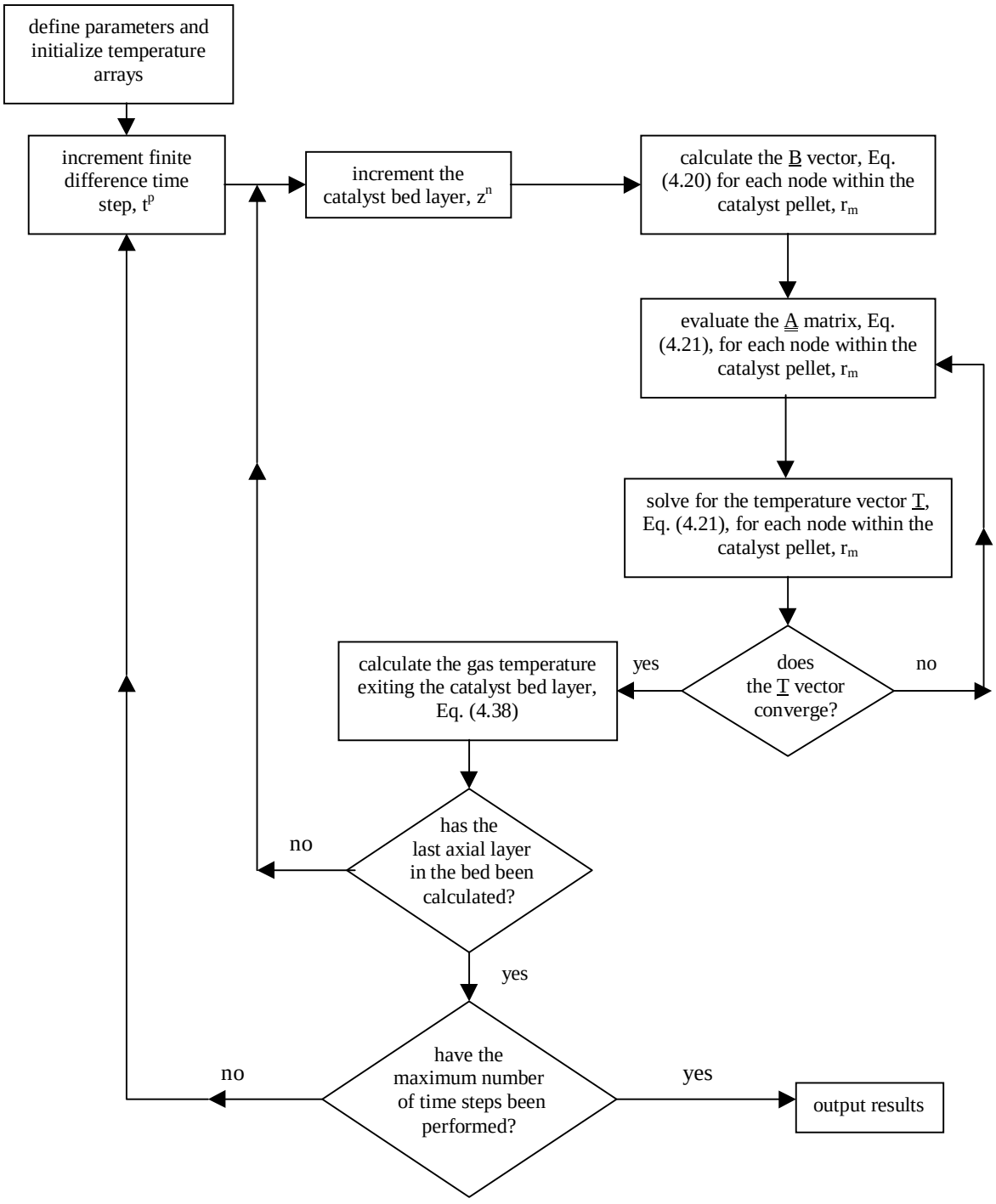

Figure 4.4 Flowchart showing the procedure for modeling both the packed and fluidized beds.

be represented as some fraction of the solid fraction for the packed bed,

$$\varphi_{mf} = 0.9 \cdot \varphi, \tag{4.37}$$

where φ is the solid fraction for the packed bed. Thus, the subsequent surface area of the catalyst pellets exposed to convection is then

$$A_s = \frac{3\pi\varphi_{mf}\left(D/2\right)^2 \Delta z}{R}. \tag{4.38}$$

The convection coefficient for the fluidized case can be represented by the correlation offered by Zabrodsky in Eq. (4.29).

Since the bed is fluidized, there is a minimum flow rate for which the drag on the particle offsets the force of gravity, suspending the pellet in the flow. Kunii and Diazo [22] give this minimum fluidizing velocity entering the bed, u_{mf}, in quadratic form as

$$\frac{1.75}{\left(1-\varphi_{mf}\right)^3}\left(\frac{d \cdot u_{mf}\rho_g}{\mu_g}\right)^2 + \frac{150\varphi_{mf}}{\left(1-\varphi_{mf}\right)^3}\left(\frac{d \cdot u_{mf}\rho_g}{\mu_g}\right) = \frac{d^3\rho_g\left(\rho-\rho_g\right)\cdot g}{{\mu_g}^2}. \tag{4.39}$$

Assuming the pellets are uniformly distributed throughout the bed at this minimum fluidization velocity, the velocity at which the the gas will flow through the bed is then

$$u_1 = \frac{u_{mf}}{1-\varphi_{mf}}. \tag{4.40}$$

At this minimum fluidization velocity, the pressure drop across the length of the catalyst bed is given by Kunii [22] as

$$\Delta p = \varphi_{mf}\left(\rho-\rho_g\right)\frac{g \cdot H}{g_c}. \tag{4.41}$$

For an inlet gas pressure near atmospheric pressure, the pressure drop across the 2.54 cm catalyst bed is less than 0.2% of the inlet pressure. With such a slight pressure drop, any pressure difference due to the fluid mechanics will be neglected in the fluidized model.

Using this formulation, the same solution approach for the packed bed can now be employed to model the fluidized case.

CHAPTER 5

RESULTS

5.1 Selective Heating Hypothesis

A single metallic catalyst particle can be modeled to determine whether the catalyst sites can achieve temperatures substantially higher than the surrounding support environment. A typical platinum particle ranges from 1 to 20 nm in diameter and is partially attached to the alumina support, exposing most of the particle to convection with the gas, as depicted in Fig. 1.3. The small size and high thermal conductivity of the platinum catalyst allows the temperature of the particle, T, to be expressed by the lumped-capacitance model

$$\rho C V \frac{dT}{dt} = \dot{q} V - h_c A_c (T - T_s) - h(A_s - A_c)(T - T_g), \tag{5.1}$$

where the density, ρ, specific heat, C, and volume, V, are those of the platinum particle. The heat generation, $\dot{q}$, is calculated using Eq. (3.22), accounting for size-dependent effects and internal electric fields. The particle losses heat to the alumina support through the contact area, A_c, and contact conductance, h_c, discussed in Section 4.3.2.2. Electron microscopy suggests that 5-10% of the particle surface area, A_s, is in contact with the support. The remainder of the catalyst is exposed to convection and radiation. The convection coefficient, h, is based on the kinetic threory of gases, and calculated with Eq. (4.24). The heat loss through radiation is negligible compared to the convective and conductive losses, and thus disregarded. Assuming the temperatures of the support,

T_s, and gas, T_g, are nearly equal allows the thermal time constant for the system to be expressed as

$$\tau_T = \frac{\rho C V}{h_c A_c + h(A_s - A_c)}. \tag{5.2}$$

Using a value of 10^5 W/m^2°C for the contact conductance and 8,500 W/m^2°C for the convection coefficient, as discussed in Section 4.3.2.2, the time required for particles 1 nm in diameter and larger to decay to a temperature 1/e times the original temperature is greater than the period of the electric field. By this analysis, the catalyst particles will remain at a fairly constant temperature in the presence of a microwave field. At steady-state conditions the particles will have a temperature rise above the support of

$$\Delta T = \frac{\dot{q} V}{h_c A_c + h(A_s - A_c)}. \tag{5.3}$$

An electric field strength as high as 10^6 V/m generates as much as $2 \cdot 10^{12}$ W/m^3 of power within the platinum particle; however, with as little as 5% of the particle surface area in contact with the support, the temperature rise of the platinum catalyst is only fractions of a degree above the support and gas temperature. Following this classical analysis, the catalyst particles cannot achieve temperatures significantly higher than the surrounding support at steady state conditions. This approach may not be entirely valid for nanometer-sized particles, though. Because the catalyst particle sizes considered are on the same order of magnitude as the mean-free-path of the phonon and electron heat carriers, 2 and 11 nm respectively, a more detailed analysis such as that of Steinbruechel and Schmidt [10] may be required.

If the platinum catalyst sites dissipate nearly all of the energy into the alumina support as predicted by the preceding analysis and Section 4.3.2.2, the effect should be noticed as an increased pellet surface temperature above that of bare alumina. Figure 5.1 shows the effect of catalyst particle size on the steady-state temperature rise of an isolated alumina catalyst pellet immersed in a 17 cm/s helium/butane flow at 25°C with an applied electric field strength of $5 \cdot 10^4$ V/m; this flow rate and electric field strength are arbitrarily chosen, but typical of conditions expected in the experiment proposed in

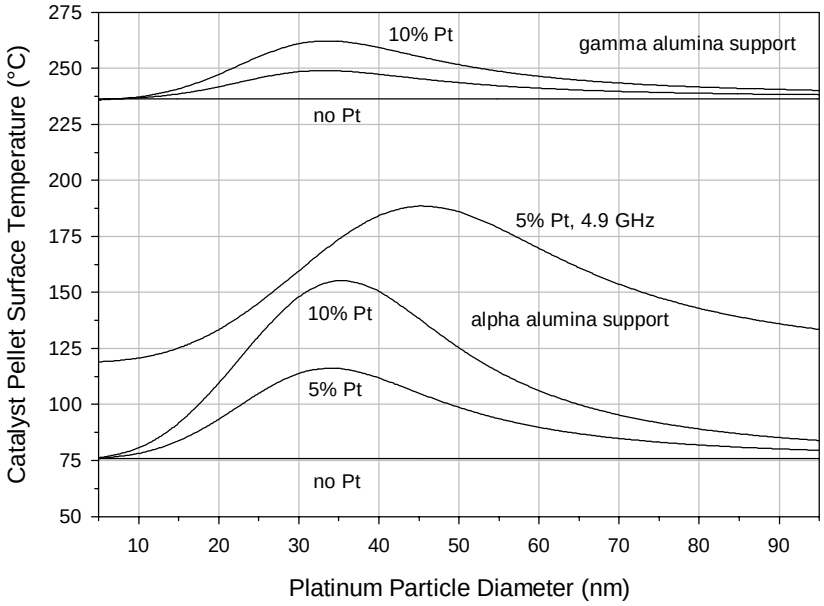

Figure 5.1 Steady state temperatures of alpha and gamma alumina catalyst pellets as a function of mean platinum particle diameter in a 2.45 GHz microwave field, except where noted.

Section 1.3. Two slightly different catalyst support materials are modeled to highlight the influence of the dielectric properties of the support. The gamma alumina, which is the support material in the proposed experiment, has a greater dielectric loss than the alpha alumina for the temperatures of interest, as shown in Fig. 5.3, thus the gamma alumina support reaches a higher overall temperature than the alpha alumina, though the presence of the platinum has a more noticeable effect on the temperature rise with an alpha alumina support.

Figure 5.1 illustrates the Maxwell-Wagner absorption peaks discussed in Section 3.5.1. Since these peaks are a function of the constitutive properties of both the platinum and the support, the temperature peaks of the alpha and gamma alumina pellets, though very similar, are not at the same catalyst particle diameter; the temperature peak for the gamma alumina support is at 33 nm, whereas the peak for the alpha alumina support is at 35 nm. This optimum particle size, and temperature rise, is also affected by the microwave frequency as seen in the case of an alpha alumina pellet with a 0.05 mass fraction of platinum in a 4.9 GHz microwave field, also shown in Fig. 5.1. It should be noted that the dielectric losses of both alpha and gamma alumina are functions of

frequency, though fairly constant over the microwave range; the dielectric properties used in this study are measured at 2.45 GHz.

The Rayleigh mixture formula, Eq, (3.16), was used to model the effective permittivity of the platinum/alumina region for the results presented in Fig. 5.1; however, two additional methods, the Maxwell-Garnet mixture theory [14] and accounting for the heat dissipated by each platinum particle, Eq.(4.25), each give results within 5.0% of those shown in Fig. 5.1.

Figure 5.1 is produced accounting for the size-dependent conductivity and subsequent electric field internal to the nanometer-sized particles. If the bulk value of platinum conductivity is used, $9.25 \cdot 10^6$ S/m, no appreciable temperature rise above that of bare alumina is observed.

5.2 Comparison of Support Materials

The previous section suggests that the maximum temperature rise above a bare alumina support will occur for platinum particles 30-35 nm in diameter, though electron microscopy suggests that the particles are less than 20 nm in diameter. Since these particles are actually smaller than the optimum size predicted by Fig. 5.1, the presence of the platinum catalysts may have very little effect on the temperature rise of the catalyst bed.

To illustrate the effect the platinum catalysts and the different supports have on the exiting gas temperatures of the proposed experiment, a packed bed is modeled using the two different alumina support materials, with and without catalyst particles of differing sizes.

For these cases, the reactor tube is oriented parallel to the electric field, as shown in Fig. 3.8. Because this tube orientation produces only a minor perturbation in the microwave field, the field internal to the bed will be modeled as the same value as the applied field. An applied electric field strength of $5 \cdot 10^4$ V/m is arbitrarily chosen to represent a strength great enough to dissipate significant energy in the catalyst sites, yet not so strong as to exceed the dielectric breakdown of the materials and produce plasma

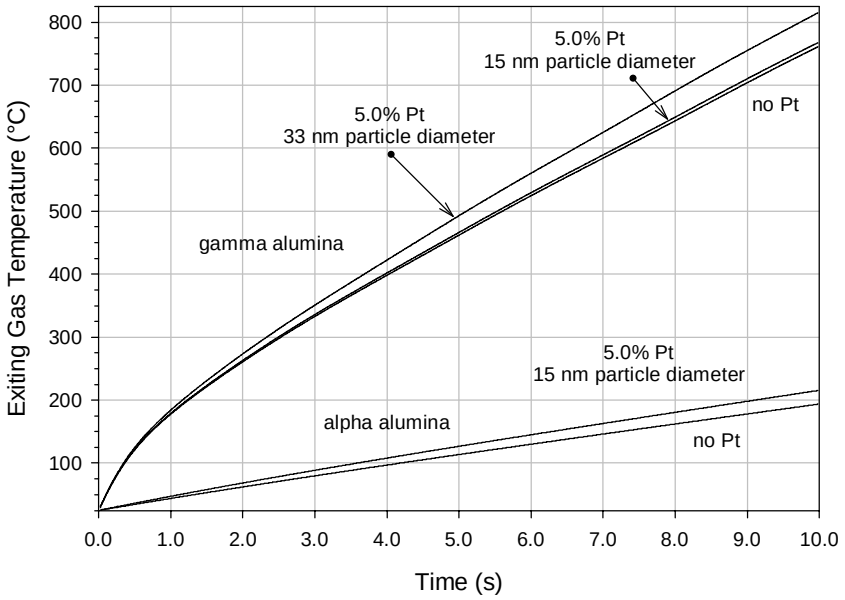

Figure 5.2 Temperature comparison using alpha and gamma alumina catalyst support materials with platinum particles of varying diameters, and without any platinum.

arcing. The inlet gas is comprised of an 80% helium and 20% butane mixture, by volume, at a temperature of 25°C flowing into the bed at a rate of 0.316 L/min, or 0.017 m/s.

First, the gamma alumina support is modeled without any platinum catalysts, and then with a 0.05 mass fraction of platinum catalysts, 15 nm in diameter; note that this mass fraction is ten times greater than the mass fraction of platinum in the proposed experiment. The exiting gas temperatures differ by only 7°C, or 0.9% , for these two cases, as shown in Fig. 5.2. This clearly indicates that the large dielectric loss of the gamma alumina support dominates over any heat dissipated by the platinum catalysts. If the same situation is modeled with platinum catalysts 33 nm in diameter, the heating effects are more pronounced. Figure 5.1 shows that catalysts of this diameter have the greatest heating effect on a single support pellet. Modeling the packed bed with 33 nm diameter catalysts, shown in Fig. 5.2, results in a 54°C, or 6.8%, temperature difference in the exiting gas temperature compared to the results obtained using bare gamma alumina.

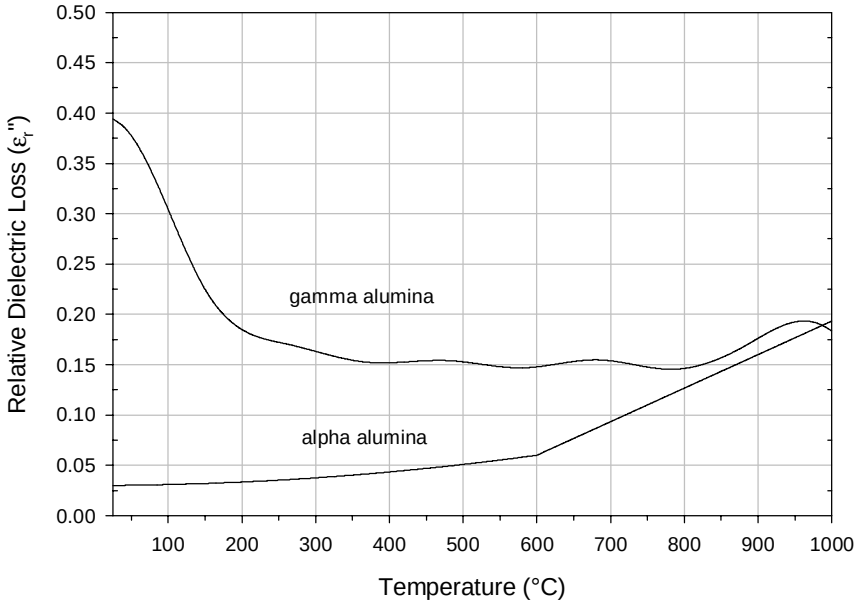

Figure 5.3 Dielectric loss of alpha [30] and gamma [31] alumina.

For comparison, the bed is modeled assuming the catalyst pellets are comprised of alpha alumina without any platinum, and then with a 0.05 mass fraction of platinum. The alpha alumina has a different crystalline form and a subsequently lower dielectric loss than gamma alumina, as shown in Fig. 5.3. Using the alpha alumina has the desirable effect of greatly reducing the overall exiting gas temperatures while maintaining a high internal electric field strength, shown in Fig. 5.2. The presence of the platinum is also more noticeable with the alpha alumina support, resulting in a 25°C, or 11.9%, difference in the exiting gas temperature when the bed is modeled with 15 nm platinum particles compared to the pellets without any platinum.

It should be noted that even though an alpha alumina support results in a lower bed temperature under these conditions, once the temperature of the alumina exceeds 600°C, the dielectric loss begins to increase rapidly with temperature. This could lead to *thermal runaway* and is a limitation of the alpha alumina support material.

5.3 Packed and Fluidized Bed Comparison

Comparing the packed and fluidized beds requires that both models operate with the same parameters. For this study, the gamma alumina catalyst pellets in both the packed

and fluidized beds are assumed to have a 3 mm diameter with a platinum mass fraction of 0.005. Furthermore, the platinum catalysts are assumed to have an average diameter of 15 nm. By assuming a mean particle size, the size-dependent issues discussed in Section 3.5 can be modeled using the Rayleigh mixing formula.

The catalyst bed can be oriented either parallel or perpendicular to the electric field, as discussed in Section 3.6, so both cases will be considered in the following sections. Increasing the strength of the microwave field increases the amount of energy dissipated in the platinum particles, and possibly promoting catalysis; however, such a strong field will rapidly heat the bed well above the temperatures required for catalysis. To allow for sufficiently high field strengths without overheating the catalyst bed, it is desirable to pulse the electric field; this will allow for the bed to cool in the absence of the microwave field. The upper bound for the electric field strength is 10^6 V/m, where the dielectric breakdown of air is encountered, so the applied electric field and any resulting internal fields should remain below this value. With this in consideration, the applied electric field strength, E_0, is arbitrarily chosen to be $5 \cdot 10^4$ V/m rms, or a peak value of $7.07 \cdot 10^4$ V/m.

The gas flowing through the reactor tube consists of an 80% helium, 20% butane mixture based on volume, though the specific flow rate differs for the packed and fluidized cases.

For the packed bed case, the solid fraction, φ, of the alumina pellets is assumed to be 0.65 to represent a randomly packed bed of spheres [21]. Using this solid fraction and the proposed gas flow rate of 0.316 l/min, the gas flows through the bed at an average rate of 0.017 m/s.

For the fluidized bed case, the solid fraction of alumina pellets is reduced slightly to allow pellet suspension at the minimum fluidization velocity. Kunii et al. [23] suggests that at the onset of fluidization the voidage is only slightly greater than that for the packed bed; to account for this increased voidage in the fluidized case, the solid fraction of the packed bed is reduced arbitrarily by ten percent to model the solid fraction of the

fluidized bed, φ_{mf}, such that $\varphi_{mf} = 0.9 \cdot \varphi$, where $\varphi = 0.65$. The inlet gas flowrate is obtained through Eq. (4.40), and for this case is 0.776 m/s, or 14.4 l/min.

5.3.1 Parallel Bed Polarization

With the reactor tube oriented parallel to the electric field and perpendicular to the direction of propagation, the electric field inside the tube differs very little from the external, applied field, and is constant along the axis of the bed, as shown in Section 3.6.2. Since the difference between the applied and internal electric fields is small, the field internal to the catalyst bed is considered to be the same strength as the applied field.

Under the operating conditions described in Section 5.3, and with a continuous electric field, the exiting gas temperature of the packed bed exceeds 750°C within the first ten seconds, as shown in Fig. 5.4 on page 56. If the microwave field is pulsed on for the first one-tenth of each second and off for the remaining nine-tenths, the bed temperature rises to only 177°C after the first ten seconds. At the end of the first ten seconds, the temperature distribution along the axis of the bed reaches a near constant state within the first third of the bed for both the continuous and pulsed fields, as shown in Fig. 5.5.

By fluidizing the bed, the exiting gas temperature reaches a steady state value just over 500°C, as shown in Figures 5.6 and 5.7, even with a continuous electric field strength of $5 \cdot 10^4$ V/m. The pulsed electric field yields an exiting gas temperature near 150°C. The flow rate of 0.776 m/s is sufficiently high for the bed and exiting gas temperature to cool in the absence of the microwave field in the pulsed case.

5.3.2 Perpendicular Bed Polarization

Orienting the reactor tube perpendicular to the electric field and direction of propagation, as shown in Fig. 3.10, produces a very different electric field distribution from the parallel polarization case. The electric field now varies sinusoidally following the relationship given in Eq. (4.22), as well as experiencing a 56% reduction in the peak electric field value, as shown in Fig. 3.11.

The exiting gas temperatures from the packed bed shown in Fig. 5.8 are 70% lower than in the parallel polarization case, though still not achieving steady state conditions. At the end of ten seconds, the temperature distribution along the axis of the bed has a maximum near the 1.5 cm position, shown in Fig. 5.9; this peak originated at the center of the bed where the electric field is strongest and migrates towards the exit of the bed with time.

With this polarization, the fluidized bed experiences a 60% reduction in exiting gas temperatures, shown in Fig 5.10. At the end of ten seconds, Fig. 5.11 shows there is no peak in the temperature distribution along the axis of the bed, as with the packed bed shown in Fig. 5.9. The higher flow rate associated with the fluidization pushes this temperature peak to the end of the bed over the course of 6 seconds, as shown in Fig. 5.12.

A limitation of this model is that it does not account for axial heat conduction through the bed from one pellet to another. Consequently, the axial temperature distributions shown in this section differ considerably between the inlet and exit regions of the bed, since the inlet gas temperature is held at a constant 25°C. This extreme temperature gradient is especially noticeable for the packed bed in a continuous microwave field, shown in Fig. 5.5. With such large temperature gradients along the axis of the bed, heat will conduct from pellet to pellet back towards the entrance of the bed, thus raising the temperature of the pellets near the entrance and lessening the temperature gradient along the axis. In the packed bed, this conduction is limited by the contact area between pellets and subsequent contact conductance; for the fluidized case, the conduction is also function of the agitation between the fluidized pellets. These conduction mechanisms should be accounted for in future work. However, with the reactor operating within the temperature range of interest for the catalysis, below 350°C, this gradient may not introduce a large error in calculating the temperatures in the upper regions of the bed.

Furthermore, the electric field distribution for both the parallel and perpendicular bed polarizations is considered constant with time, when, in fact, the field distribution will change as the dielectric properties of the bed change with temperature. This

limitation should also be accounted for in future work, especially if larger catalyst beds are to be modeled.

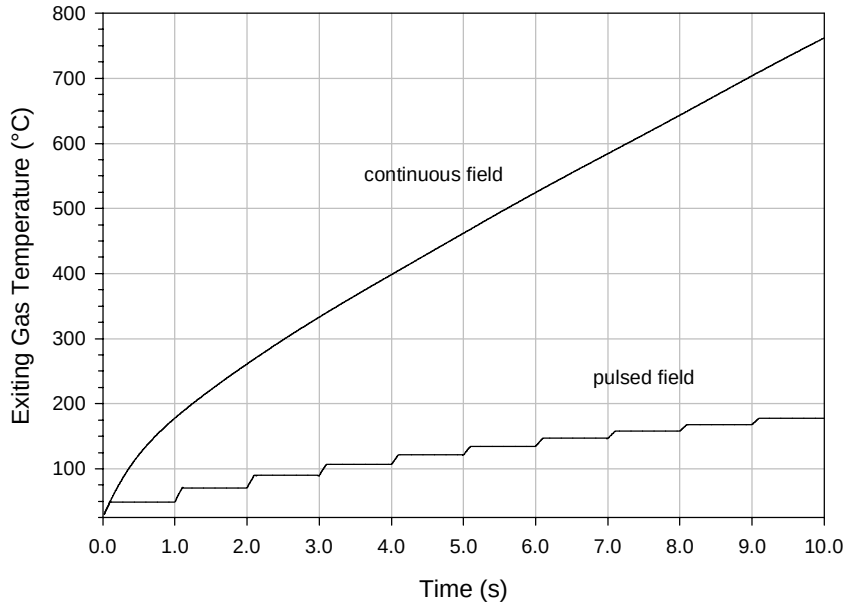

Figure 5.4 Exiting gas temperatures as a function of time for a packed bed oriented parallel to both a continuous and pulsed electric field.

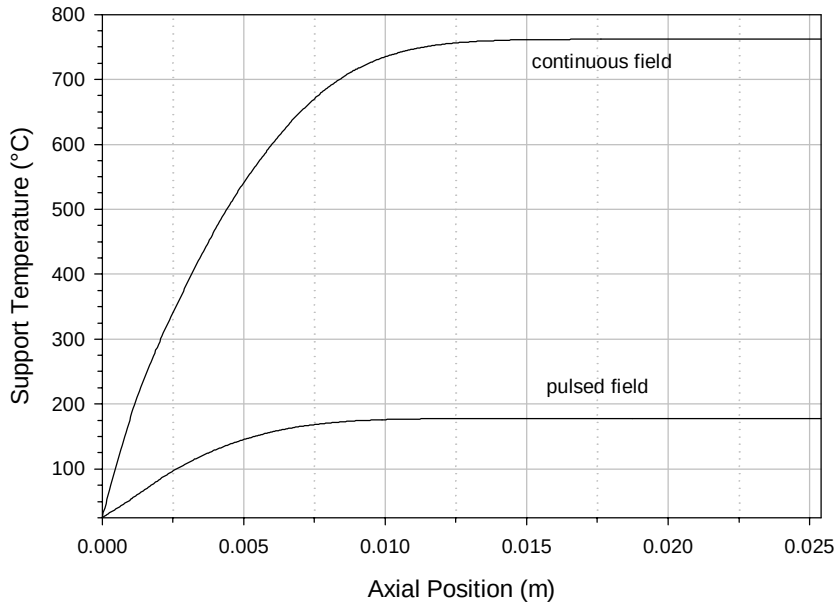

Figure 5.5 Temperature distribution of the solid support in a packed bed oriented parallel to both a continuous and pulsed electric field at the end of ten seconds.

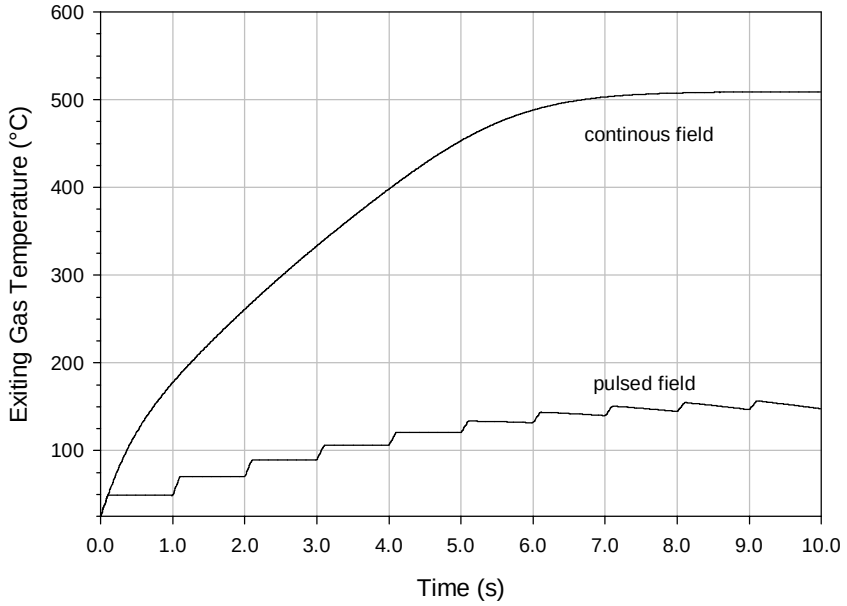

Figure 5.6 Exiting gas temperatures as a function of time for a fluidized bed oriented parallel to both a continuous and pulsed electric field.

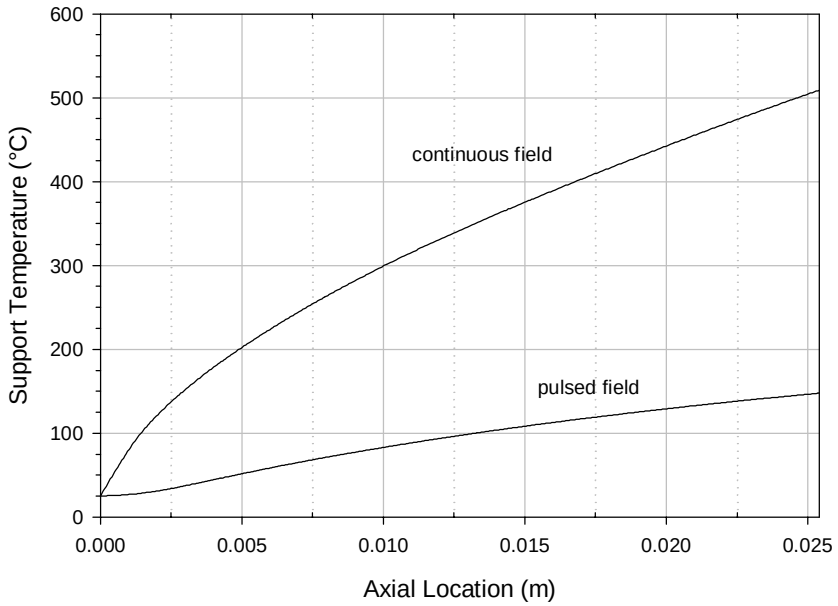

Figure 5.7 Temperature distribution of the solid support in a fluidized bed oriented parallel to both a continuous and pulsed electric field at the end of ten seconds.

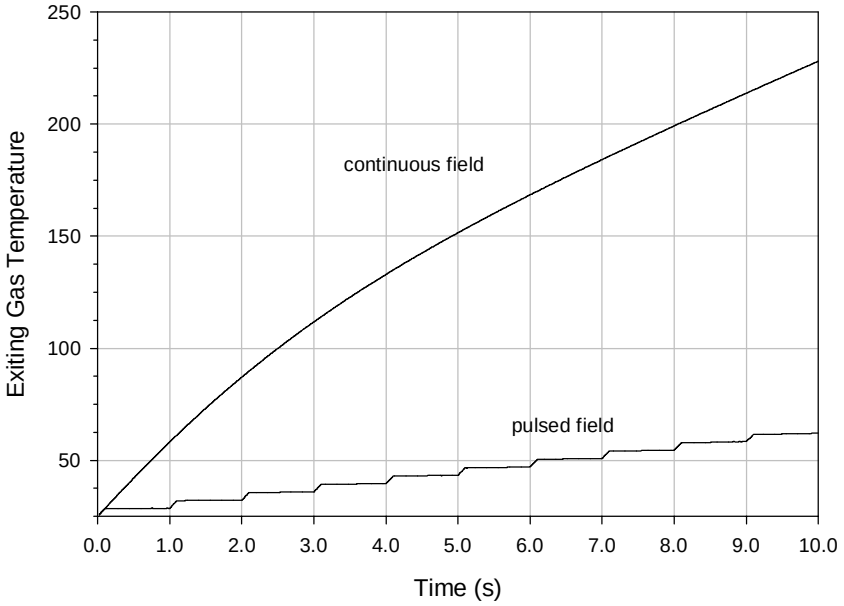

Figure 5.8 Exiting gas temperatures as a function of time for a packed bed oriented perpendicular to both a continuous and pulsed field.

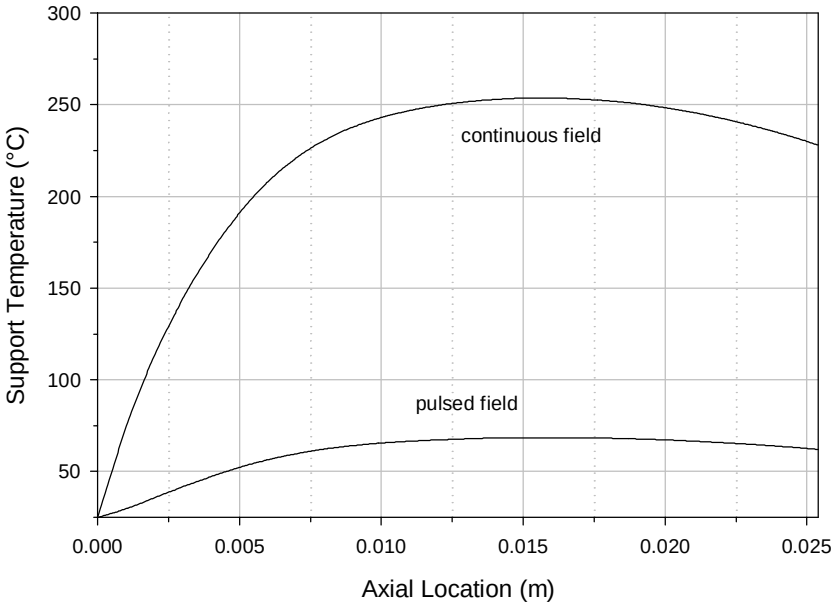

Figure 5.9 Temperature distribution of the solid support in a packed bed oriented perpendicular to both a continuous and pulsed electric field at the end of ten seconds.

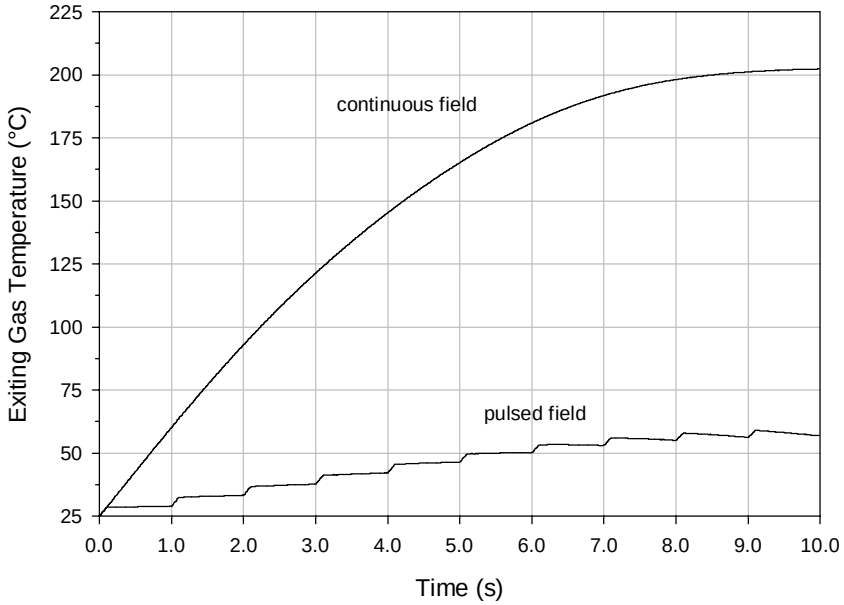

Figure 5.10 Exiting gas temperatures as a function of time for a fluidized bed oriented perpendicular to both a continuous and pulsed electric field.

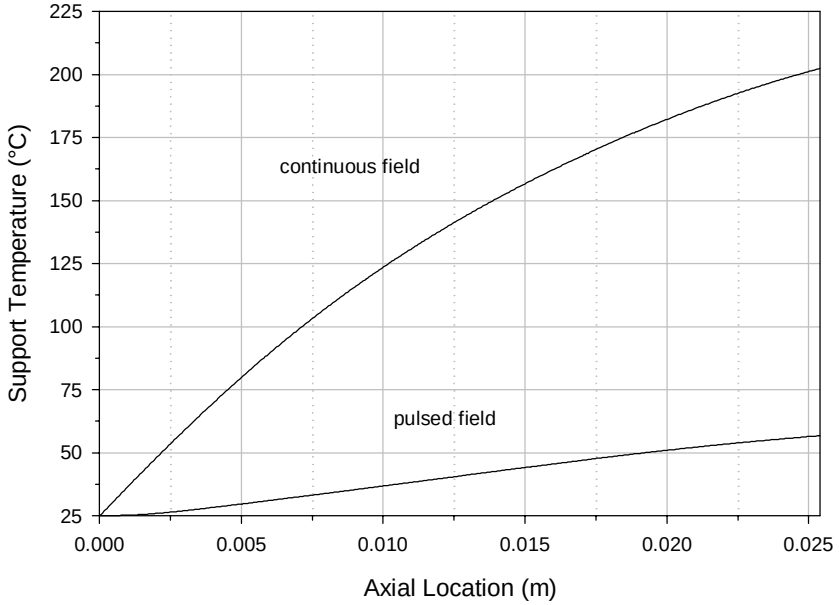

Figure 5.11 Temperature distribution of the solid support in a fluidized bed oriented perpendicular to both a continuous and pulsed electric field at the end of ten seconds.

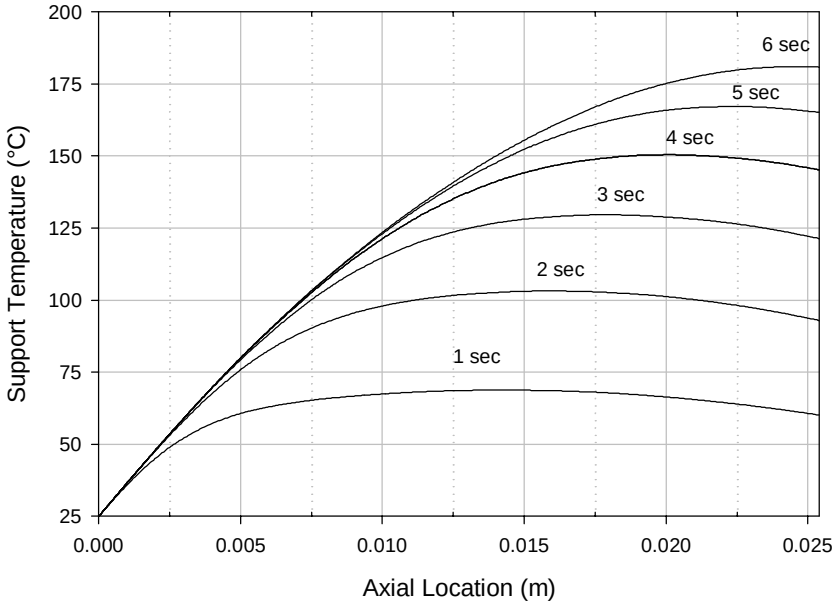

Figure 5.12 Temperature distribution of the solid support in a fluidized bed oriented perpendicular to a continuous field at various points in time.

5.4 Sensitivity Study

The metallic catalyst particles have a surprisingly small contribution to the heating of the beds. The effect of the platinum and other parameters on the temperature rise of the bed may be quantitatively compared by calculating the sensitivity coefficients of the parameters. The sensitivity coefficients are obtained by calculating the change in temperature per unit change of the parameter of interest. For instance, the non-dimensional sensitivity of the model to the conductivity of the platinum inclusions would be calculated as

$$\chi = \sigma \cdot \frac{T\big|_{\sigma+\Delta\sigma} - T\big|_{\sigma}}{\Delta\sigma}, \tag{5.4}$$

where $T\big|_{\sigma+\Delta\sigma}$ is the model temperature calculated at a slightly perturbed value of conductivity, $\sigma + \Delta\sigma$, and $T\big|_{\sigma}$ is the model temperature calculated at the unperturbed value. Using this method, the sensitivity coefficients can be calculated as functions of time.

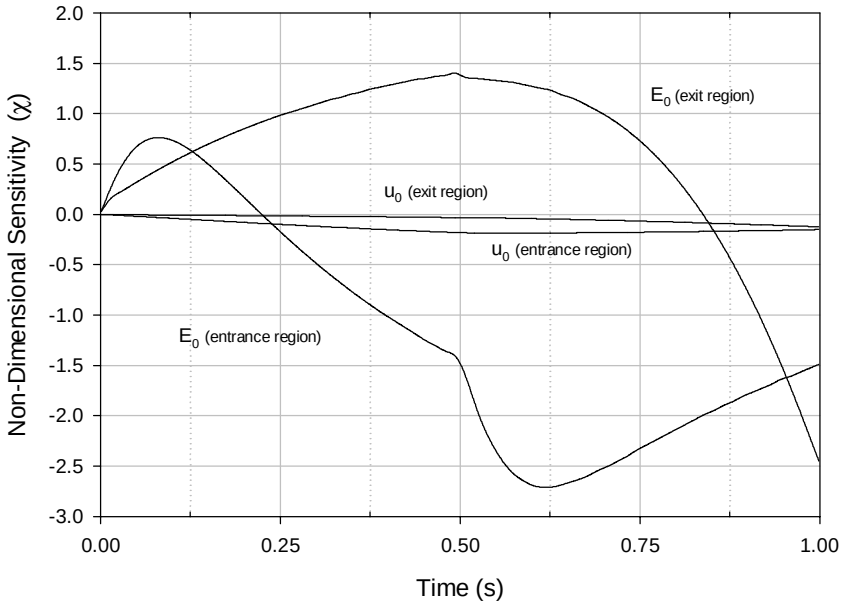

Figure 5.13 Sensitivity of the electric field strength and gas velocity.

A parametric study shows the two of the most sensitive parameters in the model to be the electric field strength and gas flow rate. Figure 5.13 shows the non-dimensional sensitivity bed temperature to these parameters for the fluidized bed case with the electric field on for the first 0.5 seconds and off for the remaining 0.5 seconds; the catalyst pellets are comprised of gamma alumina with a 0.005 mass fraction of platinum, as in the proposed experiment.

The parameters associated with the heat generated by the platinum particles have sensitivity coefficients equal to or less than 0.014, demonstrating that the model is very insensitive to the presence of the platinum. This, in conjunction with the previous results, demonstrates the difficulty in detecting the thermal effects associated with the selective heating of the catalyst particles using the experiment outlined in Section 1.3.

CHAPTER 6

CONCLUSIONS AND RECOMMENDATIONS

6.1 Conclusions

Accounting for the size-dependent conductivity of the platinum catalysts, an electric field can exist within the particles, dissipating large amounts of electromagnetic energy in the form of Joule heating. Owing to the large convection coefficient and larger contact conductance, the catalyst sites do not appear capable of achieving temperatures more than a few tenths of a degree above the support temperature at steady state conditions for microwave frequencies.

The electromagnetic energy dissipated by the catalyst particles is a function of the constitutive properties of both the platinum catalysts and alumina support. The decrease in electrical conductivity of the platinum particles allows for higher electric field strengths inside the particles, though decreasing the energy dissipated through Joule heating. This combination leads to an optimum particle size for selective heating; however, the exact size is related to the size-dependent conductivity of the platinum catalysts, which is one of the greater uncertainties in this work. In addition, a support material with a large dielectric constant will increase the electric field concentrations in and around the catalyst sites; however, due to geometrical influences, a large dielectric constant will alter the macroscopic electric field distribution, and reduce the amplitude of the field, inside the catalyst bed.

Under the experimental conditions proposed in Section 1.3, the presence of the platinum appears to have a negligibly small effect on the temperature rise of the catalyst bed. This is mainly a result of the low volume fraction of platinum, less than optimal

platinum particle size, and the large dielectric loss of the gamma alumina support. Furthermore, in the presence of a strong microwave field, the large dielectric loss of the gamma alumina support causes the bed temperatures to quickly exceed the temperatures of interest for catalysis. This overheating can be compensated for by either pulsing the electric field, or increasing the gas flow-rate, though either of these solutions may reduce the catalysis.

The primary limitation of the heat transfer model is that it does not account for thermal conduction between catalyst pellets through the bed. Consequently, an unrealistically large temperature gradient exists along the axis of the bed for some cases. However, within the temperature range of interest for catalysis, this gradient may not introduce a large error in calculating the temperatures in the upper regions of the bed.

Finally, the orientation of the reactor tube in the waveguide affects the electric field distribution within the catalyst bed. Orienting the reactor tube parallel to the electric field creates a uniform field strength along the axis of the bed, though the field strength does diminish as it nears the walls of the tube; this orientation appears to produce the most uniform field inside the reactor tube. With the reactor tube oriented perpendicular to the electric field, a large drop in electric field strength is experienced as a result of geometrical influences; the field also varies sinusoidally along the axis of the bed due to the sinusoidal variation present in the waveguide. These electric field distributions not only affect the temperature distributions within bed, but are functions of the bed temperature, as well. The macroscopic field distributions in the bed were considered constant in this study, but it should be noted that the field distributions will change as the dielectric properties of the bed change with temperature.

6.2 Recommendations

It is not likely that selective heating of the catalyst sites can be determined by measuring the thermal effects associated with the experiment outlined in Section 1.3. Using a support material with a smaller dielectric loss and a higher dielectric constant, along with catalyst particles closer to 30 nm in diameter, may promote selective heating

and subsequent measurable thermal effects. This would, however, only demonstrate that the catalyst sites are dissipating measurable amounts of energy, and not resolve the question of whether the catalyst particles are, in fact, at significantly higher temperatures than the bulk temperature. Neutron resonance radiography [11] may provide a more direct method of determining whether the catalyst sites are at higher temperatures than the support.

Future work is needed to determine the viability of microwave enhanced catalysis as an industrial process. Reactor tubes larger than the one considered in this study may lead to complicated resonant electric field distributions, which would result in uneven heating. Thus, more detailed models of the packed and fluidized beds are needed to determine if uniform and controlled heating is possible.

REFERENCES

[1] D.A.C. Stuerga and P. Gaillard. 1996. Microwave Athermal Effects in Chemistry: A Myth's Autopsy. Journal of Microwave Power and Electromagnetic Energy. Vol. 31, No. 2.

[2] G. Roussy, S. Jassm and J-M Thiebaut. 1995. Modeling of a Fluidized Bed Irradiated by a Single or a Multimode Electric Microwave Field Distribution. Journal of Microwave Power and Electromagnetic Energy. Vol. 30 No. 3.

[3] R.N. Gedye, F.E. Smith and K.C. Westaway. 1988. The rapid synthesis of organic compounds in microwave ovens. Canadian Journal of Chemistry 66:17.

[4] G. Roussy and J.A. Pearce. 1995. Foundations and Industrial Applications of Microwave and Radio Frequency Fields: Physical and Chemical Processes. John Wiley & Sons Ltd. West Sussex, England.

[5] G. Majetich and R. Hicks. 1995. The Use of Microwave Heating to Promote Organic Reactions. Journal of Microwave Power and Electromagnetic Energy. Vol. 30 No. 1.

[6] A.K. Bose, M.S. Manhas, M. Gosh, V.S. Raju, K. Tabei and Z. Urbanczyk-Lipkowska. 1990. Highly Accelerated Reactions in a Microwave Oven: Synthesis of Heterocycles. Heterocycles 30:741.

[7] K.C. Wetaway and R.N. Gedye. 1995. The Question of Specific Activation of Organic Reactions by Microwaves. Journal of Microwave Power and Electromagnetic Energy. Vol. 30 No. 4.

[8] L. Seyfried, F. Gairn, J.M. Theirbaut and G. Roussy. 1994. Microwave Electromagnetic Field Effects on Reforming Catalysts. Journal of Catalysis 148, 281.

[9] W.L. Holstein and M. Boudart. 1983. Latin American Journal of Chemical Engineering and Applied Chemistry. 13, 107

[10] Ch. Steinbruechel and L.D. Schmidt. 1973. Heat Dissipation in Catalytic Reactions on Supported Crystallites. Surface Science 40, 693

[11] J.C. Frost, P. Meehan, S.R. Morris and R.C. Ward. 1989. Non-Intrusive Temperature Measurement of the Components of a Working Catalyst by Neutron Resonance Radiography. Catalysis Letters 2, 97

[12] P. Gorkov and G. M. Eliashberg. 1965. Soviet Physics JETP 21, 940

[13] G. Nimtz, P. Marquart and H Gleiter. 1988. Size-Induced Metal-Insulator Transition in Metals and Semiconductors. Journal of Crystal Growth 86, 66

[14] J.P. Calame, A. Birman, Y. Carmel and D. Gershon. 1996. A Dielectric Mixing Law for Porous Ceramics Based on Fractal Boundaries. Journal of Applied Physics Vol. 80 No. 7

[15] C.A. Balanis. 1989. Advanced Engineering Electromagnetics. John Wiley & Sons, Inc. New York.

[16] W.H. Press, S.A. Teukolsky, W.T. Vetterling and B.P. Flannery. 1992. Numerical Recipes in Fortran 77: The Art of Scientific Computing. Press Syndicate of the University of Cambridge. Cambridge, UK.

[17] M.M.R. Williams and S.K. Loyalka. 1991. Aerosol Science Theory and Practice. Pergamon, Oxford, UK.

[18] L.B. Thomas. 1980. Accommodation of Molecules on Controlled Surfaces – Experimental Developments at the University of Missouri, 1940-1980. Rarified Gas Dynamics, Vol. 74, AIAA Progress in Astronautics and Aeronautics, 83.

[19] A. McFall. 1980. The Thermal Accommodation Coefficient of Helium and Argon on an Amorphous SiO_2 Surface. Rarified Gas Dynamics, Vol. 74, AIAA Progress in Astronautics and Aeronautics, 206.

[20] J.P. Holman. 1990. Heat Transfer. McGraw Hill Inc.

[21] T.R. Galloway and B.H. Sage. 1970. A Model of the Mechanism of Transport in Packed, Distented and Fluidized Beds. Chemical Engineering Science 25, 495

[22] D.E. Beasley and J.A. Clark. 1984. Transient Response of a Packed Bed for Thermal Energy Strorage. International Journal of Heat and Mass Transfer. Vol. 27, No. 9, 1665

[23] Kunii and Diazo. 1991. Fluidization Engineering. Butterworth-Heinemann. Boston

[24] D. Halliday and R. Resnick. 1966. Physics. John Wiley & Sons Ltd. New York.

[25] F. P. Incropera and D. P. DeWitt. 1990. Fundamentals of Heat and Mass Transfer. John Wiley & Sons, Inc. New York.

[26] R. E. Sonntag and G. J. Wan Wylen. 1984. Fundamentals of Thermodynamics. John Wiley & Sons, Inc. New York.

[27] A. F. Mills. 1992. Heat Transfer. Irwin. Homewood, Il.

[28] CRC Handbook of Chemistry and Physics. 1993. Vol. 73.

[29] W. M. Kays and M. E. Crawford. 1993. Convective Heat and Mass Transfer. McGraw Hill, Inc. New York.

[30] J. R. Thomas. 1995. Importance of Dielectric Properties in Modeling of Microwave Sintering of Ceramics. Microwaves: Theory and Application in Materials Processing III. CT 59. American Ceramic Society. Columbus Ohio.

[31] Mitchell Jackson. 1997. (personal communication).

APPENDIX

```
      PROGRAM MODEL
C..PROGRAM DESCRIPTION...
C
C..THIS PROGRAM CALLS VARIOUS SUBROUTINES WHICH MODEL EITHER A CATALYST
C  PELLET IN CROSS-FLOW, A PACKED CATALYST BED, OR A FLUIDIZED CATALYST
C  BED.
C
C..THE CROSSFLOW, PACKBED AND FLUIDIZED SUBROUTINES ARE LISTED IMMEDIATELY
C  AFTER THE MODEL PROGRAM.  ADDITIONAL SUBROUTINES AND FUNCTIONS ARE THEN
C  LISTED ALPHABETICALLY.
C
C..VARIABLE DESCRIPTIONS...
C
C  CPPT          -SPECIFIC HEAT OF PLATINUM (KJ/KG*K)
C  DAL           -DIAMETER OF CATALYST PELLETS (M)
C  DELR          -CATALYST PELLET FINITE DIFFERENCE NODE SPACING (M)
C  DELT          -FINITE DIFFERENCE TIME STEP (S)
C  DPT           -PLATINUM CATALYST PARTICLE DIAMETER (M)
C  DTUBE         -INSIDE DIAMETER OF THE REACTOR TUBE (M)
C  E0            -APPLIED ELECTRIC FIELD STRENGTH, PEAK-TO-PEAK VALUE, (V/M)
C  FHE           -PERCENT HELIUM IN THE HELIUM/BUTANE MIXTURE
C  FPT           -MASS FRACTION OF PLATINUM
C  HTUBE         -HEIGHT OF THE CATALYST BED (M)
C  IAL           -SPECIFIES WHICH ALUMINA SUPPORT IS USED, ALPHA OR GAMMA
C  IMIX          -SPECIFIES WHICH MIXTURE FORMULA IS USED
C  IPT           -SPECIFIES WHETHER THE PLATINUM CONDUCTIVITY IS EVALUATED
C                 AT THE BULK VALUE, OR COMPHENSATED FOR SIZE DEPENDENCE
C  IQDOT         -SPECIFIES HOW THE HEAT GENERATION IS CALCULATED
C  MAXDZ         -NUMBER OF AXIAL NODES THE BED AND GAS TEMPERATURES ARE
C                 EVALUATED AT
C  MODEL         -SPECIFIES WHICH MODEL IS USED: SPHERE IN CROSS-FLOW,
C                 PACKED BED, OF FLUIDIZED BED
C  MSHELL        -NUMBER OF FINITE DIFFERENCE NODES THAT LIE WITHIN THE
C                 PLATINUM/ALUMINA MIXTURE REGION
C  NPT           -TOTAL NUMBER OF MICROWAVE PULSES
C  NPULSE        -NUMBER OF MICROWAVE PULSE ITERATIONS
C  NTOTAL        -TOTAL NUMBER OF ITERATIONS
C  POROSITY      -VOIDAGE WITHIN THE BED (1 MINUS THE SOLID FRACTION)
C  PULSE         -LENGTH OF EACH MICROWAVE PULSE    (BETWEEN 0 AND 1 SECONDS, A
```

```
C                1 SECOND PULSE LENGTH DENOTES A CONSTANT FIELD WITH TIME)
C  RHOAL        -DENSITY OF THE ALUMINA (KG/M^3)
C  RHOPT        -DENSITY OF THE PLATINUM (KG/M^3)
C  SAPEL        -SURFACE AREA OF A SINGLE CATALYST PELLET (M^2)
C  SEC          -DURATION OF SIMULATION (S)
C  T0           -INLET GAS TEMPERATURE AND INITIAL TEMPERATURE OF THE
C                CATALYST BED (K)
C  TF           -FLUID TEMPERATURE (K)
C  TSHELL       -THICKNESS OF THE PT/AL2O3 MIXTURE REGION (M)
C  U0           -SUPERFICIAL, INLET FLOW VELOCTIY (M/S)
C  U1           -INTERSTICIAL FLOW VELOCITY AROUND THE CATALYST
C                PELLETS (M/S)
C  VF           -VOLUME FLOW RATE OF THE HELIUM/BUTANE MIXTURE (M^3/S)
C  VFBU         -VOLUME FLOW RATE OF THE BUTANE (M^3/S)
C  VFHE         -VOLUME FLOW RATE OF THE HELIUM (M^3/S)
C  VOLPEL       -VOLUME OF A SINGLE CATALYST PELLET (M^3)
C  VOLTUBE      -TOTAL VOLUME OF THE CATALYST BED, SOLID AND VOID (M^3)
C
      IMPLICIT DOUBLE PRECISION(A-H,O-Y)
      IMPLICIT COMPLEX*16(Z)
      PARAMETER(MTH=30)
C..ASSIGN COMMON VARIALBLE BLOCKS
      COMMON/BLOCK0/MODEL
      COMMON/BLOCK1/IAL,IPT,IMIX,IQDOT,ITRISE
      COMMON/BLOCK2/EP0,PI,FREQ,E0
      COMMON/BLOCK3/DELR,DELT,NPT,NPULSE,NTOTAL
      COMMON/BLOCK4/RHOAL,DAL,TSHELL,SAPEL,VOLPEL
      COMMON/BLOCK5/DPT,CPPT,RHOPT,FPT
      COMMON/BLOCK6/DTUBE,HTUBE,VOLTUBE,POROSITY,MAXDZ
      COMMON/BLOCK7/VFHE,VFBU,VF,FHE
      COMMON/BLOCK8/T0,TF
      DATA PI,EP0,FREQ/3.141592653589793D0,8.854D-12,2.45D+09/
C..PRINT AND WRITE FORMAT STATEMENTS
9     FORMAT(1X,I5,E20.8)
10    FORMAT(1X,4E20.8)
      ITRISE=0
C..SELECT MODEL
C  MODEL = (1) SPHERE IN CROSS FLOW  (2) PACKED BED  (3) FLUIDIZED BED
      MODEL=2
C..PROPERTIES COMMON TO THE CATALYST BED
      DTUBE=2.00D-02
      HTUBE=2.54D-02
      VOLTUBE=PI*(DTUBE/2.0D0)**2*HTUBE
      POROSITY=0.35D0
C..PROPERTIES COMMON TO ALPHA/GAMMA ALUMINA
C  IAL = (1) ALPHA ALUMINA  (2) GAMMA ALUMINA
      IAL=2
      RHOAL=7.0D+02
      DAL=3.0D-03
      TSHELL=0.07D-03
      SAPEL=4.0D0*PI*(DAL/2.0D0)**2
      VOLPEL=(4.D0/3.D0)*PI*(DAL/2.D0)**3
C..INITIAL BED AND GAS TEMPERATURE
```

```
      T0=2.98D+02
      TF=2.98D+02
C..GAS VOLUME FLOW RATES IN L/MIN CONVERTED INTO M^3/SEC
C  FOR THE SPHERE IN CROSS-FLOW AND PACKED BED
      VFHE=0.25D0
      VFHE=VFHE*1.0D-03/60.0D0
      VFHE=1.0D0*VFHE
      VFBU=0.066D0
      VFBU=VFBU*1.0D-03/60.0D0
      VFBU=1.0D0*VFBU
      VF=(VFHE+VFBU)
      FHE=(RHOHE(TF)*VFHE)/(RHOF(TF)*VF)
C..SUPERFICIAL AND INTERSTICIAL GAS VELOCITIES FOR A SPHERE IN
C  CROSS-FLOW OR PACKED BED
      U0=VF/(VOLTUBE/HTUBE)
      U1=U0/POROSITY
C..SUPERFICIAL AND SUPERSTICIAL VELOCITIES FOR A FLUIDIZED BED
      IF(MODEL.EQ.3)THEN
C..QUADRATIC SOLUTION TO EQ.(4.43)
            A1=-DAL**3*RHOF(T0)*(RHOAL-RHOF(T0))*9.81D0/VISCF(T0)**2
            A2=150.0D0*(1.0D0-POROSITY)*DAL*RHOF(T0)/(POROSITY**3*VISCF(T0))
            A3=1.75D0*(DAL*RHOF(T0))**2/(POROSITY**3*VISCF(T0))
            Q=(-1.0D0/2.0D0)*(A2+DSIGN(1.0D0,A2)*DSQRT(A2**2-4.0D0*A3*A1))
            X1=Q/A3
            X2=A1/Q
            IF(X1.GT.0.0D0)THEN
                  U0=X1
            ELSE
                  U0=X2
            ENDIF
C..UPDATE THE VOLUME FLOW RATE TO ACCOUNT FOR THE NEW FLOW VELOCITY
            VF=U0*(VOLTUBE/HTUBE)
            U1=U0/POROSITY
      ENDIF
C..PROPERTIES COMMON TO THE ELECTRIC FIELD
      E0=DSQRT(2.0D0)*5.0D+04
C..PROPERTIES COMMON TO PLATINUM
C  IPT = (1) BULK CONDUCTIVITY  (2) SIZE DEPENDENT CONDUCTIVITY
      IPT=2
      RHOPT=21.38D+03
      CPPT=0.134D+03
      DPT=33.0D-09
      FPT=0.05D0
C..CHOOSE MIXTURE FORMULA
C  IMIX =    (1) RAYLEIGH   (2) MAXWELL-GARNET THEORY
      IMIX=1
C..CHOOSE SOURCE SUBROUTINE
C  IQDOT =(1) USING MIXTURE FORMULA (2) USING PT PARTICLE HEAT GEN
C              (3) PERPENDICULAR ELECTRIC FIELD POLARIZATION, SECTION 3.6.2,
C                    & RAYLEIGH MIXTURE FORMULA
      IQDOT=1
C..FINITE DIFFERENCE PELLET NODE PARAMETERS
      DELR=(DAL/2.0D0)/(DBLE(MTH-1))
```

```
      MSHELL=NINT(MTH*TSHELL/(DAL/2.0D0))+1
C..FINITE DIFFERENCE TIME-STEP PARAMETERS
      SEC=10.0D0
      PULSE=0.10D0
      DELT=0.02D0
      NPT=NINT(SEC-1.0D0)
      NPULSE=NINT(PULSE/DELT)
      NTOTAL=NINT(1.0D0/DELT)
C..PACKED BED AXIAL NODE PARAMETERS
      MAXDZ=NINT((HTUBE/U1)/DELT)
C..FLUIDIZED BED AXIAL NODE PARAMETERS AND UPDATED TIME STEP
      IF(MODEL.EQ.3)THEN
          MAXDZ=20
          DELT=HTUBE/(DBLE(MAXDZ)*U1)
          NPULSE=NINT(PULSE/DELT)
          NTOTAL=NINT(1.0D0/DELT)
      ENDIF
      IF(MODEL.EQ.1)THEN
          PRINT*,'PERFORMING SPHERE IN CROSSFLOW MODEL...'
          CALL CROSSFLOW
      ELSEIF(MODEL.EQ.2)THEN
          PRINT*,'PERFORMING PACKED BED MODEL...'
          CALL PACKBED
      ELSEIF(MODEL.EQ.3)THEN
          PRINT*,'PERFORMING FLUIDIZED BED MODEL...'
          CALL FLUIDIZED
      ENDIF
      END
CCCCCCCCCCCCCCCCCCCCCCCCCCCCCCCCCCCCCCCCCCCCCCCCCCCCCCCCCCCCCCCCCCCCCCCCCCC
      SUBROUTINE CROSSFLOW
C..THIS SUBROUTINE   PERFORMS A ONE DIMENSIONAL, TRANSIENT,
C  FINITE DIFFERENCE MODEL OF A SINGLE CATALYST SUPPORT PELLET
C
C  CNODE        -CENTER FINITE-DIFFERENCE NODE
C  CPAL         -SPECIFIC HEAT OF ALUMINA  (J/KG K)
C  DELT         -TIME STEP (SEC)
C  EXNODE       -SURFACE FINITE-DIFFERENCE NODE
C  HCONV        -CONVECTION COEFFICIENT, EQ.(4.26),      (W/M^2)
C  INNODE       -GENERAL, INTERIOR FINITE-DIFFERENCE NODE
C  IQDOT        -SPECIFIES THE HEAT GENERATION SUBROUTINE
C  LAYER        -CATALYST BED AXIAL NODES (ALWAYS = 1 FOR
C                 CROSSFLOW SUBROUTINE)
C  M            -PELLET RADIAL NODES
C  MTH          -MAXIMUM NUMBER OF NODES WITHIN PELLET
C  MTIME        -TIME COUNTER
C  MZ           -NUMBER OF AXIAL LAYERS WITHIN THE BED
C                 (1 FOR CROSSFLOW SUBROUTINE)
C  NP           -CURRENT PULSE NUMBER
C  NPT          -TOTAL NUMBER OF MICROWAVE PULSES
C  NPULSE       -NUMBER OF ITTERATIONS WITHIN EACH PULSE
C  QDOT         -HEAT GENERATION ARRAY (W/M^3)
C  RHOAL        -DENSITY OF ALUMINA (KG/M^3)
C  RM           -CURRENT RADIAL NODE FOR THE PELLET FINITE-DIFFERENCE (M)
```

```
C  RMINUS       -AVERAGE BETWEEN THE CURRENT AND PREVIOUS NODE FOR THE
C                 PELLET FINITE-DIFFERENCE (M)
C  THETA0       -TEMPERATURE RISE ARRAY AT THE CURRENT TIME STEP (K)
C  THETA1       -TEMPERATURE RISE ARRAY AT THE FUTURE TIME STEP (K)
C  TIME         -SIMULATION TIME
C  T0           -INLET GAS TEMPERATURE (K)
C  TF           -GAS TEMPERATURE (K)
C  TS           -SURFACE TEMPERATURE ARRAY (C)
C
      IMPLICIT DOUBLE PRECISION(A-H,O-Y)
      IMPLICIT COMPLEX*16(Z)
      PARAMETER(MTH=30,MZ=1)
      DOUBLE PRECISION THETA0(1:MTH,0:MZ),THETA1(1:MTH),
     &QDOT(MTH),A(MTH),B(MTH),C(MTH),RHS(MTH),TS(0:12000,0:MZ),
     COMMON/BLOCK1/IAL,IPT,IMIX,IQDOT,ITRISE
     COMMON/BLOCK2/EP0,PI,FREQ,E0
     COMMON/BLOCK3/DELR,DELT,NPT,NPULSE,NTOTAL
     COMMON/BLOCK4/RHOAL,DAL,TSHELL,SAPEL,VOLPEL
     COMMON/BLOCK5/DPT,CPPT,RHOPT,FPT
     COMMON/BLOCK6/DTUBE,HTUBE,VOLTUBE,POROSITY,MAXDZ
     COMMON/BLOCK7/VFHE,VFBU,VF,FHE
     COMMON/BLOCK8/T0,TF
     COMMON/BLOCKSENS/ISENS,DEL
C..OPEN FILES
     OPEN(UNIT=13,FILE='TEMPVT.TXT')
C..FORMAT STATEMENTS
9    FORMAT(1X,I5,E20.8)
11   FORMAT(5X,1F10.2,5X,1F15.5,5X,1E15.5)
12   FORMAT(1F5.2,25F6.1)
100 FORMAT(1F20.4,5X,1E20.4,5X,1F20.8)
101 FORMAT(1F20.4,1E20.4,31F15.4)
C..INITIALIZE TEMPERATURE ARRAY
     DO LAYER=0,1
          DO M=1,MTH
               THETA0(M,LAYER)=T0-TF
          ENDDO
     ENDDO
C..SET THE TIME COUNTER TO 0
     MTIME=0
C..BEGIN MICROWAVE PULSE/RELAXATION DO LOOP
     DO NP=0,NPT
C..BEGIN MICROWAVE PULSE ITERATIONS
          DO J=1,NPULSE
               MTIME=MTIME+1
               TIME=MTIME*DELT
               LAYER=1
               IF(IQDOT.EQ.1)THEN
                    CALL SOURCE(MTH,MZ,LAYER,THETA0,QDOT)
               ELSEIF(IQDOT.EQ.2)THEN
                    CALL SOURCE2(MTH,MZ,LAYER,THETA0,QDOT)
               ELSE
                    PAUSE 'FAILURE OF SOURCE/SOURCE2 IN CROSSFLOW SUBROUTINE'
               ENDIF
```

```
C..CALCULATE THE RIGHT HAND SIDE, B VECTOR, OF EQ.(4.21)
            DO M=1,MTH-1
                RHS(M)=THETA0(M,LAYER)+(DELT/(RHOAL*CPAL
     &(THETA0(M,LAYER)+T0)))*QDOT(M)
            ENDDO
            TM=THETA0(MTH,LAYER)+T0
            RM=DAL/2.0D0
            RMINUS=RM-DELR/2.0D0
            RHS(MTH)=THETA0(MTH,LAYER)+(DELT/(RHOAL*CPAL(TM)))
     &*QDOT(MTH)+(TF-T0)*(3.0D0*DELT*HCONV(TM)
     &*RM**2)/(RHOAL*CPAL(TM)*(RM**3-RMINUS**3))
C..BEGIN INNER ITERATIONS   FOR T VECTOR CONVERGENCE, EQ. (4.21)
            DO IN=1,10
                CALL CNODE(MTH,MZ,LAYER,THETA0,B,C)
                CALL INNODE(MTH,MZ,LAYER,THETA0,A,B,C)
                CALL EXNODE(MTH,MZ,LAYER,THETA0,A,B)
                CALL TRIDAG(A,B,C,RHS,THETA1,MTH)
                DO M=1,MTH
                    THETA0(M,LAYER)=THETA1(M)
                ENDDO
C..END INNER INERATIONS
            ENDDO
            TS(MTIME,LAYER)=THETA0(MTH,LAYER)+(T0-2.73D+02)
            PRINT 11,TIME,TS(MTIME,LAYER)
            WRITE(13,11) TIME,TS(MTIME,LAYER)
        ENDDO
C..END MICROWAVE PULSE LOOP
C..BEGIN REST ITERATIONS WITH NO MICROWAVE FIELD
        DO J=NPULSE+1,NTOTAL
            MTIME=MTIME+1
            TIME=MTIME*DELT
      LAYER=1
            DO M=1,MTH-1
                RHS(M)=THETA0(M,LAYER)
            ENDDO
            TM=THETA0(MTH,LAYER)+T0
C..CALCULATE THE RIGHT HAND SIDE, B VECTOR, OF EQ.(4.21)
            RM=DAL/2.0D0
            RMINUS=RM-DELR/2.0D0
            RHS(MTH)=THETA0(MTH,LAYER)+(TF-T0)*(3.0D0*DELT*HCONV(TM)
     &*RM**2)/(RHOAL*CPAL(TM)*(RM**3-RMINUS**3))
C..BEGIN INNER ITERATIONS   FOR T VECTOR CONVERGENCE, EQ. (4.21)
            DO IN=1,10
                CALL CNODE(MTH,MZ,LAYER,THETA0,B,C)
                CALL INNODE(MTH,MZ,LAYER,THETA0,A,B,C)
                CALL EXNODE(MTH,MZ,LAYER,THETA0,A,B)
                CALL TRIDAG(A,B,C,RHS,THETA1,MTH)
                DO M=1,MTH
                    THETA0(M,LAYER)=THETA1(M)
                ENDDO
C..END INNER ITERATIONS
            ENDDO
            TS(MTIME,LAYER)=THETA0(MTH,LAYER)+(T0-2.73D+02)
```

```
            PRINT 11,TIME,TS(MTIME,LAYER)
            WRITE(13,11) TIME,TS(MTIME,LAYER)
         ENDDO
C..END RELAXATION   DO LOOP
      ENDDO
C..END MICROWAVE PULSE/RELAXATION DO LOOP
      END
CCCCCCCCCCCCCCCCCCCCCCCCCCCCCCCCCCCCCCCCCCCCCCCCCCCCCCCCCCCCCCCCCCCCCCCCCCC
      SUBROUTINE PACKBED
C..THIS SUBROUTINE   CALCULATES THE AXIAL TEMPERATURE DISTRIBUTION
C  OF THE PACKED CATALYST BED USING THE APPROACH OULINED
C  IN SECTION 4.5
C
C  CNODE        -CENTER FINITE-DIFFERENCE NODE
C  CPAL         -SPECIFIC HEAT OF ALUMINA  (J/KG K)
C  DELT         -TIME STEP (SEC)
C  EXNODE       -SURFACE FINITE-DIFFERENCE NODE
C  HCONV        -CONVECTION COEFFICIENT, EQ.(4.28), (W/M^2)
C  INNODE       -GENERAL, INTERIOR FINITE-DIFFERENCE NODE
C  IQDOT        -SPECIFIES THE HEAT GENERATION SUBROUTINE
C  LAYER        -CATALYST BED AXIAL NODE
C  M            -PELLET RADIAL NODES
C  MAXDZ        -TOTAL NUMBER OF AXIAL LAYERS WITHIN THE BED
C  MTH          -MAXIMUM NUMBER OF NODES WITHIN PELLET
C  MTIME        -TIME COUNTER
C  MZ           -MAXIMUM NUMBER OF AXIAL LAYERS WITHIN THE BED
C  NP           -CURRENT PULSE NUMBER
C  NPT          -TOTAL NUMBER OF MICROWAVE PULSES
C  NPULSE       -NUMBER OF ITTERATIONS WITHIN EACH PULSE
C  POROSITY     -VOID FRACTION IN THE CATALYST BED
C  QDOT         -HEAT GENERATION ARRAY (W/M^3)
C  RHOAL        -DENSITY OF ALUMINA (KG/M^3)
C  RM           -CURRENT RADIAL NODE FOR THE PELLET FINITE-DIFFERENCE (M)
C  RMINUS       -AVERAGE BETWEEN THE CURRENT AND PREVIOUS NODE FOR THE
C                PELLET FINITE-DIFFERENCE (M)
C  SA           -SURFACE AREA OF CATALYST PELLETS WITHIN ONE BED LAYER (M^2)
C  SAPEL        -SURFACE AREA OF ONE CATALYST PELLET
C  SATOT        -TOTAL SURFACE AREA OF ALL THE CATALYST PELLETS (M^2)
C  THETA0       -TEMPERATURE RISE ARRAY AT THE CURRENT TIME STEP (K)
C  THETA1       -TEMPERATURE RISE ARRAY AT THE FUTURE TIME STEP (K)
C  TIME         -SIMULATION TIME
C  T0           -INLET GAS TEMPERATURE (K)
C  TF           -GAS TEMPERATURE (K)
C  TS           -SURFACE TEMPERATURE ARRAY (C)
C  TFLUID       -FLUID TEMPERATURE ARRAY (K)
C  TOTPEL       -TOTAL NUMBER OF PELLETS WITHIN THE BED
C  TSUPPORT     -SUPPORT TEMPERATURE RISE ARRAY (K)
C  VOLAL        -TOTAL VOLUME OF THE CATALYST PELLETS (M^3)
C  VOLPEL       -VOLUME OF ONE CATALYST PELLET (M^3)
C  VOLTUBE      -VOLUME OF THE CATALYST BED (M^3)
C
      IMPLICIT DOUBLE PRECISION(A-H,O-Y)
      IMPLICIT COMPLEX*16(Z)
```

```
      PARAMETER(MTH=30,MZ=100)
      DOUBLE PRECISION THETA0(1:MTH,0:MZ),THETA1(1:MTH),
     &QDOT(MTH),A(MTH),B(MTH),C(MTH),RHS(MTH),TFLUID(0:12000,0:MZ),
     &TSUPPORT(0:12000,0:MZ),DS(1:12000,1:MZ),DF(1:12000,1:MZ)
      COMMON/BLOCK1/IAL,IPT,IMIX,IQDOT,ITRISE
      COMMON/BLOCK2/EP0,PI,FREQ,E0
      COMMON/BLOCK3/DELR,DELT,NPT,NPULSE,NTOTAL
      COMMON/BLOCK4/RHOAL,DAL,TSHELL,SAPEL,VOLPEL
      COMMON/BLOCK5/DPT,CPPT,RHOPT,FPT
      COMMON/BLOCK6/DTUBE,HTUBE,VOLTUBE,POROSITY,MAXDZ
      COMMON/BLOCK7/VFHE,VFBU,VF,FHE
      COMMON/BLOCK8/T0,TF
      COMMON/BLOCKSENS/ISENS,DEL
C     ...   OPEN FILES
      OPEN(UNIT=20,FILE='SUPPORT.TXT')
      OPEN(UNIT=21,FILE='FLUID.TXT')
C     ...   FORMAT STATEMENTS
9     FORMAT(1X,I5,E20.8)
11    FORMAT(5X,1F5.2,5X,I3,5X,2F15.5)
12    FORMAT(1F5.2,25F6.1)
C..CALCULATE THE NUMBER OF CATALYST PELLETS AND SURFACE AREA
      VOLAL=VOLTUBE*(1.0D0-POROSITY)
      TOTPEL=NINT(VOLAL/VOLPEL)
      SATOT=(SAPEL*TOTPEL)
      SA=SATOT/DBLE(MAXDZ)
C..INITIALIZE BED TEMPERATURE ARRAY
      DO LAYER=0,MAXDZ
          DO M=0,12000
              TFLUID(M,LAYER)=T0
              TSUPPORT(M,LAYER)=T0
          ENDDO
      ENDDO
C..INITIALIZE PELLET TEMPERATURE ARRAY
      DO LAYER=0,MAXDZ
          DO M=1,MTH
              THETA0(M,LAYER)=0.0D0
          ENDDO
      ENDDO
C..SET THE TIME COUNTER TO 0
      MTIME=0
C..BEGIN MICROWAVE PULSE/RELAXATION DO LOOP
      DO NP=0,NPT
C..BEGIN MICROWAVE PULSE ITERATIONS
          DO J=1,NPULSE
              MTIME=MTIME+1
              TIME=MTIME*DELT
C..BEGIN SOLUTIONS FOR EACH LAYER OF THE BED
              DO LAYER=1,MAXDZ
                  TF=TFLUID(MTIME-1,LAYER-1)
                  IF(IQDOT.EQ.1)THEN
                  CALL SOURCE(MTH,MZ,LAYER,THETA0,QDOT)
                  ELSEIF(IQDOT.EQ.2)THEN
                  CALL SOURCE2(MTH,MZ,LAYER,THETA0,QDOT)
```

```
                ELSEIF(IQDOT.EQ.3)THEN
                CALL SOURCE3(MTH,MZ,LAYER,THETA0,QDOT)
                ELSE
                PAUSE 'FAILURE OF SOURCE/SOURCE2/3 IN PACKBED SUBROUTINE'
                ENDIF
C..CALCULATE THE RIGHT HAND SIDE, B VECTOR, OF EQ.(4.21)
                DO M=1,MTH-1
                    RHS(M)=THETA0(M,LAYER)+(DELT/(RHOAL*CPAL
     &(THETA0(M,LAYER)+T0)))*QDOT(M)
                ENDDO
                TM=THETA0(MTH,LAYER)+T0
                RM=DAL/2.0D0
                RMINUS=RM-DELR/2.0D0
                RHS(MTH)=THETA0(MTH,LAYER)+(DELT/(RHOAL*CPAL(TM)))
    &*QDOT(MTH)+(TF-T0)*(3.0D0*DELT*HCONV(TM)
    &*RM**2)/(RHOAL*CPAL(TM)*(RM**3-RMINUS**3))
C..BEGIN INNER ITERATIONS   FOR CONVERGENCE OF EQ.(4.21)
                DO IN=1,10
                    CALL CNODE(MTH,MZ,LAYER,THETA0,B,C)
                    CALL INNODE(MTH,MZ,LAYER,THETA0,A,B,C)
                    CALL EXNODE(MTH,MZ,LAYER,THETA0,A,B)
                    CALL TRIDAG(A,B,C,RHS,THETA1,MTH)
                    DO M=1,MTH
                        THETA0(M,LAYER)=THETA1(M)
                    ENDDO
                ENDDO
                TSUPPORT(MTIME,LAYER)=THETA0(MTH,LAYER)+T0
                TS=TSUPPORT(MTIME,LAYER)
C..CALCULATE THE EXITTING FLUID TEMPERATURE FOR THE NODE
                TFLUID(MTIME,LAYER)=(TF-TS)*EXP(-HCONV(TS)*SA
     &/(RHOF(TS)*VF*CPF(TS)))+TS
                PRINT 11,TIME,LAYER,TS,TFLUID(MTIME,LAYER)
C..INCREMENT BED LAYER
            ENDDO
C..END MICROWAVE PULSE ITERATIONS
        ENDDO
C..BEGIN REST ITERATIONS WITH NO MICROWAVE FIELD
        DO J=NPULSE+1,NTOTAL
            MTIME=MTIME+1
            TIME=MTIME*DELT
C..BEGIN SOLUTIONS FOR EACH LAYER OF THE BED
            DO LAYER=1,MAXDZ
                TF=TFLUID(MTIME-1,LAYER-1)
C..CALCULATE THE RIGHT HAND SIDE, B VECTOR, OF EQ.(4.21)
                DO M=1,MTH-1
                    RHS(M)=THETA0(M,LAYER)
                ENDDO
                TM=THETA0(MTH,LAYER)+T0
                RM=DAL/2.0D0
                RMINUS=RM-DELR/2.0D0
                RHS(MTH)=THETA0(MTH,LAYER)+(TF-T0)*(3.0D0*DELT*HCONV(TM)
     &*RM**2)/(RHOAL*CPAL(TM)*(RM**3-RMINUS**3))
C..BEGIN INNER ITERATIONS   FOR CONVERGENCE OF EQ.(4.21)
```

```
                    DO IN=1,10
                        CALL CNODE(MTH,MZ,LAYER,THETA0,B,C)
                        CALL INNODE(MTH,MZ,LAYER,THETA0,A,B,C)
                        CALL EXNODE(MTH,MZ,LAYER,THETA0,A,B)
                        CALL TRIDAG(A,B,C,RHS,THETA1,MTH)
                        DO M=1,MTH
                            THETA0(M,LAYER)=THETA1(M)
                        ENDDO
                    ENDDO
                    TSUPPORT(MTIME,LAYER)=THETA0(MTH,LAYER)+T0
                    TS=TSUPPORT(MTIME,LAYER)
C..CALCULATE THE EXITTING FLUID TEMPERATURE FOR THE NODE
                    TFLUID(MTIME,LAYER)=(TF-TS)*EXP(-HCONV(TS)*SA
     &/(RHOF(TS)*VF*CPF(TS)))+TS
                    PRINT 11,TIME,LAYER,TS,TFLUID(MTIME,LAYER)
C..INCREMENT THE BED LAYER
                ENDDO
C..END RELAXATION DO LOOP
            ENDDO
C..END MICROWAVE PULSE/RELAXATION DO LOOP
        ENDDO
C..WRITE OUTPUT TO FILES
C     IF(ISENS.EQ.0)THEN
        IDZ=NINT(DBLE(MAXDZ)/20.0D0)
       DO M=1,MTIME
            DO LAYER=1,MAXDZ,IDZ
                DS(M,LAYER)=TSUPPORT(M,LAYER)-273.0D0
                DF(M,LAYER)=TFLUID(M,LAYER)-273.0D0
            ENDDO
        ENDDO
        DO M=1,MTIME
            TIME=DBLE(M)*DELT
            WRITE(20,12) TIME,(DS(M,LAYER),LAYER=1,MAXDZ,IDZ)
            WRITE(21,12) TIME,(DF(M,LAYER),LAYER=1,MAXDZ,IDZ)
        ENDDO
C     ENDIF
C     ..    END OUTPUT TO FILES
        RETURN
        END
CCCCCCCCCCCCCCCCCCCCCCCCCCCCCCCCCCCCCCCCCCCCCCCCCCCCCCCCCCCCCCCCCCCCCCCCCCCCCCC
        SUBROUTINE FLUIDIZED
C..THIS SUBROUTINE   CALCULATES THE AXIAL TEMPERATURE DISTRIBUTION,
C  OF THE FLUIDIZED CATALYST BED USING THE APPROACH OULINED
C  IN SECTION 4.5 AND 4.6
C
C  CNODE        -CENTER FINITE-DIFFERENCE NODE
C  CPAL         -SPECIFIC HEAT OF ALUMINA  (J/KG K)
C  DELT         -TIME STEP (SEC)
C  EXNODE       -SURFACE FINITE-DIFFERENCE NODE
C  HCONV        -CONVECTION COEFFICIENT, EQ.(4.29), (W/M^2)
C  INNODE       -GENERAL, INTERIOR FINITE-DIFFERENCE NODE
C  IQDOT        -SPECIFIES THE HEAT GENERATION SUBROUTINE
C  LAYER        -CATALYST BED AXIAL NODE
```

```
C  M            -PELLET RADIAL NODES
C  MAXDZ         -TOTAL NUMBER OF AXIAL LAYERS WITHIN THE BED
C  MTH           -MAXIMUM NUMBER OF NODES WITHIN PELLET
C  MTIME         -TIME COUNTER
C  MZ            -MAXIMUM NUMBER OF AXIAL LAYERS WITHIN THE BED
C  NP            -CURRENT PULSE NUMBER
C  NPT           -TOTAL NUMBER OF MICROWAVE PULSES
C  NPULSE        -NUMBER OF ITTERATIONS WITHIN EACH PULSE
C  POROSITY      -VOID FRACTION IN THE CATALYST BED
C  QDOT          -HEAT GENERATION ARRAY (W/M^3)
C  RHOAL         -DENSITY OF ALUMINA (KG/M^3)
C  RM            -CURRENT RADIAL NODE FOR THE PELLET FINITE-DIFFERENCE (M)
C  RMINUS        -AVERAGE BETWEEN THE CURRENT AND PREVIOUS NODE FOR THE
C                 PELLET FINITE-DIFFERENCE (M)
C  SA            -SURFACE AREA OF CATALYST PELLETS WITHIN ONE BED LAYER (M^2)
C  SAPEL         -SURFACE AREA OF ONE CATALYST PELLET
C  SATOT         -TOTAL SURFACE AREA OF ALL THE CATALYST PELLETS (M^2)
C  THETA0        -TEMPERATURE RISE ARRAY AT THE CURRENT TIME STEP (K)
C  THETA1        -TEMPERATURE RISE ARRAY AT THE FUTURE TIME STEP (K)
C  TIME          -SIMULATION TIME
C  T0            -INLET GAS TEMPERATURE (K)
C  TF            -GAS TEMPERATURE (K)
C  TS            -SURFACE TEMPERATURE ARRAY (C)
C  TFLUID        -FLUID TEMPERATURE ARRAY (K)
C  TOTPEL        -TOTAL NUMBER OF PELLETS WITHIN THE BED
C  TSUPPORT      -SUPPORT TEMPERATURE RISE ARRAY (K)
C  VOLAL         -TOTAL VOLUME OF THE CATALYST PELLETS (M^3)
C  VOLPEL        -VOLUME OF ONE CATALYST PELLET (M^3)
C  VOLTUBE       -VOLUME OF THE CATALYST BED (M^3)
C
      IMPLICIT DOUBLE PRECISION(A-H,O-Y)
      IMPLICIT COMPLEX*16(Z)
      PARAMETER(MTH=30,MZ=100)
      DOUBLE PRECISION THETA0(1:MTH,0:MZ),THETA1(1:MTH),
     &QDOT(MTH),A(MTH),B(MTH),C(MTH),RHS(MTH),TFLUID(0:12000,0:MZ),
     &TSUPPORT(0:12000,0:MZ),DS(1:12000,1:MZ),DF(1:12000,1:MZ)
      COMMON/BLOCK1/IAL,IPT,IMIX,IQDOT,ITRISE
      COMMON/BLOCK2/EP0,PI,FREQ,E0
      COMMON/BLOCK3/DELR,DELT,NPT,NPULSE,NTOTAL
      COMMON/BLOCK4/RHOAL,DAL,TSHELL,SAPEL,VOLPEL
      COMMON/BLOCK5/DPT,CPPT,RHOPT,FPT
      COMMON/BLOCK6/DTUBE,HTUBE,VOLTUBE,POROSITY,MAXDZ
      COMMON/BLOCK7/VFHE,VFBU,VF,FHE
      COMMON/BLOCK8/T0,TF
C..OPEN FILES
      OPEN(UNIT=13,FILE='FLUID.TXT')
      OPEN(UNIT=15,FILE='SUPPORT.TXT')
C..FORMAT STATEMENTS
9     FORMAT(1X,I5,E20.8)
10    FORMAT(1F5.2,10F7.1)
11    FORMAT(5X,1F5.2,5X,I3,5X,2F15.4)
12    FORMAT(1F5.2,25F6.1)
C..CALCULATE THE NUMBER OF PELLETS AND TOTAL SURFACE AREA
```

```
      VOLAL=0.9D0*(VOLTUBE*(1.0D0-POROSITY))
      TOTPEL=NINT(VOLAL/VOLPEL)
      SATOT=(SAPEL*TOTPEL)
      SA=SATOT/DBLE(MAXDZ)
C..INITIALIZE BED TEMPERATURE ARRAY
      DO LAYER=0,MAXDZ
          DO M=0,12000
              TFLUID(M,LAYER)=T0
              TSUPPORT(M,LAYER)=T0
          ENDDO
      ENDDO
C..INITIALIZE PELLET TEMPERATURE ARRAY
      DO LAYER=0,MAXDZ
          DO M=1,MTH
              THETA0(M,LAYER)=0.0D0
          ENDDO
      ENDDO
C..SET THE TIME COUNTER TO 0
      MTIME=0
C..BEGIN MICROWAVE PULSE/RELAXATION DO LOOP
      DO NP=0,NPT
C..BEGIN MICROWAVE PULSE ITERATIONS
          DO J=1,NPULSE
              MTIME=MTIME+1
              TIME=MTIME*DELT
C..BEGIN SOLUTIONS FOR EACH LAYER OF THE BED
              DO LAYER=1,MAXDZ
                  TF=TFLUID(MTIME-1,LAYER-1)
                  IF(IQDOT.EQ.1)THEN
                      CALL SOURCE(MTH,MZ,LAYER,THETA0,QDOT)
                  ELSEIF(IQDOT.EQ.2)THEN
                      CALL SOURCE2(MTH,MZ,LAYER,THETA0,QDOT)
                  ELSEIF(IQDOT.EQ.3)THEN
                      CALL SOURCE3(MTH,MZ,LAYER,THETA0,QDOT)
                  ELSE
                  PAUSE 'FAILURE OF SOURCE/SOURCE2/3 IN FLUIDIZED SUBROUTINE'
                  ENDIF
C..CALCULATE THE RIGHT HAND SIDE, B VECTOR, OF EQ.(4.21)
                  DO M=1,MTH-1
                      RHS(M)=THETA0(M,LAYER)+(DELT/(RHOAL*CPAL
   &(THETA0(M,LAYER)+T0)))*QDOT(M)
                  ENDDO
                  TM=THETA0(MTH,LAYER)+T0
                  RM=DAL/2.0D0
                  RMINUS=RM-DELR/2.0D0
                  RHS(MTH)=THETA0(MTH,LAYER)+(DELT/(RHOAL*CPAL(TM)))
   &*QDOT(MTH)+(TF-T0)*(3.0D0*DELT*HCONV(TM)
   &*RM**2)/(RHOAL*CPAL(TM)*(RM**3-RMINUS**3))
C..BEGIN INNER ITERATIONS   FOR CONVERGENCE OF EQ.(4.21)
                  DO IN=1,10
                      CALL CNODE(MTH,MZ,LAYER,THETA0,B,C)
                      CALL INNODE(MTH,MZ,LAYER,THETA0,A,B,C)
                      CALL EXNODE(MTH,MZ,LAYER,THETA0,A,B)
```

```
                    CALL TRIDAG(A,B,C,RHS,THETA1,MTH)
                    DO M=1,MTH
                        THETA0(M,LAYER)=THETA1(M)
                    ENDDO
                ENDDO
                TSUPPORT(MTIME,LAYER)=THETA0(MTH,LAYER)+T0
                TS=TSUPPORT(MTIME,LAYER)
C..CALCULATE THE EXITTING FLUID TEMPERATURE FOR THE NODE
                TFLUID(MTIME,LAYER)=(TF-TS)*EXP(-HCONV(TS)*SA
     &/(RHOF(TS)*VF*CPF(TS)))+TS
                PRINT 11,TIME,LAYER,TS,TFLUID(MTIME,LAYER)
C..INCREMENT TO NEXT BED LAYER
            ENDDO
C..END MICROWAVE PULSE DO LOOP
        ENDDO
C..BEGIN REST ITERATIONS WITH NO MICROWAVE FIELD
        DO J=NPULSE+1,NTOTAL
            MTIME=MTIME+1
            TIME=MTIME*DELT
            DO LAYER=1,MAXDZ
                TF=TFLUID(MTIME-1,LAYER-1)
                DO M=1,MTH-1
                    RHS(M)=THETA0(M,LAYER)
                ENDDO
                TM=THETA0(MTH,LAYER)+T0
                RM=DAL/2.0D0
                RMINUS=RM-DELR/2.0D0
                RHS(MTH)=THETA0(MTH,LAYER)+(TF-T0)*(3.0D0*DELT*HCONV(TM)
     &*RM**2)/(RHOAL*CPAL(TM)*(RM**3-RMINUS**3))
C..BEGIN INNER ITERATIONS FOR CONVERGENCE OF EQ.(4.21)
                DO IN=1,10
                    CALL CNODE(MTH,MZ,LAYER,THETA0,B,C)
                    CALL INNODE(MTH,MZ,LAYER,THETA0,A,B,C)
                    CALL EXNODE(MTH,MZ,LAYER,THETA0,A,B)
                    CALL TRIDAG(A,B,C,RHS,THETA1,MTH)
                    DO M=1,MTH
                        THETA0(M,LAYER)=THETA1(M)
                    ENDDO
                ENDDO
                TSUPPORT(MTIME,LAYER)=THETA0(MTH,LAYER)+T0
                TS=TSUPPORT(MTIME,LAYER)
C..CALCULATE THE EXITTING FLUID TEMPERATURE FOR THE NODE
                TFLUID(MTIME,LAYER)=(TF-TS)*EXP(-HCONV(TS)*SA
     &/(RHOF(TS)*VF*CPF(TS)))+TS
                PRINT 11,TIME,LAYER,TS,TFLUID(MTIME,LAYER)
C..INCREMENT TO NEXT BED LAYER
            ENDDO
C..END RELAXATION DO LOOP
        ENDDO
C..END MICROWAVE PULSE/RELAXATION DO LOOP
        ENDDO
C..WRITE OUTPUT TO FILES
         IDZ=NINT(DBLE(MAXDZ)/20.0D0)
```

```
      DO M=1,MTIME
        DO LAYER=1,MAXDZ,IDZ
         DS(M,LAYER)=TSUPPORT(M,LAYER)-273.0D0
         DF(M,LAYER)=TFLUID(M,LAYER)-273.0D0
        ENDDO
       ENDDO
       DO M=1,MTIME
        TIME=DBLE(M)*DELT
        WRITE(15,12) TIME,(DS(M,LAYER),LAYER=1,MAXDZ,IDZ)
        WRITE(13,12) TIME,(DF(M,LAYER),LAYER=1,MAXDZ,IDZ)
       ENDDO
      RETURN
      END
CCCCCCCCCCCCCCCCCCCCCCCCCCCCCCCCCCCCCCCCCCCCCCCCCCCCCCCCCCCCCCCCCCCCCCCCCCC
      FUNCTION BSIGPT(T)
C..BULK CONDUCTANCE OF PLATINUM
C  FROM HALLIDAY & RESNICK [24]
C
C  ALPHA        -RESISITIVITY COEFFICIENT
C  BSIGPT       -BULK CONDUCTIVITY OF PLATINUM (S/M)
C  RHO0         -RESISITIVITY AT 293K (OHMS)
C  T0           -BASE TEMPRERATURE (K)
C
      IMPLICIT DOUBLE PRECISION(A-H,O-Y)
      DATA RHO0,ALPHA,T0/10.6D-08,3.9D-03,2.93D+02/
      BSIGPT=1.0D0/(RHO0*ALPHA*(T-T0)+RHO0)
      RETURN
      END
CCCCCCCCCCCCCCCCCCCCCCCCCCCCCCCCCCCCCCCCCCCCCCCCCCCCCCCCCCCCCCCCCCCCCCCCCCC
      SUBROUTINE CNODE(MTH,MZ,LAYER,THETA0,B,C)
C..CALCULATES THE COEFFICIENTS OF THE CENTER NODE EQUATION
C  FOR THE A MATRIX IN EQ.(4.21)
C
C  B                -COEFFICIENT FOR MATRIX A IN EQ.(4.21)
C  C                -COEFFICIENT FOR MATRIX A IN EQ.(4.21)
C  CPAL             -SPECIFIC HEAT OF ALUMINA (J/KG K)
C  DELR             -DISTANCE BETWEEN FINITE-DIFFERENCE NODES (M)
C  DELT             -TIME STEP (S)
C  KPLUS            -AVERAGED THERMAL CONDUCTIVITY (W/M K)
C  LAYER            -CURRENT LAYER IN THE BED
C  RHOAL            -DENSITY OF ALUMINA (KG/M^3)
C  RM               -RADIAL POSITION (M)
C  RMINUS           -RADIAL POSITION MINUS DELR/2 (M)
C  RPLUS            -RADIAL POSITION PLUS DELR/2 (M)
C  THETA0           -TEMPERATURE RISE ARRAY AT THE CURRENT TIME STEP (K)
C  TM               -TEMPERATURE AT RM (K)
C  TMPLUS           -TEMPERATURE AT RMPLUS (K)
C
      IMPLICIT DOUBLE PRECISION(A-H,O-Y)
      IMPLICIT COMPLEX*16(Z)
      DOUBLE PRECISION B(1),C(1),THETA0(1:MTH,0:MZ),KAL,KPLUS
      COMMON/BLOCK3/DELR,DELT,NPT,NPULSE,NTOTAL
      COMMON/BLOCK4/RHOAL,DAL,TSHELL,SAPEL,VOLPEL
```

```
      COMMON/BLOCK8/T0,TF
      RM=0.0D0
      TM=THETA0(1,LAYER)+T0
      TMPLUS=THETA0(2,LAYER)+T0
      RPLUS=RM+DELR/2.0D0
      RMINUS=RM-DELR/2.0D0
      KPLUS=(KAL(TMPLUS)+KAL(TM))/2.0D0
      B(1)=1.0D0+6.0D0*(DELT/(RHOAL*CPAL(TM)*DELR**2))*KPLUS
      C(1)=-6.0D0*(DELT/(RHOAL*CPAL(TM)*DELR**2))*KPLUS
      RETURN
      END
CCCCCCCCCCCCCCCCCCCCCCCCCCCCCCCCCCCCCCCCCCCCCCCCCCCCCCCCCCCCCCCCCCCCCCCCCCC
      FUNCTION CPAL(T)
C..CALCULATES THE SPECIFIC HEAT OF THE ALUMINA USING A CUBIC SPLINE
C  INTERPOLATION OF DATA FROM INCROPERA AND DEWITT [25]
C
C  CPAL          -SPECIFIC HEAT OF ALUMINA (J/KG K)
C  NX            -NUMBER OF DATA POINTS
C  T             -TEMPERATURE (K)
C  XTEMP         -TEMPERATURE DATA POINTS (K)
C  Y2            -SECOND DERIVITIVES OBTAINED FROM SPLINE SUBROUTINE [REF]
C  YCPAL         -SPECIFIC HEAT DATA POINTS (J/KG K)
C  YINT          -CUBIC SPLINE INTERPOLATION FOR THE SPECIFIC HEAT
C                 OF ALUMINA (J/KG K)
C
      IMPLICIT DOUBLE PRECISION(A-H,O-Y)
      DOUBLE PRECISION XTEMP(4),YCPAL(4),Y2(4)
      DATA XTEMP/300.0D0,400.0D0,600.0D0,1000.0D0/
      DATA YCPAL/765.0D0,940.0D0,1110.0D0,1225.0D0/
      DATA Y2/0.0D+00,-8.5367647D-03,-1.3897059D-03,0.0D+00/
      DATA NX/4/
C..CALL THE INTERPOLATION SUBROUTINE
      CALL SPLINT(XTEMP,YCPAL,Y2,NX,T,YINT)
      CPAL=YINT
      RETURN
      END
CCCCCCCCCCCCCCCCCCCCCCCCCCCCCCCCCCCCCCCCCCCCCCCCCCCCCCCCCCCCCCCCCCCCCCCCCCC
      FUNCTION CPBU(T)
C..CALCULATES THE SPECIFIC HEAT CAPACITY OF BUTANE
C  FROM THE POLYNOMIAL FIT IN SONNTAG AND VAN WYLEN   [26]
C
C  A,B,C,D       -COEFFICIENTS
C  CPBU          -SPECIFICE HEAT OF BUTANE (J/KG/ K)
C  T             -TEMPERERATURE (K)
C  THETA         -TEMPORARY VARIABLE
C
      IMPLICIT DOUBLE PRECISION(A-H,O-Y)
      DATA A,B,C,D/3.954D0,37.12D0,-1.833D0,0.03498D0/
      THETA=T/100.0D0
      CPBU=A+B*THETA+C*THETA**2+D*THETA**3
      CPBU=CPBU/58.124D-03
      RETURN
```

```
      END
CCCCCCCCCCCCCCCCCCCCCCCCCCCCCCCCCCCCCCCCCCCCCCCCCCCCCCCCCCCCCCCCCCCCCCCCCCC
      FUNCTION CPF(T)
C..CALCULATES THE SPECIFIC HEAT OF THE GAS MIXTURE
C  FOLLOWS THE FORM OF THE PMIX FUNCTION
C
C  CPBU         -SPECIFIC HEAT FUNCTION FOR BUTANE (J/KG K)
C  CPF          -SPECIFIC HEAT OF THE GAS MIXTURE (J/KG K)
C  CPHE         -SPECIFIC HEAT OF HELIUM (J/KG K)
C  DEN          -TEMPORARY VARIABLE
C  RHOBU        -DENSITY FUNCTION FOR BUTANE (KG/M^3)
C  RHOHE        -DENSITY FUNCTION FOR HELIUM (KG/M^3)
C  TERM1        -TEMPORARY VARIABLE
C  TERM2        -TEMPORARY VARIABLE
C  VFBU         -VOLUME FLOW-RATE OF BUTANE (M^3/S)
C  VFHE         -VOLUME FLOW-RATE OF HELIUM (M^3/S)
C
      IMPLICIT DOUBLE PRECISION(A-H,O-Y)
      COMMON/BLOCK7/VFHE,VFBU,VF,FHE
      CPHE=5.193D+03
      TERM1=RHOHE(T)*VFHE
      TERM2=RHOBU(T)*VFBU
      DEN=TERM1+TERM2
      CPF=(TERM1/DEN)*CPHE+(TERM2/DEN)*CPBU(T)
      RETURN
      END
CCCCCCCCCCCCCCCCCCCCCCCCCCCCCCCCCCCCCCCCCCCCCCCCCCCCCCCCCCCCCCCCCCCCCCCCCCC
      FUNCTION E2(T)
C..CALCULATES THE ELECTRIC FIELD INSIDE THE PLATINUM PARTICLES
C  FROM ROUSSY [4]
C
C  E0           -APPLIED ELECTRIC FIELD
C  E2           -INTERNAL ELECTRIC FIELD (V/M)
C  EPDPA        -DIELECTRIC LOSS OF ALPHA ALUMINA (F/M)
C  EPDPG        -DIELECTRIC LOSS OF GAMMA ALUMINA (F/M)
C  EPPA         -DIELECTRIC CONSTANT OF ALPHA ALUMINA (F/M)
C  EPPG         -DIELECTRIC CONSTANT OF GAMMA ALUMINA (F/M)
C  IAL          -SPECIFIES SUPPORT MATERIAL
C  ZE2          -COMPLEX INTERNAL ELECTRIC FIELD VALUE (V/M)
C  ZCONJ        -COMPLEX CONJUGATE FUNCTION
C  ZEP1         -COMPLEX PERMITTIVITY OF THE ALUMINA SUPPORT (F/M)
C  ZEP2         -COMPLEX PERMITTIVITY OF THE PLATINUM (F/M)
C
      IMPLICIT DOUBLE PRECISION(A-H,O-Y)
      IMPLICIT COMPLEX*16(Z)
      COMMON/BLOCK1/IAL,IPT,IMIX,IQDOT,ITRISE
      COMMON/BLOCK2/EP0,PI,FREQ,E0
      IF (IAL.EQ.1) THEN
          ZEP1=DCMPLX(EPPA(T),-EPDPA(T))
       ELSEIF (IAL.EQ.2) THEN
          ZEP1=DCMPLX(EPPG(T),-EPDPG(T))
       ELSE
          PAUSE 'E2 FUNCTION FAILED'
```

```
      ENDIF
      ZEP2=DCMPLX(1.0D0,-EPDPPT(T))
      ZE2=E0*(3.0D0*ZEP1)/(2.0D0*ZEP1+ZEP2)
      E2=DSQRT(DREAL(ZE2*ZCONJ(ZE2)))
      RETURN
      END
CCCCCCCCCCCCCCCCCCCCCCCCCCCCCCCCCCCCCCCCCCCCCCCCCCCCCCCCCCCCCCC
      FUNCTION EPDPA(T)
C..DIELECTRIC LOSS OF ALPHA ALUMINA [30]
C  FROM A POLYNOMIAL FIT TO DATA OF CROSS AND BINNER
C
C  EPDPA    -DIELECTRIC LOSS OF ALPHA ALUMINA (F/M)
C
     IMPLICIT DOUBLE PRECISION(A-H,O-Z)
     DOUBLE PRECISION B(2)
     DATA B/-0.1400,3.3333D-04/
     DATA TREF/2.73D+02/
     BASE=3.0D-02
     X=T-TREF
     IF(X.LE.6.0D+02)THEN
       EPDPA=(0.06D0-BASE)*(X/6.0D+02)**2+BASE
     RETURN
      ELSE
     EPDPA=B(1)+B(2)*X
     ENDIF
      END
CCCCCCCCCCCCCCCCCCCCCCCCCCCCCCCCCCCCCCCCCCCCCCCCCCCCCCCCCCCCCCC
      FUNCTION EPDPG(T)
C..DIELECTRIC LOSS OF GAMMA ALUMINA USING A CUBIC SPLINE INTERPOLATION [31]
C
C  EPDPG          -DIELECTRIC LOSS OF GAMMA ALUMINA (F/M)
C  NX             -NUMBER OF DATA POINTS
C  T              -TEMPERATURE (K)
C  XTEMP          -TEMPERATURE DATA POINTS (K)
C  Y2             -SECOND DERIVATIVE OBTAINED THROUGH SPLINE SUBROUTINE
C  YEPDP          -DIELECTRIC LOSS DATA POINTS (F/M)
C  YINT           -CUBIC SPLINE INTERPOLATION (F/M)
C
      IMPLICIT DOUBLE PRECISION(A-H,O-Y)
      DOUBLE PRECISION XTEMP(12),YEPDP(12),Y2(12)
      DATA XTEMP/302.0D0,308.0D0,422.0D0,535.0D0,644.0D0,751.0D0,
      &855.0D0,957.0D0,1057.0D0,1154.0D0,1249.0D0,1341.0D0/
      DATA YEPDP/0.39213D0,0.38927D0,0.22602D0,0.17027D0,0.15228D0,
      &0.15409D0,0.14686D0,0.15471D0,0.14539D0,0.16813D0,0.19206D0,
      &0.13106D0/
      DATA Y2/0.0D+00,-3.4071793D-05,2.1448466D-05,-1.9600969D-06,
      &3.8211751D-06,-3.2273509D-06,4.1775541D-06,-4.9669384D-06,
      &5.5956789D-06,2.6576733D-06,-1.5353231D-05,0.0D+00/
      DATA NX/12/
      IF(T.GT.1341.0D0)THEN
           EPDPG=0.16156D0
        ELSE
           CALL SPLINT(XTEMP,YEPDP,Y2,NX,T,YINT)
```

```
          EPDPG=YINT
      ENDIF
      RETURN
      END
CCCCCCCCCCCCCCCCCCCCCCCCCCCCCCCCCCCCCCCCCCCCCCCCCCCCCCCCCCCCCCCCCCCCCCCCCCCCCC
      FUNCTION EPDPPT(T)
C..DIELECTRIC LOSS OF PLATINUM
C
C  BSIGPT       -BULK CONDUCTIVITY FUNCTION FOR PLATINUM (S/M)
C  EP0          -PERMITTIVITY OF FREE SPACE
C  EPDPPT       -DIELECTRIC LOSS OF PLATINUM (F/M)
C  FREQ         -MICROWAVE FREQUENCY
C  IPT          -SPECIFIES BULK OR SIZE DEPENDENT VALUES
C  QSIGPT       -SIZE-DEPENDENT CONDUCTIVITY FUNCTION FOR PLATINUM (S/M)
C
      IMPLICIT DOUBLE PRECISION(A-H,O-Y)
      COMMON/BLOCK1/IAL,IPT,IMIX,IQDOT,ITRISE
      COMMON/BLOCK2/EP0,PI,FREQ,E0
      IF (IPT.EQ.1) THEN
          EPDPPT=BSIGPT(T)/(2.0D0*PI*FREQ*EP0)
       ELSEIF(IPT.EQ.2) THEN
          EPDPPT=QSIGPT(T)/(2.0D0*PI*FREQ*EP0)
       ELSE
          PAUSE 'EPDPT FUNCTION FAILED'
      ENDIF
      RETURN
      END
CCCCCCCCCCCCCCCCCCCCCCCCCCCCCCCCCCCCCCCCCCCCCCCCCCCCCCCCCCCCCCCCCCCCCCCCCCCCCC
      FUNCTION EPPA(T)
C..DIELECTRIC CONSTANT OF ALPHA ALUMINA [30]
C  FROM A POLYNOMIAL FIT TO DATA OF CROSS AND BINNER
C
      IMPLICIT DOUBLE PRECISION(A-H,O-Z)
      DOUBLE PRECISION A(5)
      DATA A/7.331D0,-9.120D-04,6.428D-06,-6.531D-09,2.578D-12/
      DATA TREF/2.73D+02/
      SUM=0.0D0
      DO 5 I=1,4
          SUM=(T-TREF)*(SUM+A(6-I))
5     CONTINUE
      EPPA=SUM+A(1)
      RETURN
      END
CCCCCCCCCCCCCCCCCCCCCCCCCCCCCCCCCCCCCCCCCCCCCCCCCCCCCCCCCCCCCCCCCCCCCCCCCCCCCC
      FUNCTION EPPG(T)
C..DIELECTRIC CONSTANT OF GAMMA ALUMINA [31]

C  USING A CUBIC SPLINE INTERPOLATION
C
C  EPPG         -DIELECTRIC CONSTANT OF GAMMA ALUMINA (F/M)
C  NX           -NUMBER OF DATA POINTS
C  T            -TEMPERATURE (K)
C  Y2           -SECOND DERIVITIVES FROM SPLINE SUBROUTINE
```

```
C  YEPP          -DIELECTRIC CONSTANT DATA (F/M)
C  YINT          -CUBIC SPLINE INTERPOLATION (F/M)
C
      IMPLICIT DOUBLE PRECISION(A-H,O-Y)
      DOUBLE PRECISION XTEMP(12),YEPP(12),Y2(12)
      DATA XTEMP/302.0D0,308.0D0,422.0D0,535.0D0,644.0D0,751.0D0,
     &855.0D0,957.0D0,1057.0D0,1154.0D0,1249.0D0,1341.0D0/
      DATA YEPP/4.487D0,4.4982D0,5.0396D0,4.4478D0,4.6517D0,4.9169D0,
     &4.6465D0,4.441D0,4.3126D0,4.196D0,4.0462D0,3.7173D0/
      DATA Y2/0.0D+00,1.7357089D-04,-2.1370419D-04,1.5324666D-04,
     &-1.143195D-05,-7.5870177D-05,2.6628896D-05,4.2270398D-06,
     &-3.963615D-07,2.320529D-06,-3.2645448D-05,0.0D+00/
      DATA NX/12/
      IF(T.GT.1341)THEN
          EPPG=3.7173D0
       ELSE
          CALL SPLINT(XTEMP,YEPP,Y2,NX,T,YINT)
          EPPG=YINT
      ENDIF
      RETURN
      END
CCCCCCCCCCCCCCCCCCCCCCCCCCCCCCCCCCCCCCCCCCCCCCCCCCCCCCCCCCCCCCCCCCCCCCCCCCC
      SUBROUTINE EXNODE(MTH,MZ,LAYER,THETA0,A,B)
C..CALCULATES THE COEFFICIENTS OF THE EXTERIOR NODE
C  FOR THE A MATRIX IN EQ.(4.21)
C
C  A               -COEFFICIENT FOR MATRIX A IN EQ.(4.21)
C  B               -COEFFICIENT FOR MATRIX A IN EQ.(4.21)
C  CPAL            -SPECIFIC HEAT OF ALUMINA (J/KG K)
C  DELR            -DISTANCE BETWEEN FINITE-DIFFERENCE NODES (M)
C  DELT            -TIME STEP (S)
C  KMINUS          -AVERAGED THERMAL CONDUCTIVITY (W/M K)
C  KPLUS           -AVERAGED THERMAL CONDUCTIVITY (W/M K)
C  LAYER           -CURRENT LAYER IN THE BED
C  MTH             -EXTERIOR NODE NUMBER
C  RHOAL           -DENSITY OF ALUMINA (KG/M^3)
C  RM              -RADIAL POSITION (M)
C  RMINUS          -RADIAL POSITION MINUS DELR/2 (M)
C  THETA0          -TEMPERATURE RISE ARRAY AT THE CURRENT TIME STEP (K)
C  TM              -TEMPERATURE AT RM (K)
C  TMMINUS         -TEMPERATURE AT MTH-1(K)
C  TMPLUS          -TEMPERATURE AT RMPLUS (K)
C
      IMPLICIT DOUBLE PRECISION(A-H,O-Y)
      IMPLICIT COMPLEX*16(Z)
      DOUBLE PRECISION A(MTH),B(MTH),THETA0(1:MTH,0:MZ),KMINUS,KAL
      COMMON/BLOCK3/DELR,DELT,NPT,NPULSE,NTOTAL
      COMMON/BLOCK4/RHOAL,DAL,TSHELL,SAPEL,VOLPEL
      COMMON/BLOCK8/T0,TF
      TMMINUS=THETA0(MTH-1,LAYER)+T0
      TM=THETA0(MTH,LAYER)+T0
      RM=DAL/2.0D0
      RMINUS=RM-DELR/2.0D0
```

```
      KMINUS=(KAL(TMMINUS)+KAL(TM))/2.0D0
      A(MTH)=-(3.0D0*DELT*KMINUS*RMINUS**2)/(RHOAL*CPAL(TM)*DELR*
     &(RM**3-RMINUS**3))
      B(MTH)=(1.0D0+
     &(3.0D0*DELT*KMINUS*RMINUS**2)/(RHOAL*CPAL(TM)*DELR*
     &(RM**3-RMINUS**3))+(3.0D0*DELT*HCONV(TM)*RM**2)/
     &(RHOAL*CPAL(TM)*(RM**3-RMINUS**3)))
      RETURN
      END
CCCCCCCCCCCCCCCCCCCCCCCCCCCCCCCCCCCCCCCCCCCCCCCCCCCCCCCCCCCCCCCCCCCCCCCCCC
      FUNCTION HCONV(T)
C..CONVECTION COEFFICIENT USING CORRELATIONS FOR A SPHERE IN CROSS-FLOW,
C  PACKED BED, OR FLUIDIZED BED
C
C  C1              -CONSTANT FOR EQ.(4.28)
C  C2              -CONSTANT FOR EQ.(4.28)
C  CPF             -SPECIFIC HEAT OF THE GAS (J/KG K)
C  DAL             -DIAMETER OF THE ALUMINA PELLET (M)
C  HCONV           -CONVECTION COEFFICIENT (W/M^2)
C  HTUBE           -HEIGHT OF THE CATALYST BED (M)
C  KF              -THERMAL CONDUCTIVITY OF THE GAS (W/M K)
C  MODEL           -SPECIFIES CROSS-FLOW, PACKED BED, OR FLUIDIZED BED
C  POROSITY        -VOID FRACTION OF THE BED
C  PR              -PRANDTL NUMBER OF THE GAS
C  RE              -REYNOLDS NUMBER BASED ON ALUMINA PELLET DIAMETER
C  RHOF            -DENSITY OF THE GAS MIXTURE (KG/M^3)
C  T               -PELLET SURFACE TEMPERATURE (K)
C  TF              -MEAN GAS TEMPERATURE (K)
C  U0              -SUPERFICIAL GAS VELOCITY (M/S)
C  VF              -VOLUME FLOW OF THE MIXTURE (M^3/S)
C  VISCF           -VISCOSITY OF THE GAS MIXTURE (KG/M S)
C  VOLTUBE         -VOLUME OF THE CATALYST BED (M^3)
C
      IMPLICIT DOUBLE PRECISION(A-H,O-Y)
      DOUBLE PRECISION KF
      COMMON/BLOCK0/MODEL
      COMMON/BLOCK4/RHOAL,DAL,TSHELL,SAPEL,VOLPEL
      COMMON/BLOCK6/DTUBE,HTUBE,VOLTUBE,POROSITY,MAXDZ
      COMMON/BLOCK7/VFHE,VFBU,VF,FHE
      COMMON/BLOCK8/T0,TF
      U0=VF/(VOLTUBE/HTUBE)
      RE=U0*DAL*RHOF(T)/VISCF(T)
      PR=(CPF(T)*VISCF(T))/KF(T)
      IF(MODEL.EQ.1)THEN
C..CORRELATION FOR A SPHERE IN CROSS-FLOW FROM J.P.HOLMAN, EQ.(4.26)
         HCONV=(KF(T)/DAL)*(2.0D0+(0.4D0*RE**(0.5D0)+0.06*RE**(1.0D0/3.0D0)
     &)*(PR**0.4D0)*((VISCF(TF)/VISCF(T))**0.25D0))
         RETURN
      ELSEIF(MODEL.EQ.2)THEN
C..CORRELATION FOR A PACKED BED OFFERED BY BEASLEY AND CLARK, EQ.(4.28)
         C1=2.031D0
         C2=0.049D0
         HCONV=(KF(T)/DAL)*(2.0D0+C1*RE**(0.5D0)*PR**(1.0D0/3.0D0)+
```

```
   &C2*RE*PR**(0.5D0))
         RETURN
      ELSEIF(MODEL.EQ.3)THEN
C..CORRELATION FOR A FLUIDIZED BED OFFERED BY ZABRODSKY, EQ.(4.29)
         HCONV=(KF(T)/DAL)*(2.0D0/(1.0D0-(1.0D0-POROSITY)**(1.0D0/3.0D0)))
         RETURN
      ELSE
         PAUSE 'H FUNCTION NOT SPECIFIED'
      ENDIF
      RETURN
      END
CCCCCCCCCCCCCCCCCCCCCCCCCCCCCCCCCCCCCCCCCCCCCCCCCCCCCCCCCCCCCCCCCCCCCCCCCCC
      SUBROUTINE INNODE(MTH,MZ,LAYER,THETA0,A,B,C)
C..CALCULATES THE COEFFICIENTS OF THE GENERAL, INTERIOR NODES
C  FOR THE A MATRIX IN EQ.(4.21)
C
C  A              -COEFFICIENT FOR MATRIX A IN EQ.(4.21)
C  B              -COEFFICIENT FOR MATRIX A IN EQ.(4.21)
C  C              -COEFFICIENT FOR MATRIX A IN EQ.(4.21)
C  CPAL           -SPECIFIC HEAT OF ALUMINA (J/KG K)
C  DELR           -DISTANCE BETWEEN FINITE-DIFFERENCE NODES (M)
C  DELT           -TIME STEP (S)
C  KMINUS         -AVERAGED THERMAL CONDUCTIVITY (W/M K)
C  KPLUS          -AVERAGED THERMAL CONDUCTIVITY (W/M K)
C  LAYER          -CURRENT LAYER IN THE BED
C  M              -NODE  NUMBER
C  MTH            -EXTERIOR NODE NUMBER
C  RHOAL          -DENSITY OF ALUMINA (KG/M^3)
C  RM             -RADIAL POSITION (M)
C  RMINUS         -RADIAL POSITION MINUS DELR/2 (M)
C  RPLUS          -RADIAL POSITION PLUS DELR/2 (M)
C  THETA0         -TEMPERATURE RISE ARRAY AT THE CURRENT TIME STEP (K)
C  TM             -TEMPERATURE AT RM (K)
C  TMMINUS        -TEMPERATURE AT THE PREVIOUS NODE (K)
C  TMPLUS         -TEMPERATURE AT RMPLUS (K)
C
      IMPLICIT DOUBLE PRECISION(A-H,O-Y)
      IMPLICIT COMPLEX*16(Z)
      DOUBLE PRECISION A(MTH),B(MTH),C(MTH),THETA0(1:MTH,0:MZ),
     &KPLUS,KMINUS,KAL
      COMMON/BLOCK3/DELR,DELT,NPT,NPULSE,NTOTAL
      COMMON/BLOCK4/RHOAL,DAL,TSHELL,SAPEL,VOLPEL
      COMMON/BLOCK8/T0,TF
      DO M=2,(MTH-1)
       RM=DBLE(M-1)*DELR
       TMMINUS=THETA0(M-1,LAYER)+T0
       TM=THETA0(M,LAYER)+T0
       TMPLUS=THETA0(M+1,LAYER)+T0
       RPLUS=RM+DELR/2.0D0
       RMINUS=RM-DELR/2.0D0
       KPLUS=(KAL(TMPLUS)+KAL(TM))/2.0D0
       KMINUS=(KAL(TMMINUS)+KAL(TM))/2.0D0
       A(M)=-(3.0D0*DELT*KMINUS*RMINUS**2)/(RHOAL*CPAL(TM)*DELR
```

```
     &*(RPLUS**3-RMINUS**3))
       B(M)=(1.0D0+((3.0D0*DELT*(KMINUS*RMINUS**2+KPLUS*RPLUS**2))
     &/(RHOAL*CPAL(TM)*DELR*(RPLUS**3-RMINUS**3))))
       C(M)=-(3.0D0*DELT*KPLUS*RPLUS**2)/(RHOAL*CPAL(TM)*DELR
     &*(RPLUS**3-RMINUS**3))
      ENDDO
      RETURN
      END
CCCCCCCCCCCCCCCCCCCCCCCCCCCCCCCCCCCCCCCCCCCCCCCCCCCCCCCCCCCCCCCCCCCCCCCCCCC
      FUNCTION KAL(T)
C..THERMAL CONDUCTIVITY OF ALUMINA
C  USING A CUBIC SPLINE INTERPOLATION OF DATA FROM A. F. MILLS [27]
C
C  KAL              -THERMAL CONDUCTIVITY OF ALUMINA (W/M K)
C  T                -TEMPERATURE (K)
C  XTEMP            -TEMPERATURE DATA (K)
C  Y2               -SECOND DERIVATIVES FROM SPLINE SUBROUTINE
C  YINT             -CUBIC SPLINE INTERPOLATION (W/M K)
C  YKAL             -THERMAL CONDUCTIVITY DATA (W/M K)
C
      IMPLICIT DOUBLE PRECISION(A-H,O-Y)
      DOUBLE PRECISION XTEMP(5),YKAL(5),Y2(5),KAL
      DATA XTEMP/300.0D0,400.0D0,600.0D0,1000.0D0,1500.0D0/
      DATA YKAL/36.0D0,27.0D0,16.0D0,7.6D0,5.4D0/
      DATA Y2/0.0D+00,3.1429787D-04,1.0710638D-04,3.1531915D-05,0.0D+00/
      DATA NX/5/
      CALL SPLINT(XTEMP,YKAL,Y2,NX,T,YINT)
      KAL=YINT
      RETURN
      END
CCCCCCCCCCCCCCCCCCCCCCCCCCCCCCCCCCCCCCCCCCCCCCCCCCCCCCCCCCCCCCCCCCCCCCCCCCC
      FUNCTION KBU(T)
C..THERMAL CONDUCTIVITY OF BUTANE
      IMPLICIT DOUBLE PRECISION(A-H,O-Y)
      DOUBLE PRECISION KBU
      DOUBLE PRECISION TPTS(4),KBUS(4)
      DATA TPTS/2.73D+02,2.98D+02,4.73D+02,6.73D+02/
      DATA KBUS/0.015D0,0.0162D0,0.039D0,0.074D0/
      IF(T.GE.TPTS(4))THEN
        A=(KBUS(4)-KBUS(3))/(TPTS(4)-TPTS(3))
        B=KBUS(4)-A*TPTS(4)
        KBU=A*T+B
        RETURN
      ENDIF
      DO I=1,3
        X=TPTS(I)
        Y=TPTS(I+1)
        IF(T.EQ.X)THEN
           KBU=KBUS(I)
           RETURN
        ELSEIF(T.GT.X.AND.T.LT.Y)THEN
          KBU=KBUS(I)+(T-X)*(KBUS(I+1)-KBUS(I))/(Y-X)
           RETURN
```

```
      ENDIF
     ENDDO
     RETURN
     END
CCCCCCCCCCCCCCCCCCCCCCCCCCCCCCCCCCCCCCCCCCCCCCCCCCCCCCCCCCCCCCCCCCCCCCCCCCCCCC
     FUNCTION KF(T)
C..THERMAL CONDUCTION OF THE GAS MIXTURE USING PMIX FUNCTION
C
C  KBU          -THERMAL CONDUCTIVITY OF BUTANE (W/M K)
C  KF           -THERMAL CONDUCTIVITY OF THE GAS MIXTURE (W/M K)
C  KHE          -THERMAL CONDUCTIVITY OF HELIUM (W/M K)
C  P1           -THERMAL CONDUCTIVITY OF HELIUM (W/M K)
C  P2           -THERMAL CONDUCTIVITY OF BUTANE (W/M K)
C  PMIX         -PROPERTY MIXTURE FUNCTION
C
     IMPLICIT DOUBLE PRECISION(A-H,O-Y)
     DOUBLE PRECISION KHE,KBU,KF
     P1=KHE(T)
     P2=KBU(T)
     KF=PMIX(P1,P2)
     RETURN
     END
CCCCCCCCCCCCCCCCCCCCCCCCCCCCCCCCCCCCCCCCCCCCCCCCCCCCCCCCCCCCCCCCCCCCCCCCCCCCCC
     FUNCTION KHE(T)
C..THERMAL CONDUCTIVITY OF HELIUM
C  USING A CUBIC SPLINE INTERPOLATION OF DATA FROM KAYS AND CRAWFORD [28]
C
C  KHE          -THERMAL CONDUCTIVITY OF HELIUM (W/M K)
C  T            -TEMPERATURE (K)
C  XTEMP        -TEMPERATURE DATA (K)
C  Y2           -SECOND DERIVATIVES FROM SPLINE SUBROUTINE
C  YINT         -CUBIC SPLINE INTERPOLATION (W/M K)
C  YKHE         -THERMAL CONDUCTIVITY DATA (W/M K)
C
     IMPLICIT DOUBLE PRECISION(A-H,O-Y)
     DOUBLE PRECISION XTEMP(15),YKHE(15),Y2(15),KHE
     DATA XTEMP/2.5D+02,3.0D+02,3.5D+02,4.0D+02,4.5D+02,5.0D+02,
    &6.0D+02,7.0D+02,8.0D+02,9.0D+02,1.0D+03,1.1D+03,1.2D+03,
    &1.3D+03,1.4D+03/
     DATA YKHE/13.7D-02,15.5D-02,17.2D-02,18.9D-02,20.5D-02,22.1D-02,
    &25.1D-02,28.0D-02,30.7D-02,33.4D-02,36.0D-02,38.5D-02,41.0D-02,
    &43.4D-02,45.7D-02/
     DATA Y2/0.0D+00,-6.9124103D-07,3.6496411D-07,-7.686154D-07,
    &3.0949749D-07,-4.6937455D-07,5.3374894D-08,-3.4412503D-07,
    &1.2312522D-07,-1.4837586D-07,-1.2962178D-07,6.6862976D-08,
    &-1.3783013D-07,-1.1554247D-07,0.0D+00/
     DATA NX/15/
    CALL SPLINT(XTEMP,YKHE,Y2,NX,T,YINT)
     KHE=YINT
     RETURN
     END
CCCCCCCCCCCCCCCCCCCCCCCCCCCCCCCCCCCCCCCCCCCCCCCCCCCCCCCCCCCCCCCCCCCCCCCCCCCCCC
     FUNCTION PMIX(P1,P2)
```

```
C..FINDS VISCOSITY AND THERMAL CONDUCTION OF GAS MIXTURES
C
C  FHE          -VOLUME FRACTION OF HELIUM
C  MW1          -MOLECULAR WEIGHT OF HELIUM
C  MW2          -MOLECULAR WEIGHT OF BUTANE
C  P1           -VISCOSITY OR CONDUCTIVITY OF HELIUM
C  P2           -VISCOSITY OR CONDUCTIVITY OF BUTANE
C
      IMPLICIT DOUBLE PRECISION(A-H,O-Y)
      DOUBLE PRECISION MW1,MW2
      COMMON/BLOCK7/VFHE,VFBU,VF,FHE
      DATA MW1,MW2/4.0D0,58.12D0/
      X1=(FHE/MW1)/(FHE/MW1+(1.0D0-FHE)/MW2)
      X2=1.0D0-X1
      TERM1=1.0D0+DSQRT(P1/P2)*(MW2/MW1)**(0.25D0)
      TERM1=TERM1/DSQRT(8.0D0*(1.0D0+MW1/MW2))
      PHI12=TERM1
      TERM1=1.0D0+DSQRT(P2/P1)*(MW1/MW2)**(0,25D0)
      TERM1=TERM1/DSQRT(8.0D0*(1.0D0+MW2/MW1))
      PHI21=TERM1
      PHI11=1.0D0
      PHI22=1.0D0
      PMIX=X1*P1/(X1*PHI11+X2*PHI12)+X2*P2/(X1*PHI21+X2*PHI22)
      RETURN
      END
CCCCCCCCCCCCCCCCCCCCCCCCCCCCCCCCCCCCCCCCCCCCCCCCCCCCCCCCCCCCCCCCCCCCCCCCCCCCCCC
      FUNCTION QSIGPT(T)
C..SIZE DEPENDENT ELECTRICAL CONDUCTIVITY OF PLATINUM
C
C  BSIGPT       -BULK CONDUCTIVITY OF PT (S/M)
C  DPT          -PLATINUM PARTICLE DIAMETER (M)
C
      IMPLICIT DOUBLE PRECISION(A-H,O-Y)
      COMMON/BLOCK5/DPT,CPPT,RHOPT,FPT
      QSIGPT=BSIGPT(T)*((DPT/5.0D-06)**3)
      RETURN
      END
CCCCCCCCCCCCCCCCCCCCCCCCCCCCCCCCCCCCCCCCCCCCCCCCCCCCCCCCCCCCCCCCCCCCCCCCCCCCCCC
      FUNCTION RHOBU(T)
C..CALCULATES THE DENSITY OF BUTANE BY INTERPOLATING A
C  CUBIC SPLINE FOR DATA GIVEN IN THE CRC HANDBOOK [28]
C
C  NX               -NUMBER OF DATA POINTS
C  RHOBU            -DENSITY OF BUTANE (KG/M^3)
C  T                -TEMPERATURE (K)
C  XTEMP            -TEMPERATURE DATA (K)
C  Y2               -SECOND DERIVATIVES FROM SPLINE SUBROUTINE
C  YINT             -CUBIC SPLINE INTERPOLATION (KG/M^3)
C  YRHO             -DENSITY DATA (KG/M^3)
C
      IMPLICIT DOUBLE PRECISION(A-H,O-Y)
      DOUBLE PRECISION XTEMP(7),YRHO(7),Y2(7)
      DATA XTEMP/2.73D02,3.73D02,4.73D02,5.73D02,6.73D02,7.73D02,
```

```
   &8.73D02/
     DATA YRHO/2.59D0,1.9D0,1.5D0,1.24D0,1.05D0,9.16D-01,8.12D-01/
     DATA Y2/0.0D+00,4.1250769D-05,8.9969231D-06,6.7615385D-06,
   &5.9569231D-06,3.0107692D-06,0.0D+00/
     DATA NX/7/
     IF(T.GT.8.73D02)THEN
          RHOBU=8.12D-01
     ELSE
          CALL SPLINT(XTEMP,YRHO,Y2,NX,T,YINT)
          RHOBU=YINT
     ENDIF
     RETURN
     END
CCCCCCCCCCCCCCCCCCCCCCCCCCCCCCCCCCCCCCCCCCCCCCCCCCCCCCCCCCCCCCCCCCCCCCCCCCC
     FUNCTION RHOF(T)
C..CALCULATES THE DENSITY OF THE HELIUM-BUTANE MIXTURE
C
C  RHOBU          -DENSITY OF BUTANE (KG/M^3)
C  RHOF           -DENSITY OF THE GAS MIXTURE (KG/M^3)
C  RHOHE          -DENSITY OF HELIUM (KG/M^3)
C  VF             -VOLUME FLOW RATE OF THE GAS (M^3/S)
C  VFBU           -VOLUME FLOW RATE OF THE BUTANE (M^3/S)
C  VFHE           -VOLUME FLOW RATE OF THE HELIUM (M^3/S)
C
     IMPLICIT DOUBLE PRECISION(A-H,O-Y)
     COMMON/BLOCK7/VFHE,VFBU,VF,FHE
     RHOF=(RHOHE(T)*VFHE+RHOBU(T)*VFBU)/VF
     RETURN
     END
CCCCCCCCCCCCCCCCCCCCCCCCCCCCCCCCCCCCCCCCCCCCCCCCCCCCCCCCCCCCCCCCCCCCCCCCCCC
     FUNCTION RHOHE(T)
C..CALCULATES THE DENSITY OF HELIUM USING THE IDEAL GAS EQUATION OF STATE
C
C  PATM        -PRESSURE OF THE GASS ASSUMING ATMOSPHERIC PRESSURE
C  RHE         -GAS CONSTANT OF HELIUM
C  RHOHE       -DENSITY OF HELIUM (KG/M^3)
C  T           -TEMPERATURE (K)
C
     IMPLICIT DOUBLE PRECISION(A-H,O-Y)
     DATA PATM,RHE/101.325D+03,2.07703D+03/
     RHOHE=PATM/(RHE*T)
     RETURN
     END
CCCCCCCCCCCCCCCCCCCCCCCCCCCCCCCCCCCCCCCCCCCCCCCCCCCCCCCCCCCCCCCCCCCCCCCCCCC
SUBROUTINE SPLINE(X,Y,N,YP1,YPN,Y2)
C..CALCULATES THE SECOND DERIVITIVES FOR THE CUBIC SPLINE INTERPOLATION
C  FROM NUMERICAL RECIPIES IN FORTRAN 77 [16]
    INTEGER N,NMAX
    DOUBLE PRECISION YP1,YPN,X(N),Y(N),Y2(N)
    PARAMETER (NMAX=500)
    INTEGER I,K
    DOUBLE PRECISION P,QN,SIG,UN,U(NMAX)
    IF (YP1.GT..99E30) THEN
```

```
      Y2(1)=0.
      U(1)=0.
     ELSE
      Y2(1)=-0.5
      U(1)=(3./(X(2)-X(1)))*((Y(2)-Y(1))/(X(2)-X(1))-YP1)
     ENDIF
     DO 11 I=2,N-1
      SIG=(X(I)-X(I-1))/(X(I+1)-X(I-1))
      P=SIG*Y2(I-1)+2.
      Y2(I)=(SIG-1.)/P
      U(I)=(6.*((Y(I+1)-Y(I))/(X(I+
    *1)-X(I))-(Y(I)-Y(I-1))/(X(I)-X(I-1)))/(X(I+1)-X(I-1))-SIG*

    *U(I-1))/P
11    CONTINUE
     IF (YPN.GT..99E30) THEN
      QN=0.
      UN=0.
     ELSE
      QN=0.5
      UN=(3./(X(N)-X(N-1)))*(YPN-(Y(N)-Y(N-1))/(X(N)-X(N-1)))
     ENDIF
     Y2(N)=(UN-QN*U(N-1))/(QN*Y2(N-1)+1.)
     DO 12 K=N-1,1,-1
      Y2(K)=Y2(K)*Y2(K+1)+U(K)
12    CONTINUE
     RETURN
     END
CCCCCCCCCCCCCCCCCCCCCCCCCCCCCCCCCCCCCCCCCCCCCCCCCCCCCCCCCCCCCCCCCCCCCCCCCCC
      SUBROUTINE SPLINT(XA,YA,Y2A,N,X,Y)
C..CUBIC SPLINE INTERPOLATION SUBROUTINE
C  FROM NUMERICAL RECIPIES IN FORTRAN 77 [16]
     INTEGER N
     DOUBLE PRECISION X,Y,XA(N),Y2A(N),YA(N)
     INTEGER K,KHI,KLO
     DOUBLE PRECISION A,B,H
     KLO=1
     KHI=N
1     IF (KHI-KLO.GT.1) THEN
      K=(KHI+KLO)/2
      IF(XA(K).GT.X)THEN
        KHI=K
      ELSE
        KLO=K
      ENDIF
     GOTO 1
     ENDIF
     H=XA(KHI)-XA(KLO)
     IF (H.EQ.0.) PAUSE 'BAD XA INPUT IN SPLINT'
     A=(XA(KHI)-X)/H
     B=(X-XA(KLO))/H
     Y=A*YA(KLO)+B*YA(KHI)+((A**3-A)*Y2A(KLO)+(B**3-B)*Y2A(KHI))*(H**
    *2)/6.
```

```
      RETURN
      END
CCCCCCCCCCCCCCCCCCCCCCCCCCCCCCCCCCCCCCCCCCCCCCCCCCCCCCCCCCCCCCCCCCCCCCCCCCCCCCC
      SUBROUTINE SOURCE(MTH,MZ,NLAYER,THETA0,QDOT)
C..CALCULATES THE HEAT GENERATION WITHIN THE ALUMINA PELLET
C  USING A MIXTURE FORMULA TO MODEL THE EFFECTIVE PERMITTIVITY OF
C  THE PT/AL2O3 MIXTURE REGION
C
C  DAL          -DIAMETER OF ALUMINA PELLET (M)
C  E0           -APPLIED ELECTRIC FIELD STRENGTH (V/M)
C  EP0          -PERMITTIVITY OF FREE SPACE (F/M)
C  EPDPA        -DIELECTRIC LOSS OF ALPHA ALUMINA (F/M)
C  EPDPG        -DIELECTRIC LOSS OF GAMMA ALUMINA (F/M)
C  FREQ         -FREQUENCY OF THE MICROWAVE FIELD (HZ)
C  IAL          -SPECIFIES ALPHA OR GAMMA ALUMINA
C  MTH          -NUMBER OF FINITE-DIFFERENCE NODES WITHIN THE ALUMINA PELLET
C  NLAYER       -CURRENT CATALYST BED LAYER
C  NODES        -NUMBER OF FINITE-DIFFERENCE NODES WITHIN THE PT/AL2O3
C                MIXTURE REGION
C  QDOT         -VOLUMETRIC HEAT GENERATION VECTOR (W/M^3)
C  RATIO        -TEMPORARY VARIABLE
C  THETA0       -TEMPERATURE RISE ARRAY AT THE CURRENT TIME STEP (K)
C  TSHELL       -THICKNESS OF THE PT/AL2O3 MIXTURE REGION
C  ZEPM         -COMPLEX PERMITTIVITY OF THE MIXTURE REGION (F/M)
C
      IMPLICIT DOUBLE PRECISION(A-H,O-Y)
      IMPLICIT COMPLEX*16(Z)
      DOUBLE PRECISION QDOT(MTH),THETA0(1:MTH,0:MZ)
      COMMON/BLOCK1/IAL,IPT,IMIX,IQDOT,ITRISE
      COMMON/BLOCK2/EP0,PI,FREQ,E0
      COMMON/BLOCK4/RHOAL,DAL,TSHELL,SAPEL,VOLPEL
      COMMON/BLOCK5/DPT,CPPT,RHOPT,FPT
      COMMON/BLOCK8/T0,TF
C..CALCULATE THE NUMBER OF NODES WITHING THE SHELL
      RATIO=TSHELL/(DAL/2.0D0)
      NODES=NINT(RATIO*MTH)+1
C..CALCULATE THE INTERIOR HEAT GENERATION OF THE PELLET
      DO M=1,(MTH-NODES)
          IF (IAL.EQ.1) THEN
              QDOT(M)=ABS(PI*FREQ*EP0*EPDPA(THETA0(M,NLAYER)+T0)*E0**2)
          ELSEIF (IAL.EQ.2) THEN
              QDOT(M)=ABS(PI*FREQ*EP0*EPDPG(THETA0(M,NLAYER)+T0)*E0**2)
          ELSE
              PAUSE 'SOURCE SUBROUTINE FAILED'
          ENDIF
      ENDDO
C..CALCULATE THE HEAT GENERATION WITHIN THE SHELL OF THE PELLET
      DO M=(MTH-NODES+1),MTH
          QDOT(M)=ABS(PI*FREQ*EP0*AIMAG(ZEPM(THETA0(M,NLAYER)+T0))*E0**2)
      ENDDO
      RETURN
      END
CCCCCCCCCCCCCCCCCCCCCCCCCCCCCCCCCCCCCCCCCCCCCCCCCCCCCCCCCCCCCCCCCCCCCCCCCCCCCCC
```

```
      SUBROUTINE SOURCE2(MTH,MZ,NLAYER,THETA0,QDOT)
C..CALCULATES THE HEAT GENERATION WITHIN THE ALUMINA PELLET
C  ACCOUNTING FOR THE HEAT GENERATED BY THE INDIVIDUAL PT PARTICLES
C  WITHIN THE PT/AL2O3 MIXTURE REGION
C
C  BSIGPT       -BULK CONDUCTIVITY OF PLATINUM (S/M)
C  DAL          -DIAMETER OF ALUMINA PELLET (M)
C  E0           -APPLIED ELECTRIC FIELD STRENGTH (V/M)
C  E2           -ELECTRIC FIELD INTERNAL TO THE PLATINUM PARTICLES,
C                EQ.(3.21), (V/M)
C  EP0          -PERMITTIVITY OF FREE SPACE (F/M)
C  EPDPA        -DIELECTRIC LOSS OF ALPHA ALUMINA (F/M)
C  EPDPG        -DIELECTRIC LOSS OF GAMMA ALUMINA (F/M)
C  FPT          -MASS FRACTION OF PLATINUM
C  FREQ         -FREQUENCY OF THE MICROWAVE FIELD (HZ)
C  IAL          -SPECIFIES ALPHA OR GAMMA ALUMINA
C  IPT          -SPECIFIES BULK OR SIZE DEPENDENT PLATINUM CONDUCTIVITY
C  MTH          -NUMBER OF FINITE-DIFFERENCE NODES WITHIN THE ALUMINA PELLET
C  NLAYER       -CURRENT CATALYST BED LAYER
C  NODES        -NUMBER OF FINITE-DIFFERENCE NODES WITHIN THE PT/AL2O3
C                MIXTURE REGION
C  PTMASS       -TOTAL MASS OF THE PLATINUM (KG)
C  Q1           -HEAT GENERATED BY THE PLATINUM PARTICLES (W/M^3)
C  Q2           -HEAT GENERATED BY THE ALUMINA SUPPORT (W/M^3)
C  QDOT         -VOLUMETRIC HEAT GENERATION VECTOR (W/M^3)
C  QSIGPT       -SIZE DEPENDENT CONDUCTIVITY (S/M)
C  RATIO        -TEMPORARY VARIABLE
C  RHOPT        -DENSITY OF PLATINUM (KG/M^3)
C  THETA0       -TEMPERATURE RISE ARRAY AT THE CURRENT TIME STEP (K)
C  TSHELL       -THICKNESS OF THE PT/AL2O3 MIXTURE REGION
C  VOLPEL       -VOLUME OF THE ALUMINA PELLET (M^3)
C  VSHELL       -VOLUME OF THE PT/AL2O3 MIXTURE REGION (M^3)
C  ZEPM         -COMPLEX PERMITTIVITY OF THE MIXTURE REGION (F/M)
C
      IMPLICIT DOUBLE PRECISION(A-H,O-Y)
      IMPLICIT COMPLEX*16(Z)
      DOUBLE PRECISION QDOT(MTH),THETA0(1:MTH,0:MZ)
      COMMON/BLOCK1/IAL,IPT,IMIX,IQDOT,ITRISE
      COMMON/BLOCK2/EP0,PI,FREQ,E0
      COMMON/BLOCK4/RHOAL,DAL,TSHELL,SAPEL,VOLPEL
      COMMON/BLOCK5/DPT,CPPT,RHOPT,FPT
      COMMON/BLOCK8/T0,TF
C..COMPUTE THE VOLUME FRACTION OF PT
      VSHELL=(4.D0/3.D0)*PI*((DAL/2.0D0)**3-((DAL/2.0D0)-TSHELL)**3)
      PTMASS=(FPT/(1.0D0-FPT))*VOLPEL*RHOAL
      VOLFRAC=(PTMASS/RHOPT)/((PTMASS/RHOPT)+VSHELL)
C..CALCULATE THE NUMBER OF NODES WITHING THE SHELL
      RATIO=TSHELL/(DAL/2.0D0)
      NODES=NINT(RATIO*MTH)+1
C..CALCULATE THE INTERIOR HEAT GENERATION OF THE PELLET
     DO M=1,(MTH-NODES)
          IF (IAL.EQ.1) THEN
               QDOT(M)=ABS(PI*FREQ*EP0*EPDPA(THETA0(M,NLAYER)+T0)*E0**2)
```

```
            ELSEIF (IAL.EQ.2) THEN
                  QDOT(M)=ABS(PI*FREQ*EP0*EPDPG(THETA0(M,NLAYER)+T0)*E0**2)
            ELSE
                  PAUSE 'SOURCE SUBROUTINE FAILED'
            ENDIF
      ENDDO
C..CALCULATE THE HEAT GENERATION WITHIN THE SHELL OF THE PELLET
C  USING THE HEAT GENERATION OF THE INDIVIDUAL PT PARTICLES
     DO M=(MTH-NODES+1),MTH
            IF (IAL.EQ.1) THEN
                  Q2=ABS(PI*FREQ*EP0*EPDPA(THETA0(M,NLAYER)+T0)*E0**2)
            ELSEIF (IAL.EQ.2) THEN
                  Q2=ABS(PI*FREQ*EP0*EPDPG(THETA0(M,NLAYER)+T0)*E0**2)
            ELSE
                  PAUSE 'SOURCE2 SUBROUTINE FAILED'
            ENDIF
            IF(IPT.EQ.1)THEN
                  Q1=0.5D0*BSIGPT(THETA0(M,NLAYER)+T0)*E2(THETA0(M,NLAYER)+T0)
      &**2
            ELSEIF(IPT.EQ.2)THEN
                  Q1=0.5D0*QSIGPT(THETA0(M,NLAYER)+T0)*E2(THETA0(M,NLAYER)+T0)
      &**2
            ELSE
                  PAUSE 'SOURCE2 SUBROUTINE FAILED'
            ENDIF
            QDOT(M)=(VOLFRAC*Q1+(1.0-VOLFRAC)*Q2)
      ENDDO
      RETURN
      END
CCCCCCCCCCCCCCCCCCCCCCCCCCCCCCCCCCCCCCCCCCCCCCCCCCCCCCCCCCCC
      SUBROUTINE SOURCE3(MTH,MZ,NLAYER,THETA0,QDOT)
C..CALCULATES THE HEAT GENERATION WITHIN THE ALUMINA PELLET
C  USING A MIXTURE FORMULA TO MODEL THE EFFECTIVE PERMITTIVITY OF
C  THE PT/AL2O3 MIXTURE REGION
C..ALSO ACCOUNTS FOR A VARYING ELECTRIC FIELD ALONG THE AXIS OF THE
C  CATALYST BED
C
C  A          -WIDTH OF THE WAVEGUIDE (M)
C  BASE       -TEMPORARY VARIABLE
C  CONST      -ELECTRIC FIELD DISTRIVBUTION CALCULATED BY EQ.(4.22)
C  DAL        -DIAMETER OF ALUMINA PELLET (M)
C  E0         -APPLIED ELECTRIC FIELD STRENGTH (V/M)
C  E0IN       -ELECTRIC FIELD DISTRIBUTION WITHIN THE CATALYST BED (V/M)
C  EP0        -PERMITTIVITY OF FREE SPACE (F/M)
C  EPDPA      -DIELECTRIC LOSS OF ALPHA ALUMINA (F/M)
C  EPDPG      -DIELECTRIC LOSS OF GAMMA ALUMINA (F/M)
C  FREQ       -FREQUENCY OF THE MICROWAVE FIELD (HZ)
C  IAL        -SPECIFIES ALPHA OR GAMMA ALUMINA
C  MTH        -NUMBER OF FINITE-DIFFERENCE NODES WITHIN THE ALUMINA PELLET
C  NLAYER     -CURRENT CATALYST BED LAYER
C  NODES      -NUMBER OF FINITE-DIFFERENCE NODES WITHIN THE PT/AL2O3
C              MIXTURE REGION
C  QDOT       -VOLUMETRIC HEAT GENERATION VECTOR (W/M^3)
```

```
C  RATIO        -TEMPORARY VARIABLE
C  THETA0       -TEMPERATURE RISE ARRAY AT THE CURRENT TIME STEP (K)
C  TSHELL       -THICKNESS OF THE PT/AL2O3 MIXTURE REGION
C  ZEPM         -COMPLEX PERMITTIVITY OF THE MIXTURE REGION (F/M)
C
      IMPLICIT DOUBLE PRECISION(A-H,O-Y)
      IMPLICIT COMPLEX*16(Z)
      DOUBLE PRECISION QDOT(MTH),THETA0(1:MTH,0:MZ)
      COMMON/BLOCK1/IAL,IPT,IMIX,IQDOT,ITRISE
      COMMON/BLOCK2/EP0,PI,FREQ,E0
      COMMON/BLOCK4/RHOAL,DAL,TSHELL,SAPEL,VOLPEL
      COMMON/BLOCK5/DPT,CPPT,RHOPT,FPT
      COMMON/BLOCK6/DTUBE,HTUBE,VOLTUBE,POROSITY,MAXDZ
      COMMON/BLOCK8/T0,TF
C..CALCULATE THE NUMBER OF NODES WITHING THE SHELL
      RATIO=TSHELL/(DAL/2.0D0)
      NODES=NINT(RATIO*MTH)+1
C..CALCULATE THE EFIELD VARIATION
      A=7.21D-02
      BASE=(A-HTUBE)/2.0D0
      CONST=0.44D0*SIN((PI/A)*(BASE+(DBLE(NLAYER)/DBLE(MAXDZ))*HTUBE))
      E0IN=CONST*E0
C..CALCULATE THE INTERIOR HEAT GENERATION OF THE PELLET
     DO M=1,(MTH-NODES)
          IF (IAL.EQ.1) THEN
               QDOT(M)=ABS(PI*FREQ*EP0*EPDPA(THETA0(M,NLAYER)+T0)*E0IN**2)
          ELSEIF (IAL.EQ.2) THEN
               QDOT(M)=ABS(PI*FREQ*EP0*EPDPG(THETA0(M,NLAYER)+T0)*E0IN**2)
          ELSE
               PAUSE 'SOURCE SUBROUTINE FAILED'
          ENDIF
      ENDDO
C..CALCULATE THE HEAT GENERATION WITHIN THE SHELL OF THE PELLET
      DO M=(MTH-NODES+1),MTH
           QDOT(M)=ABS(PI*FREQ*EP0*AIMAG(ZEPM(THETA0(M,NLAYER)+T0))*E0IN**2)
      ENDDO
      RETURN
      END
CCCCCCCCCCCCCCCCCCCCCCCCCCCCCCCCCCCCCCCCCCCCCCCCCCCCCCCCCCCCCCCCCCCCCCCCCC
      SUBROUTINE TRIDAG(A,B,C,R,U,N)
C..THOMAS ALGORITHM FOR SOLUTION OF TRIDIAGONAL SYSTEMS
C  FROM NUMERICAL RECIPIES IN FORTRAN 77 [16]
      INTEGER N,NMAX
      DOUBLE PRECISION A(N),B(N),C(N),R(N),U(N)
     PARAMETER (NMAX=500)
     INTEGER J
     REAL BET,GAM(NMAX)
     IF(B(1).EQ.0.)PAUSE 'TRIDAG: REWRITE EQUATIONS'
     BET=B(1)
     U(1)=R(1)/BET
     DO 11 J=2,N
      GAM(J)=C(J-1)/BET
      BET=B(J)-A(J)*GAM(J)
```

```
      IF(BET.EQ.0.)PAUSE 'TRIDAG FAILED'
      U(J)=(R(J)-A(J)*U(J-1))/BET
11    CONTINUE
     DO 12 J=N-1,1,-1
      U(J)=U(J)-GAM(J+1)*U(J+1)
12    CONTINUE
     RETURN
     END
CCCCCCCCCCCCCCCCCCCCCCCCCCCCCCCCCCCCCCCCCCCCCCCCCCCCCCCCCCCCCCCCCCCCCCCCCCC
      FUNCTION VISCBU(T)
C..VISCOCITY OF BUTANE FROM A CUBIC SPLINE INTERPOLATION
C  FROM DATA IN THE CRC HANDBOOK [28]
C
C  NX            -NUMBER OF DATA POINTS
C  VISCBU        -VISCOCITY OF BUTANE (KG/M S)
C  T             -TEMPERATURE (K)
C  XTEMP         -TEMPERATURE DATA (K)
C  Y2            -SECOND DERIVATIVES FROM SPLINE SUBROUTINE
C  YINT          -CUBIC SPLINE INTERPOLATION (KG/M S)
C  YVISC         -VISCOCITY DATA (KG/M S)
C
      IMPLICIT DOUBLE PRECISION(A-H,O-Y)
      DOUBLE PRECISION XTEMP(7),YVISC(7),Y2(7)
      DATA XTEMP/2.73D02,3.73D02,4.73D02,5.73D02,6.73D02,7.73D02,
    &8.73D02/
      DATA YVISC/6.84D-06,9.26D-06,1.17D-05,1.4D-05,1.64D-05,1.87D-05,
    &2.11D-05/
      DATA Y2/0.0D+00,1.0784615D-11,-3.1138462D-11,2.9769231D-11,
    &-2.7938462D-11,2.1984615D-11,0.0D+00/
      DATA NX/7/
      CALL SPLINT(XTEMP,YVISC,Y2,NX,T,YINT)
      VISCBU=YINT
      RETURN
      END
CCCCCCCCCCCCCCCCCCCCCCCCCCCCCCCCCCCCCCCCCCCCCCCCCCCCCCCCCCCCCCCCCCCCCCCCCCC
      FUNCTION VISCF(T)
C..CALCULATES THE DYNAMIC VISCOCITY OF THE GAS MIXTURE
C  USING PMIX FUNCTION
C
C  P1            -VISCOCITY OF HELIUM
C  P2            -VISCOCITY OF BUTANE
C  VISCF         -VISCOCITY OF HELIUM/BUTANE MIXTURE
C
      IMPLICIT DOUBLE PRECISION(A-H,O-Y)
      P1=VISCHE(T)
      P2=VISCBU(T)
      VISCF=PMIX(P1,P2)
      RETURN
      END
CCCCCCCCCCCCCCCCCCCCCCCCCCCCCCCCCCCCCCCCCCCCCCCCCCCCCCCCCCCCCCCCCCCCCCCCCCC
      FUNCTION VISCHE(T)
C..VISCOCITY OF HELLIUM FROM A CUBIC SPLINE INTERPOLATION OF
C  DATA FROM KAYS AND CRAWFORD [29]
```

```
C
C  NX            -NUMBER OF DATA POINTS
C  VISCHE        -VISCOCITY OF HELIUM (KG/M S)
C  T             -TEMPERATURE (K)
C  XTEMP         -TEMPERATURE DATA (K)
C  Y2            -SECOND DERIVATIVES FROM SPLINE SUBROUTINE
C  YINT          -CUBIC SPLINE INTERPOLATION (KG/M S)
C  YVISC         -VISCOCITY DATA (KG/M S)
C
      IMPLICIT DOUBLE PRECISION(A-H,O-Y)
      DOUBLE PRECISION XTEMP(15),YVISC(15),Y2(15)
      DATA XTEMP/2.5D+02,3.0D+02,3.5D+02,4.0D+02,4.5D+02,5.0D+02,
     &6.0D+02,7.0D+02,8.0D+02,9.0D+02,1.0D+03,1.1D+03,1.2D+03,
     &1.3D+03,1.4D+03/
      DATA YVISC/17.6D-06,19.9D-06,22.2D-06,24.3D-06,26.4D-06,28.4D-06,
     &32.2D-06,35.9D-06,39.4D-06,42.8D-06,46.2D-06,49.4D-06,52.5D-06,
     &55.6D-06,58.6D-06/
      DATA Y2/0.0D+00,3.5460893D-11,-1.4184357D-10,5.1913389D-11,
     &-6.5809984D-11,-2.8673453D-11,-1.074648D-12,-2.7027955D-11,
     &-1.0813533D-11,1.0282088D-11,-3.0314818D-11,-9.0228167D-12,
     &6.4060844D-12,-1.6601521D-11,0.0D+00/
      DATA NX/15/
      CALL SPLINT(XTEMP,YVISC,Y2,NX,T,YINT)
      VISCHE=YINT
      RETURN
      END
CCCCCCCCCCCCCCCCCCCCCCCCCCCCCCCCCCCCCCCCCCCCCCCCCCCCCCCCCCCCCCCCCCCCCCCCCCCCCCC
      FUNCTION ZCONJ(Z)
C..RETURNS THE CONJUGATE OF A COMPLEX NUMBER
      IMPLICIT DOUBLE PRECISION(A-H,O-Y)
      IMPLICIT COMPLEX*16(Z)
      ZI=DCMPLX(0.0D0,1.0D0)
      R1=Z
      R2=-ZI*Z
      ZCONJ=DCMPLX(R1,-R2)
      RETURN
      END
CCCCCCCCCCCCCCCCCCCCCCCCCCCCCCCCCCCCCCCCCCCCCCCCCCCCCCCCCCCCCCCCCCCCCCCCCCCCCCC
      FUNCTION ZEPM(T)
C..EFFECTIVE DIELECTRIC LOSS OF AL2O3 & PT MIXTURE
C
C  DAL           -DIAMETER OF THE ALUMINA CATALYST PELLET (M)
C  EPDPA         -DIELECTRIC LOSS OF ALPHA ALUMINA (F/M)
C  EPDPG         -DIELECTRIC LOSS OF GAMMA ALUMINA (F/M)
C  EPPA          -DIELECTRIC CONSTANT OF ALPHA ALUMINA (F/M)
C  EPPG          -DIELECTRIC CONSTANT OF GAMMA ALUMINA (F/M)
C  FPT           -MASS FRACTION OF PLATINUM \
C  IAL           -SPECIFIED ALPHA OR GAMMA ALUMINA SUPPORT
C  IMIX          -SPECIFIES THE MIXTURE FORMULA
C  PTMASS        -TOTAL MASS OF PLATINUM    (KG/M^3)
C  R             -TEMPORARY VARIABLE
C  RHOAL         -DENSITY OF ALUMINA (KG/M^3)
C  RHOPT         -DENSITY OF PLATINUM (KG/M^3)
```

```
C  TSHELL      -THICKNESS OF THE PT/AL2O3 MIXTURE REGION (M^3)
C  VOLFRAC    -VOLUME FRACTION OF PLATINUM
C  VSHELL      -VOLUME OF THE PT/AL2O3 MIXTURE REGION (M^3)
C  ZEP1         -COMPLEX PERMITTIVITY OF ALUMINA (F/M)
C  ZEP2         -COMPLEX PERMITTIVITY OF PLATINUM (F/M)
C  ZEPM         -COMPLEX PERMITTIVITY OF THE MIXTURE (F/M)
C  ZDEN         -TEMPORARY VARIABLE
C  ZNUM         -TEMPORARY VARIABLE
C
      IMPLICIT DOUBLE PRECISION(A-H,O-Y)
      IMPLICIT COMPLEX*16(Z)
      COMMON/BLOCK1/IAL,IPT,IMIX,IQDOT,ITRISE
      COMMON/BLOCK2/EP0,PI,FREQ,E0
      COMMON/BLOCK4/RHOAL,DAL,TSHELL,SAPEL,VOLPEL
      COMMON/BLOCK5/DPT,CPPT,RHOPT,FPT
C..COMPUTE THE VOLUME FRACTION OF PT
      VSHELL=(4.D0/3.D0)*PI*((DAL/2.0D0)**3-((DAL/2.0D0)-TSHELL)**3)
      PTMASS=(FPT/(1.0D0-FPT))*VOLPEL*RHOAL
      VOLFRAC=(PTMASS/RHOPT)/((PTMASS/RHOPT)+VSHELL)
      IF (IAL.EQ.1) THEN
          ZEP1=DCMPLX(EPPA(T),-EPDPA(T))
       ELSEIF (IAL.EQ.2) THEN
          ZEP1=DCMPLX(EPPG(T),-EPDPG(T))
       ELSE
          PAUSE 'ZEPM FUNCTION FAILED'
      ENDIF
      ZEP2=DCMPLX(1.0D0,-EPDPPT(T))
      IF (IMIX.EQ.1) THEN
C..USING THE RAYLEIGH FORMULA EQ.(3.16)
          ZNUM=ZEP1*(2.0D0*ZEP1+ZEP2)+2.0D0*VOLFRAC*ZEP1*(ZEP2-ZEP1)
          ZDEN=(2.0D0*ZEP1+ZEP2)-VOLFRAC*(ZEP2-ZEP1)
          ZEPM=ZNUM/ZDEN
C..USING THE MAXWELL-GARNET THEORY [14]
       ELSEIF(IMIX.EQ.2)THEN
         R=1.0D0-VOLFRAC
          ZNUM=ZEP1*(ZEP2*(3.0D0-2.0D0*R)+2.0D0*R*ZEP1)
          ZDEN=R*ZEP2+ZEP1*(3.0D0-R)
        ZEPM=ZNUM/ZDEN
       ELSE
          PAUSE 'ZEPM UNCTION FAILED'
     ENDIF
     RETURN
     END
```